SOLIDIFICATION OF METAL DROPLETS DURING FREE FALL ATOMIZATION

A thesis submitted in partial fulfillment of the Requirements for the Degree of

MASTERS OF TECHNOLOGY

by

Shiba Narayan Sahu

to the

DEPARTMENT OF MATERIALS AND METALLURGICAL ENGINNERING
INDIAN INSTITUTE OF TECHNOLOGY, KANPUR-208016

13 FEB 2003 /MME
पुरुषोत्तम काशीनाथ केलकर पुस्तकालय
भारतीय प्रौद्योगिकी संस्थान कानपुर
अवाप्ति क्र० A 141829

POST GRADUATE OFFICE
THESIS SUBMITTED
ON 3-5-02
I.I.T., KANPUR 16

CERTIFICATE

This is to certify that Mr. Shiba Narayan Sahu has completed the work contained in the thesis entitled "*Solidification of Metal Droplets during Free Fall Atomization*" under my supervision and it has not been submitted elsewhere for a degree.

Prof. S.C. Koria
Dept. of Materials and Metallurgical Engg.
I.I.T., Kanpur-208016
April 2002

ACKNOWLEDGEMENT

I would like to express my deep sense of gratitude to my guide and mentor Dr. S.C. Koria for his invaluable guidance and help through out my M. Tech. programme. I am sincerely thankful for his valuable suggestions and encouragement, which made the work interesting and enjoyable.

I am greatly inspired by my friends who helped me in troubled times and stood by me. Nevertheless, their presence in my life made the stay at I.I.T., Kanpur memorable and enjoyable one. The numbers are many; Trailokya, Preeti, Sampurna, Lenka Bhai, Suraj Bhai, Ranjan Bhai, Emila, Sushant, Himanshu Bhai, are few of them. Also I am thankful to Ph.D. scholar Mr. Anil with whom I shared the lab as well as feelings.

Lastly, I am deeply owed to my parents and sisters whose continuous encouragement helped me to succeed all goals in my life. I dedicate my thesis to them.

ABSTARCT:

Spray atomization and deposition is an emerging technology to produce near net shape products directly from melts. As a consequence, this technology eliminates casting as a separate step and leads to significant energy savings and improved microstructures in the product. The process integrates atomization of liquid metals into droplets, solidification of droplets during flight and deposition of droplets into a there dimensional perform in order to get the product of the desired properties.

In the present study a mathematical model is developed to study solidification behavior of droplets produced by free fall atomization. Momentum and heat transfer equations are coupled to predict the extent of solidification of droplets as a function of several parameters like atomizing gas velocity, droplet size, flight distance, degree of superheat etc. The following results may be noted.

- For a given velocity of the atomizing gas field, the fine droplets acquire a higher velocity initially than the coarser ones. Later during their motion downstream their velocity decreases below the velocity of coarser ones. It means that the atomized droplets of different sizes will hit the substrate at different velocities.

- For a given droplet size, the difference between velocity of gas and the droplet decreases rapidly with the increase in flight distance and becomes zero at a particular flight distance. This particular flight distance is found to increase with the increase in the droplet size.

- As a consequence of the above observation, heat transfer coefficient at first decreases, then attains a minimum value and thereafter increases with the increase in the flight distance.

- The calculations are performed for solidification under rapid cooling for Al and Cu droplets in He and Nitrogen mediums. Al droplets are

found to be solidifying at a longer distance than Cu droplets in both the mediums. Due to higher cooling rate in Helium medium all droplets are found to be solidifying at a distance much lower than the Nitrogen medium. In terms of flight distance finer droplets tend to solidify earlier than the coarser ones This suggests that the atomizer-substrate distance must be selected on the basis of amount of liquid fraction in the spray. It is because higher amount of solid fraction in the spray will lead to improper adhesion and higher amount of liquid in the spray will lead to the improper microstructure

NOMENCLATURE:

A	projected area of the droplet on a plane perpendicular to its motion
a_0	lattice parameter
A_d	total surface area of the droplet
A_s	molar solid surface area
C_0	number of atoms per unit volume
C_{drag}	fluid drag coefficient
C_{pl}	specific heat of the droplet in liquid state
C_{psub}	specific heat of the substrate
C_{ps}	specific heat of the droplet in the solid state
C_{psl}	specific heat of the semiliquid droplet
d	droplet diameter
D	effective nozzle diameter
D_0	diffusion coefficient in the liquid state
d_m	mean diameter
F	focal length
f_r	fraction solidified at the end of recalescence
f_0	atom attaching frequency
g	gravitational constant
h_c	heat transfer coefficient
$h_{s,d}$	heat transfer coefficient from deposit to substrate
$h_{a,d}$	heat transfer coefficient from deposit to surrounding gas
$h_{a,s}$	heat transfer coefficient from substrate to gas
H_1	rate of evolution of latent heat
H_2	rate of extraction of heat by gas
H_f	latent heat of fusion per kg
H_{fm}	molar heat of fusion
H_{fv}	latent heat of fusion per unit volume

I_s	steady state nucleation rate
I_t	transient nucleation rate
K	Boltzman's constant
k_g	thermal conductivity of gas
M	molecular weight
m_g	flow rate of gas
m_l	flow rate of molten metal
N	gas constant used for atomization
Nu	Nusselt Number
P	plenum pressure
Pr	Prandtl Number
R	universal gas constant
Re	Reynolds number
R_i	interfacial velocity
T	temperature of the droplet
T_g	gas temperature
T_m	melting point
T_N	nucleation temperature
T_0	initial deposit temperature
$T_{0,s}$	initial substrate temperature
V	volume of the droplet
V_d	droplet velocity
V_g	initial gas velocity
V_m	volume per atom
Z	distance
Z_c	critical distance up to which the gas velocity remains constant
d_m	mean droplet diameter
Cd	discharge coefficient
Hc	height of the molten metal
σ_g	standard deviation

k_s	thermal conductivity of metal
k_{sub}	thermal conductivity of substrate
β	dimensionless factor for limited diffusion
α	geometric constant of the metal used
τ	Incubation period
λ	jump distance
Ω	molar volume of the metal
ρ_a	density of air
ρ_g	density of gas used for atomization
ν_g	kinematic viscosity of gas
μ_g	dynamic viscosity of molten metal
ΔGc	critical free energy
ΔG_v	volume free energy
ρ_l	density of molten metal
ν_l	kinematic viscosity of molten metal
μ_l	dynamic viscosity of molten metal
γ_{lv}	surface tension of liquid metal
ρ_s	density of metal in the solid state
σ_{sl}	solid-liquid interfacial energy
ρ_{sl}	density of the semiliquid droplet
σ_l	melt superheat tension
γ	Cp/Cv for atomizing gas
ρ_{sub}	density of the substrate

THERMOPHYSICAL DATA:

A) ATOMIZING MEDIUMS:

Nitrogen gas:

C_{pg}	1030 J/kg/^{0}C
k_g	0 0252 J/m/ ^{0}C
μ_g	1 78 * 10^{-5} kg $m^{-1}s^{-1}$
T_g	25^{0}C
ρ_g	1 137 kg/m^3

Helium gas:

C_{pg}	5250.0 J/kg/^{0}C
k_g	0.1394 J/m/ ^{0}C
μ_g	1.72× 10^{-5} kg $m^{-1}s^{-1}$
T_g	25^{0}C
ρ_g	0.1635 kg/m^3

B) METALS:

Aluminium:

a_0	4 049 ×10^{-10} m
C_{pl}	862 5 J/kg/^{0}C
C_{ps}	755 8 J/kg/^{0}C
D_0	4.0 ×10^{-10} m^2/s
H_f	397746 J/kg
H_{fm}	10739 142 J/mol
H_{fv}	1.0739×10^9 J/m^3
T_m	660^{0}C
μ_l	0.001 kg $m^{-1}s^{-1}$
ρ_s	2700 kg/m^3
ρ_l	2540 kg/m^3

Copper

a_0	$3\ 63\times10^{-10}$ m
C_{pl}	495.5J/kg/^{0}C
C_{ps}	428 4J/kg/^{0}C
D_0	4.02×10^{-10} m^2/s
H_f	205700J/kg
H_{fm}	13061J/mol
H_{fv}	1.84×10^9 J/m^3
T_m	1083^{0}C
μ_l	0 0017 kg m^{-1}s^{-1}
ρ_s	8960.0kg/m^3
ρ_l	8598.8kg/m^3

OTHER DATA:

D	0.004m
F	0.09m
K	1.38×10^{-23} J/K
P	10 bar
R	8.314 J/mol/K
ρ_a	1.2 kg/m^3

LIST OF FIGURES:

LIST OF FIGURES:

LIST OF TABLES

CHAPTER 1 INTRODUCTION

1.1 SPRAY ATOMIZATION AND DEPOSITION: AN OVERVIEW

Spay deposition is an integrated process which is a combination of three consecutive steps, namely atomization of a liquid metal into droplets, then motion of the droplets in the atomization gas and lastly deposition of the droplets into a preform. At first the metal is melted in a container to attain a desired level of superheat. Then the molten metal is disintegrated by a high velocity gas jet into a dispersion of droplets, which is known as atomization. The droplets thus formed, travel a predetermined distance in the gaseous environment and accumulate on the substrate to form a preform, which is known as deposition. Fig. 1.1 [1] shows the principles of spray atomization and deposition processing.

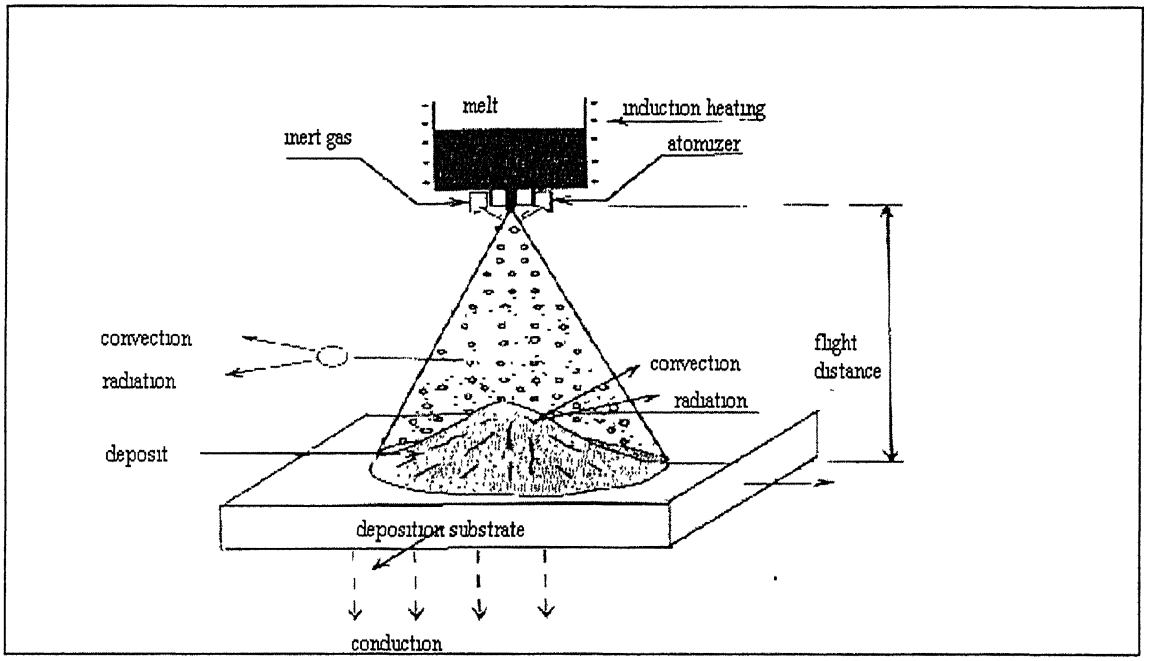

Figure 1.1: Principles of spray atomization and deposition

In order to avoid extensive oxidation of the material during processing or to synthesize the material under a controlled atmosphere, spray deposition processes are generally conducted in an environmental chamber. The selection of the atomization media depends primarily on the metals and alloys to be sprayed and on the final microstructure desired. Generally, an inert gas such as nitrogen, argon or helium is used

for atomization since these gases do not react with most metals. Nitrogen for example, is inert to many alloy systems; it is inexpensive and is widely used for atomizing a wide variety of metals and alloys. Helium, despite its attractive thermal transport characteristics, is having restricted use due to its high cost. There are several factors that are essential towards the understanding of the spray deposition process. These are the key processing parameters, the microstructure and macroscopic characteristics of the spray deposited performs.

Key processing parameters:

Fig. 1.1 illustrates the critical governing parameters in the spray deposition process. There are a number of factors that critically influence the size distribution of the droplets that are produced during atomization, such as the flow rate of the molten metal and the flow rate of the atomization gas. The deposition distance is also an important parameter since it is inherently coupled to the solidification conditions of the droplets during impingement with a deposition surface. The total heat contained in the dispersion of atomized droplets is dissipated during two stages: droplet flight and deposition. During the droplet flight stage, the primary mechanism of heat transfer is thermal energy exchange between droplets and atomizing gas. As a result of high relative velocity exists between the droplets and gas, the droplets loose heat in a very rapid rate by the mechanism of forced convection. This rapid rate of cooling leads to the formation of rapidly solidified microstructures. During the deposition stage, the distribution of droplets accumulates into a thick preform. There are two major heat transfer mechanisms that influence the thermal conditions that are present in this stage: heat convection through the upper surface of the spray deposited material into the cooling substrate and heat loss through the top of the deposit to the surrounding gas.

Micro structural characteristics:

An important incentive for developing spray deposition technique as an alternative approach to conventional materials fabrication techniques such as powder metallurgy and ingot metallurgy, results from the unusual combinations of microstructure and physical properties that may be achieved using this method. Spray deposition provides the benefits associated with fine particle technology that is microstructural refinement and alloying flexibility etc., while avoiding some of the drawbacks that is fine

particle reactivity, surface reactions etc. In addition, spray deposition offers the opportunity for extensive micro structural control and under some conditions, near-net-shape manufacturing. In addition, there are two characteristics that are singular about spray deposition. First, droplets exchange thermal energy with an atomization gas media as they travel towards a deposition surface. The deposition distance that is, the distance from the atomizer to the collecting substrate is selected such that the average droplet will contain a predetermined proportion of solid phases. During deposition, liquid, semisolid and solid droplets repeatedly impinge the substrate of the spray deposited material. Accordingly, fragmentation of dendrites that evolve during atomization offers potential nucleation sites for grain refinement. This is in contrast with materials processed utilizing other rapid solidification techniques in which nucleation events rely, to a large extent, on the presence of heterogeneous nucleation reagents or a high level of undercooling. Second, during deposition, a bulk material is formed from the accumulation of isolated droplets or powders. In this case, the potential segregation distances are generally very small as compared with those associated with conventional processing techniques. Hence, the scale of segregation in spray-deposited material is limited by the sizes of the droplets, which are generally smaller than a few hundred micrometers. But in conventional casting processes the segregation stays in the range of several thousands of micrometers. Spray-deposited materials are therefore characterized by a uniform, rapidly solidified microstructure. Some of the microstructural features for spray-deposited material are listed below.

(a) microstructural refinement that is characterized by a fine grain microstructure and fine, uniformly distributed secondary phase parameters.

(b) reduced segregation that is characterized by relatively small segregation distances in the microscopic scale.

(c) Formation of metastable phases that are energetically favorable only under thermodynamic conditions that are far from equilibrium.

1.2 HISTORY AND RECENT DEVELOPMENTS:

Singer at the University College of Swansea, UK pioneered the technology of spray atomization and deposition during the 1970s. Singer proposed the production of rolled metal strip directly from the molten metal, known as spray rolling, as an alternative to the casting and forming of a wide variety of spray-based technologies. These technologies include spray forging, spray peening, liquid dynamic compaction, variable co-deposition of multiphase materials and spray forming of metal matrix composites. Now a days in an effort to increase material yields and decrease energy consumption, spray deposition technology is presently being developed for the near net shape manufacturing of aluminum sheets. Spray deposition technology has continued to evolve and has undergone various modification and improvements since its incorporation. The different areas where modifications had taken place are

(a) Spray deposition atmosphere

(b) Atomizer design

(c) Control of porosity

(a) Spray deposition atmosphere:

A strict control of the atmosphere becomes necessary, if optimal combinations of microstructure and properties are desired. It is because reactive metals like Al and Mg undergo extensive oxidation during the process, if the atmosphere contains oxygen.

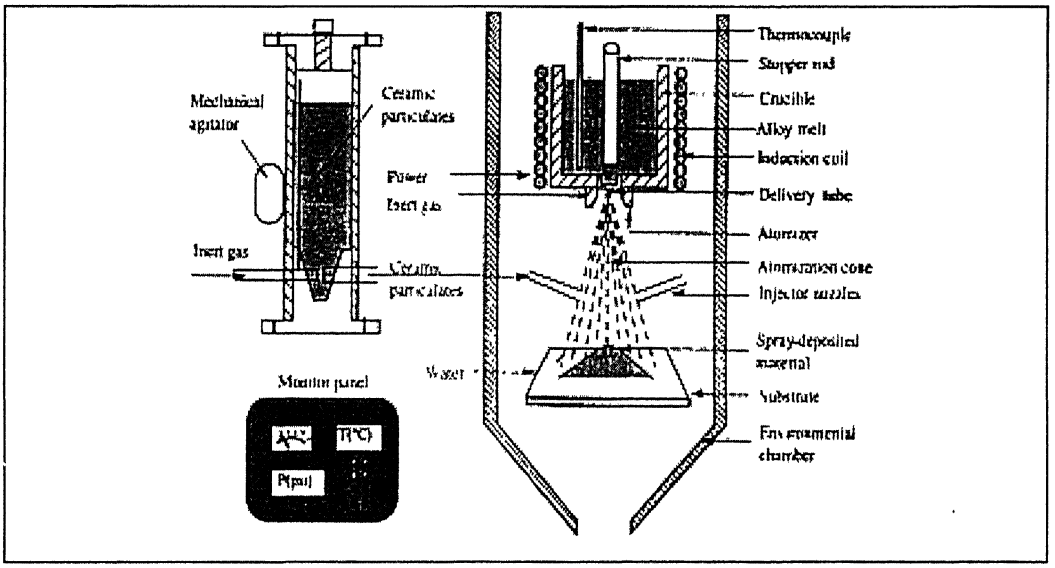

Figure 1.2.1: Experimental apparatus used for spray deposition of alloys and metal matrix composites.

Therefore, modern spray deposition equipments incorporates controlled atmosphere, such that melting, atomization and deposition all occur under a high purity, inert atmosphere. One example of such an experimental apparatus is shown in Fig. 1.2.1 [2]. In this particular experimental arrangement melting, atomization and deposition are conducted inside of an environmental chamber that is first evacuated down to a vacuum of 0.1-1 torr and subsequently backfilled with an inert gas.

(b) Atomizer design:

A critical aspect of spray deposition technology involves atomizer design. The atomizer is used to disintegrate the molten metal into a dispersion of droplets and therefore different designs result in various distributions of droplets sizes. Since, size distributions is an important variable that governs the solidification behavior of droplets, atomizer design influences the resultant quality of the preform and the microstructure and properties of spray-deposited materials. Various atomizer design influences the resultant quality of the preform. The atomizers can be classified into two types. Singer conducted his early spray deposition experiments using a closed type atomizer [3]. A closed type atomizer is illustrated in Fig. 1.2.2. It normally contains 10-18 gas jets symmetrically arranged around a cavity designed to contain the metal delivery tube. Typically, the gas

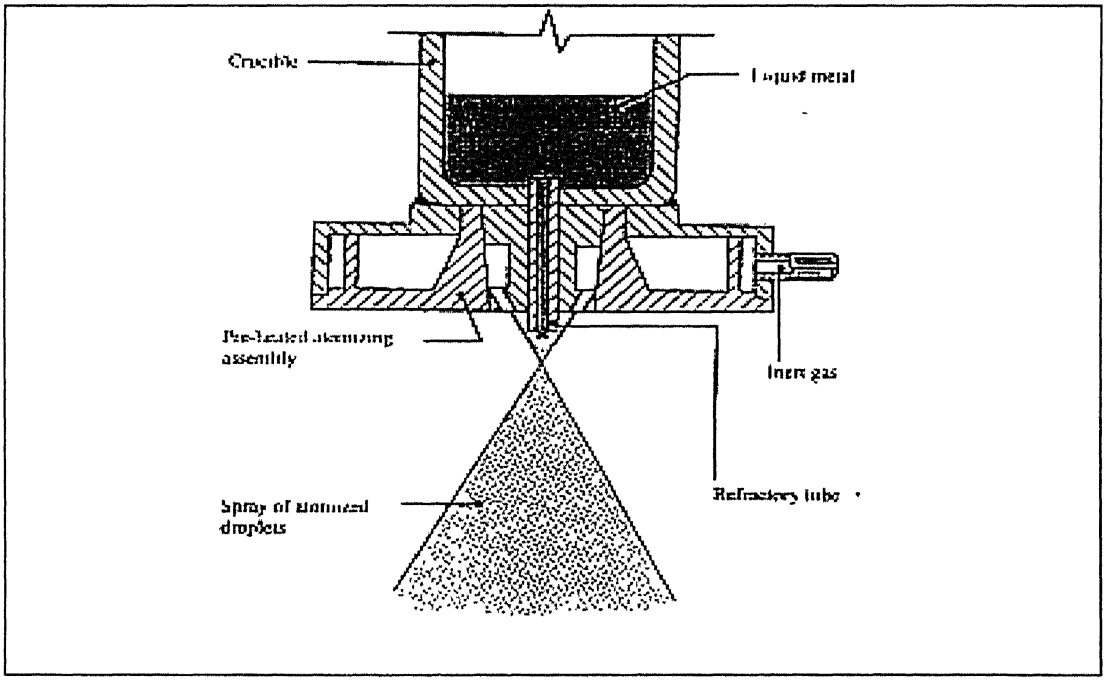

Figure 1.2.2: Closed-type atomizer used for spray deposition processing

nozzles are positioned at a distance of 10-15 diameters apart, depending on the desired powder characteristics. The geometry of the gas nozzles is designed in order to provide maximum kinetic energy to the atomization gas, thereby avoiding instability of the metal stream and producing a stable atomized droplet spray. The major problem that is associated with this type of atomizer is that it is very sensitive to metal freeze up, a condition that occurs when the liquid metal at the end of the delivery tube solidifies prematurely as a result of the rapid heat extraction that occurs in this region.

In view of the difficulties associated with the metal freeze-up phenomenon, many of the later experiments by Singer were conducted using an open-type atomizer. A schematic diagram of such an atomizer is illustrated in Fig. 1.2.3 [2]. An open-type atomizer is also preferred as free-fall design. In the free-fall design, liquid metal is allowed to fall freely to the atomization point (i.e. the focal point of the atomization gas jets). Since, the metal delivery nozzle tube is not direct contact with the atomization gas jets, nozzle freeze-up is avoided. The principal problem that is associated with open-type atomizers however is the instability of the molten metal stream that leads to oscillation and asymmetry of the atomization cone. This instability occurs because of the fact that

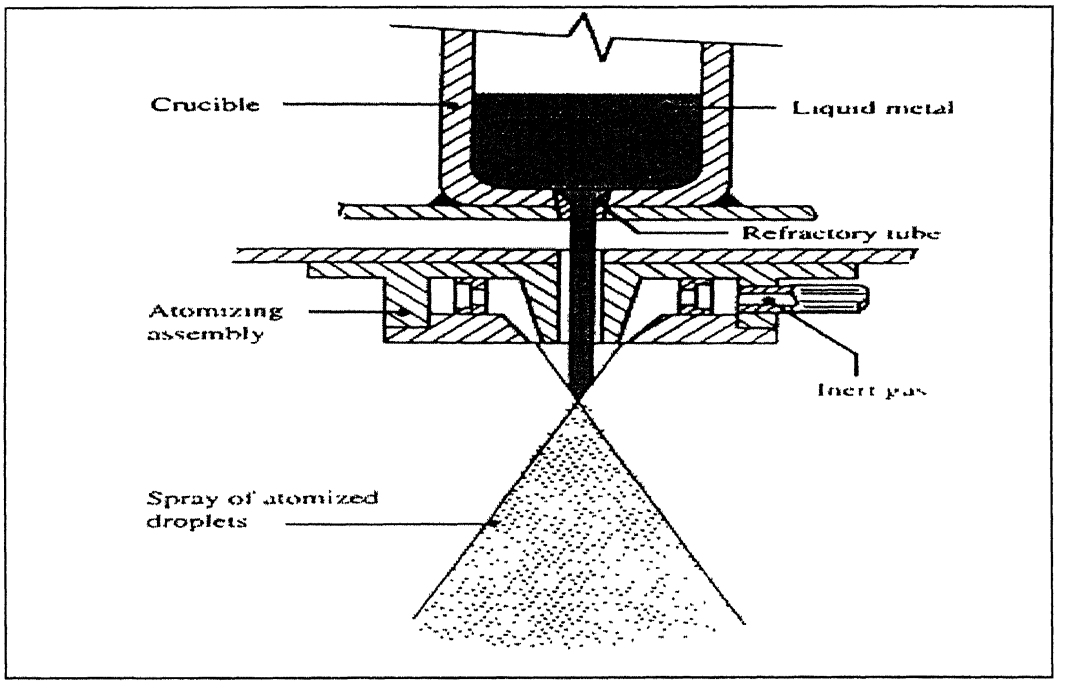

Figure 1.2.3: Open-type atomizer used for spray deposition processing

the free falling molten metal stream is easily deflected by the turbulence in the surrounding gas envelope. In the 1980s the liquid dynamic compaction process (LDC)

was developed. The major difference between the (LDC) process and the early spray deposition experiments involves atomizer design. The LDC process incorporates an ultrasonic gas atomizer, designed in principle to provide more efficient atomization.

(c) Control of porosity:

In spray deposited materials, there exist a certain fraction of porosity. The presence of this porosity requires that these materials be stored under inert conditions in order to avoid internal oxidation. Moreover, extensive hot working is necessary in order to densify such porous materials completely. The two prime factors which influences porosity are, the low spray density and the solidification condition of the impinging droplet. Some reported density values for spray-deposited materials are summarized in Table-1 [1].

Table-1: Relative density of metals and alloys

Material	Relative density(%)	Year
Al alloy	80-85	1970
13% C steel	85-97	1982
IN718	99.5	1987
Rene 80	99.4	1986
Rene 95	99.8	1987
390(Al-Si)	98.1	1993
Al-Si-X	98.7	1990

The results in this table reveal that large gains in density values in recent years, although a finite amount of porosity appears unavoidable. There are two primary factors, which are responsible for the observed trend, namely, the generation of a high spray density and the careful control of solidification conditions during impingement. Both of these factors contribute to maintaining a relatively continuous semisolid layer on the upper surface of the preforms during deposition. A high spray density may be rapidly achieved through atomizer design. Moreover, advances in knowledge of process fundamentals through experimentation and modeling have led to a better understanding of the thermal and solidification conditions that are necessary in order to obtain optimal microstructural refinement and minimal porosity.

1.3 SCOPE OF SPRAY DEPOSOTION TECHNIQUE:

Spray atomization and deposition technique is now being utilized to deposit metals, alloys and composites in a wide variety of geometries including sheets, tubes, discs and plates. The various techniques is which these shapes are produced are described below.

(a) Spray rolling

(b) Spray forging

(c) Spray forming of sheet metals

(d) Spray peening

(e) Near-net-shape forming

(a) Spray rolling:

Spray rolling is used to produce a flat shape by spray deposition, which is rolled into sheet geometry. A requirement in this process is that the material be rolled immediately following spray deposition while it remained at an elevated temperature and hence have a certain degree of plasticity. Efforts to spray-form dense sheets in an integrated approach led to the development of the Mark-IV equipment for spray rolling. The Mark-IV apparatus contained a rotating substrate, which is shown in Fig. 1.3.1 [3].

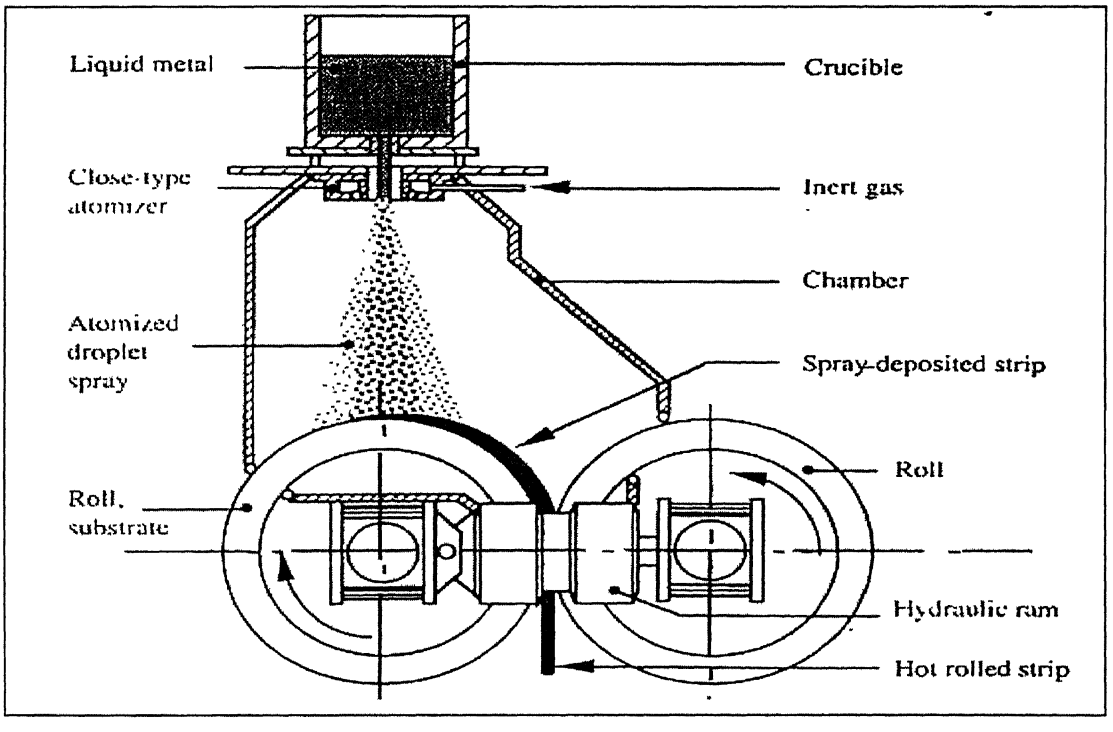

Figure 1.3.1: Mark IV equipment for spray rolling

This apparatus incorporates twin wheels with an appropriate gap in between. The spray of droplets was also generated using a single circular gas atomizer. During spray rolling, droplets are deposited on the surface of one of the rolls or on the surface of both rolls. The spray-deposited material was directly deformed between the rolls while it remained at a relatively high temperature. Following spray deposition and hot rolling, the rolled metal strip peeled off continuously from the rolls. Since, a large proportion of the porosity was closed during the elevated temperature deformation immediately following deposition, the sheet metal released from the roll gap was relatively dense. One of the advantages of this early spray deposition, direct rolling approach is that the thermal energy that is released during phase transformation is utilized to enhance plasticity during hot deformation. In addition, this processing approach provides the flexibility of producing laminated materials, where two different metals or alloys can be deposited on the surface of two separate rolls. Hence, the rotating rolls deform and weld the two separate layers of material simultaneously, which yields a laminate.

(b) Spray forging:

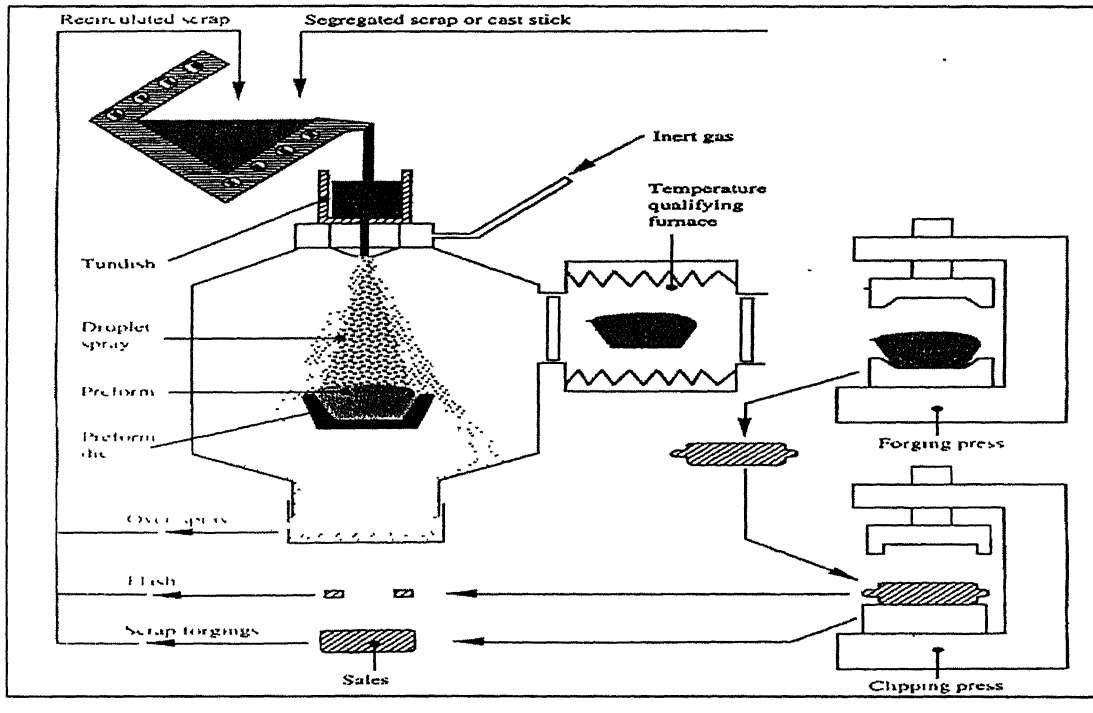

Figure 1.3.2: The spray forging process

Osprey Metals Ltd. produced the forging preforms by spray deposition. The Osprey process was considered to be an attractive alternative to the two existing basic

methods of producing forgings (i) forging of pre-rolled ingot castings, and (ii) forging of metal powder products. The conventional forging route from ingot castings generates large quantities of scrap. The powder metallurgy process is relatively expensive as a result of the necessary reducing, sieving, blending, compacting and heating steps that are involved. Fig. 1.3.2 shows a schematic diagram of the spray forging process. The three primary components of an integrated spray forging plant are [4] (i) the melting unit (ii) the Osprey preform production unit and (iii) the forging unit. The Osprey preform production unit consists of a heated tundish, an atomizer, gas-controlling equipment, and preform collection and removal equipment. In the spray-forging process, the starting material is melted and poured from a tundish into an atomizer. The molten metal is atomized using high velocity inert gas. The resulting atomized spray of droplets is directed into a shaped collector to form a spray-deposited preform. Following spray deposition, the preform is removed from the collector and is transferred into a temperature-qualifying furnace, which is located inside of the spray deposition chamber. The shaped preform may be hot deformed in a single-blow forging operation to produce a fully densified product.

(c) Spray forming of sheet metals:

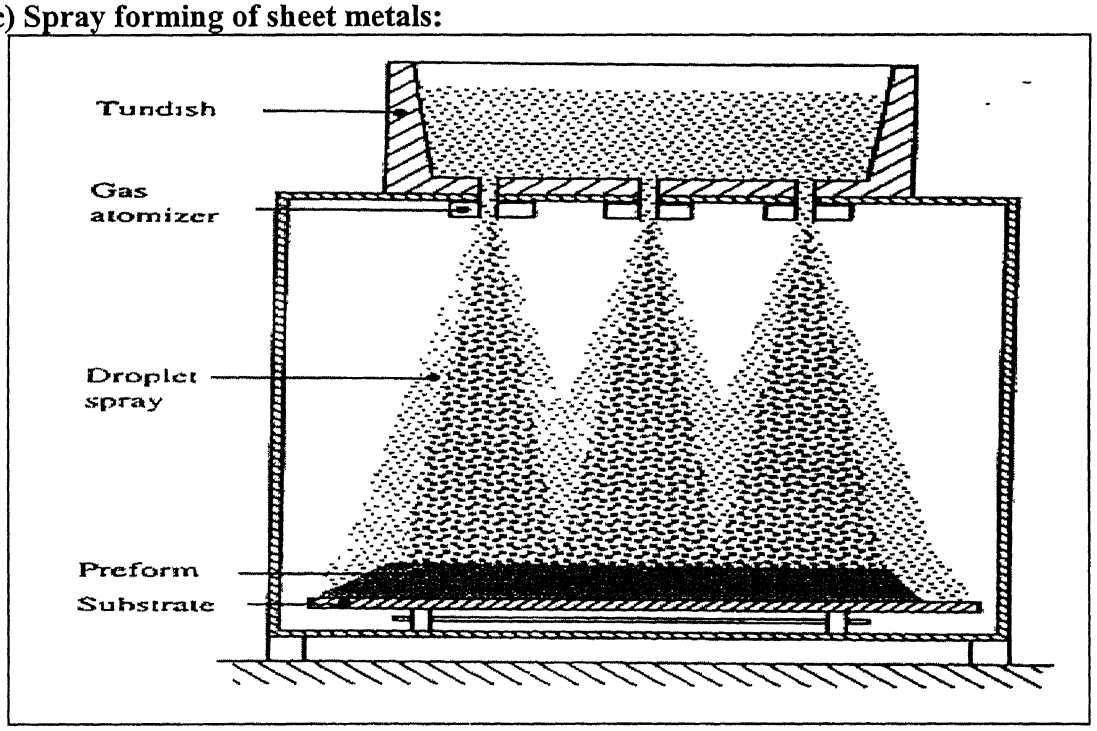

Figure 1.3.3: A multi nozzle spray deposition unit

A major problem during spray formation of sheet metals using spray-forming techniques is the formation of sheets with variable thickness. It is because the mass flux of droplets within the atomization cone produced by a conical atomizer is spatially non-uniform. In view of the limitations imposed by non-uniform mass flux, several modifications are done to improve the morphology of the spray-deposited materials, namely multi-nozzle spray deposition technique [1]. The schematic diagram of a multi-nozzle spray-deposition apparatus is shown in Fig. 1.3.3. The apparatus consists of multiple atomization nozzles and a moving substrate; all components are enclosed in a chamber. The nozzles are aligned so as to increase the width of the spray deposited preform. During spray deposition, the nozzles atomize multiple molten metal streams supplied by a tundish to produce several sprays of metallic droplets, thereby achieving a relatively uniform spray density across the width direction of the substrate. Thickness variations in the length direction of the spray-deposited materials can be controlled by altering the translation velocity of the moving substrate.

(d) Spray peening:

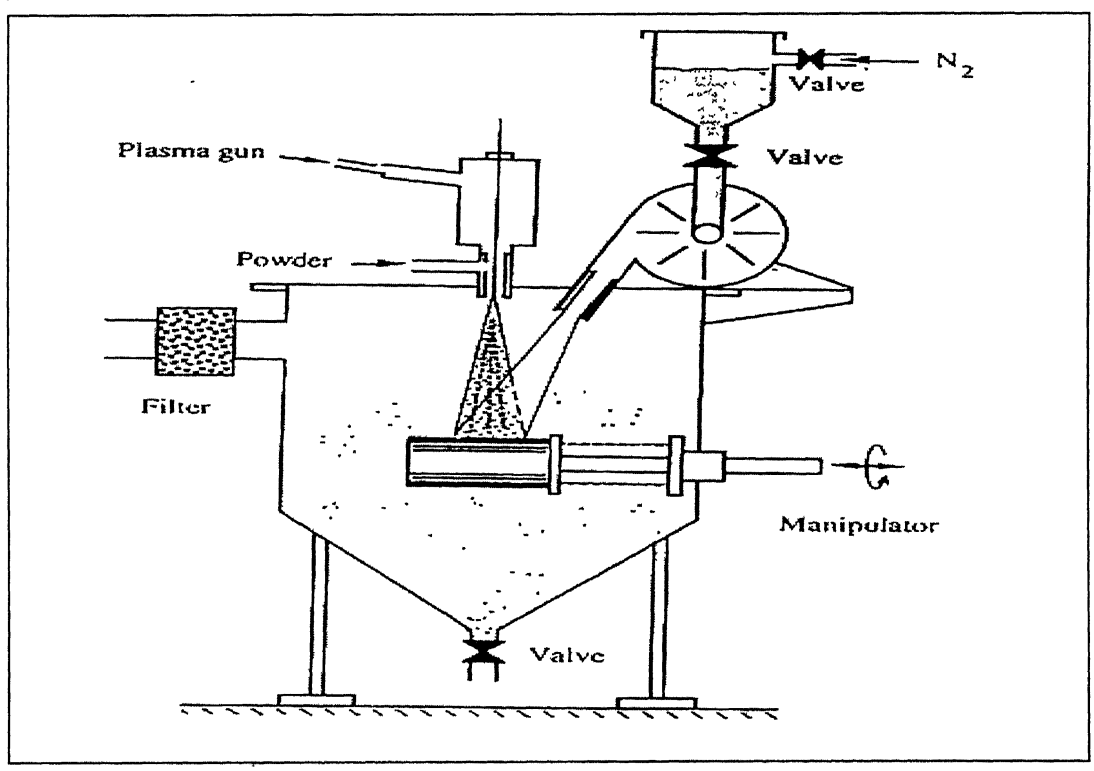

Figure 1.3.4: The principle of spray peening

The principle of spray peening is shown in Fig. 1.3.4 [6]. A typical spray-peening unit consists of a gas atomizer, a peening shot injector and a collecting substrate. In the

spray-peening process, a conical atomizer produces a spray of metallic droplets. The droplets are then directed to and deposited on the surface of a spray-deposited material, while simultaneously peening shots are directed at the deposition surface. Hence, the surface region of the spray-deposited material deforms and densifies under the continuous impact of peening shots. The spray-peening process differs from other spray-forming processes in that the droplets are consolidated simultaneously during spray deposition by the continuous bombardment of peening shots.

In principle, the advantages of spray peening are two fold. First, this process allows spray-deposited materials to achieve full density simultaneously as the deposition progress. In this case, oxidation reactions related to interconnected porosity are avoided. Second, the continuous impact of peening shots enables the materials to solidify more rapidly relative to conventional spray deposition conditions.

(e) Near-net-shape forming:

Spray deposition processing involves the production of bulk preforms from the continuous impingement and collection of solid, liquid and semiliquid droplets. Accordingly, by controlling the deposition rate and spatial distribution of droplets, it is possible to fabricate near-net-shape preforms using spray deposition. The advantages of near-net-shape spray forming are summarized as follows [1].

(i) formation of near-net-shape parts or preforms with rapidly solidified microstructures, i.e., fine grain size, very limited micro segregation and homogeneous element distribution in a macroscopic scale.

(ii) relatively high density in the as spray-deposited condition with isolated porosity levels of less than 2%.

(iii) reduced oxygen and nitrogen pick-up and ceramic inclusion contamination as compared with conventional powder metallurgy materials.

(iv) excellent forgeability

(v) improved materials utilization.

The technologies that are currently used for the production near-net-shape preforms are described below.

- **Tubular preforms**: Fig 1.3.5 schematically illustrates the principles of near-net-shape forming of tubular preforms using spray deposition processing [7] .Generally, the spray forming unit consists of a heated ladle, an atomization unit and a specially designed collection substrate. The ladle serves as a supplier of molten metal, and it is generally heated to maintain a constant temperature during spray-forming. The

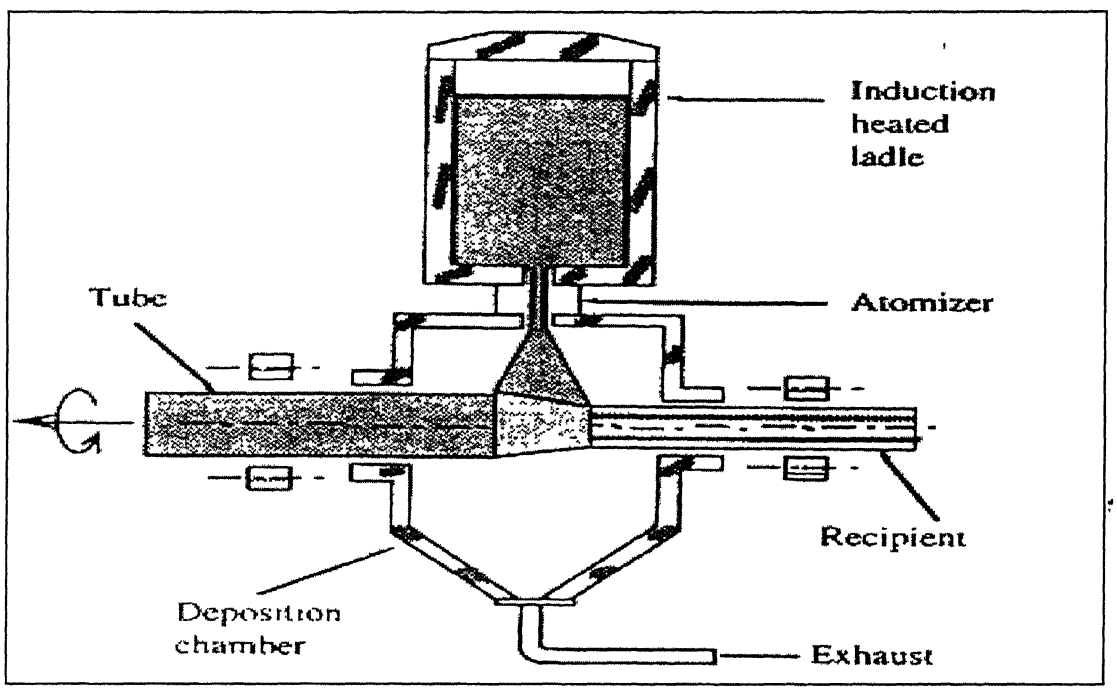

Figure 1.3.5: Spray atomization and deposition processing of tubular materials

ladle arrangement may also be used to control the mass flow rate of molten metal, for example, by controlling the pressure inside the ladle. Here, the distribution of solid, liquid and semi liquid droplets is deposited on to a cylindrical steel mandrel. During spray deposition, the substrate is rotated and translated at predetermined speeds. Accordingly, the atomized metallic droplets impinge and collect, to form a tubular preform of predetermined wall thickness. Following spray deposition, the core material of the original substrate is removed by machining. The as-spray-deposited tubing may then be directly extruded to achieve full density, final finish and desired dimensions.

- **Short rings:** Spray- deposited short rings are produced principally for gas turbine applications. The alloys that are used for the spray deposition of short rings are typically nickel-based superalloys [1]. Since these materials are heavily alloyed, an

increase in strength is generally accompanied by a decrease in hot workability. Accordingly, spray deposition of short rings of Ni-based superalloys provides the following advantages.

(i) increase in workability

(ii) decrease in material and tubing costs

(iii) elimination of several processing steps which other wise would be essential if an ingot metallurgy processing route is employed.

(iv) reduced oxygen and ceramic contamination as compared with powder metallurgy products.

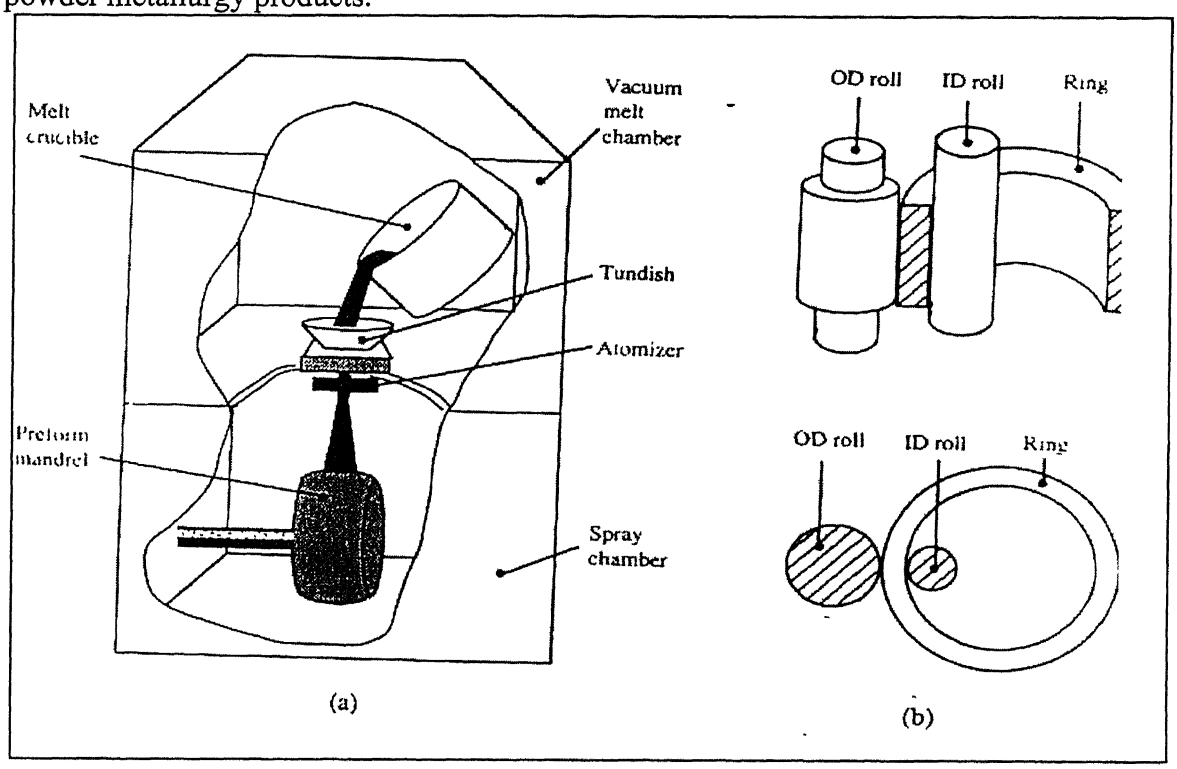

Figure 1.3.6 (a) The spray deposition of short rings (b) Ring rolling

There are two distinct spray deposition technologies, which are been presently used for production of short ring preforms. These are spray deposition and centrifugal spray deposition. There are two important differences between these two deposition techniques. First, the former method uses a gas atomizer to produce the spray of droplets where as the latter uses centrifugal atomization to produce droplets. Second, the former method uses a hollow mandrel as a collecting substrate where droplets are deposited onto

increase in strength is generally accompanied by a decrease in hot workability. Accordingly, spray deposition of short rings of Ni-based superalloys provides the following advantages.

(i) increase in workability

(ii) decrease in material and tubing costs

(iii) elimination of several processing steps which other wise would be essential if an ingot metallurgy processing route is employed.

(iv) reduced oxygen and ceramic contamination as compared with powder metallurgy products.

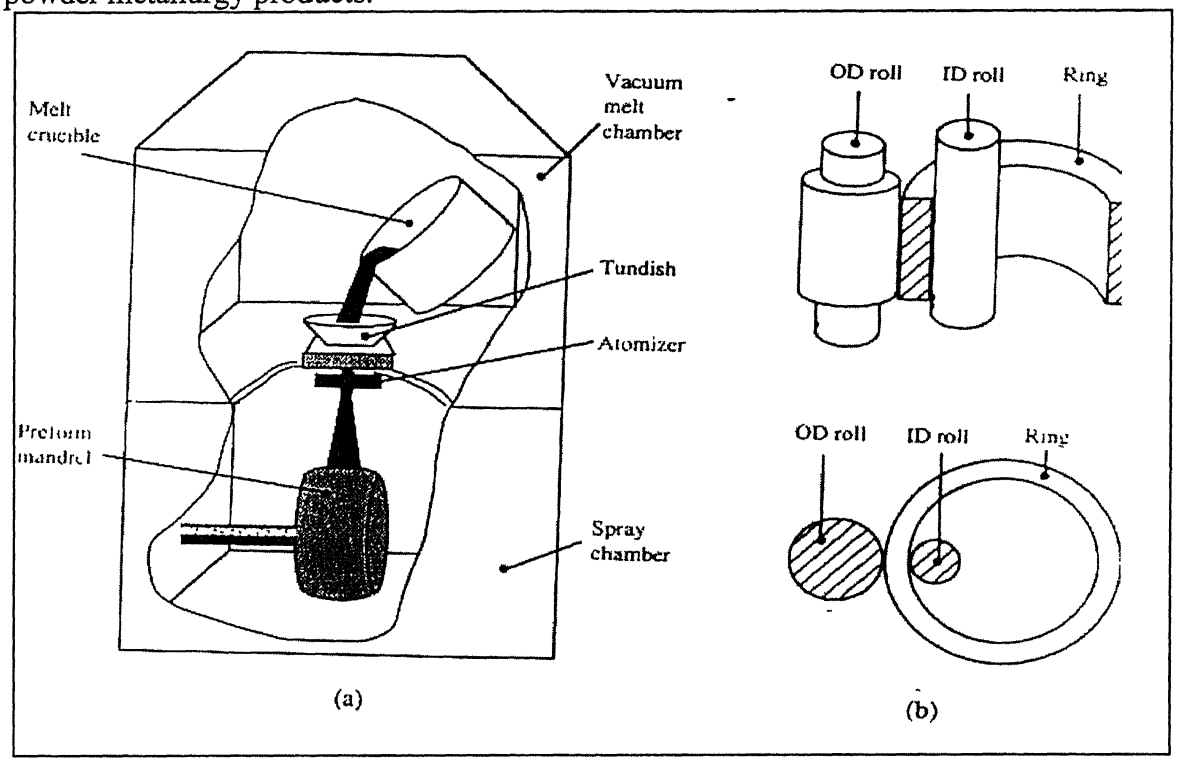

Figure 1.3.6 (a) The spray deposition of short rings (b) Ring rolling

There are two distinct spray deposition technologies, which are been presently used for production of short ring preforms. These are spray deposition and centrifugal spray deposition. There are two important differences between these two deposition techniques. First, the former method uses a gas atomizer to produce the spray of droplets where as the latter uses centrifugal atomization to produce droplets. Second, the former method uses a hollow mandrel as a collecting substrate where droplets are deposited onto

the outer surface of the mandrel, where as the latter method uses a large diameter cylindrical as a collecting substrate where droplets are deposited onto the inner surface.

In the case of fabricating short ring preforms using spray deposition, atomized droplets are deposited on a large diameter rotating mandrel. The as-spray-deposited rings are subsequently densified using hot isostatic pressing (HIP) and ring rolling operations. Fig. 1.3.6 illustrates the principle of spray deposition of short rings and the ring rolling operation following spray deposition [1]. In the centrifugal spray deposition approach, molten metal is atomized by a high speed rotating discs. Fig. 1.3.6 shows the spray-deposited rings in the hot isostatic pressed and machined condition.

- **Mill rolls:** Sumitomo Heavy Foundry and Forging Co. (Japan) introduced the spray deposition technology for mill rolls [8]. The technology is used for the processing of high speed steels. The spray deposition processing apparatus used in the production of mill rolls is similar to that used for the fabrication of tubings.

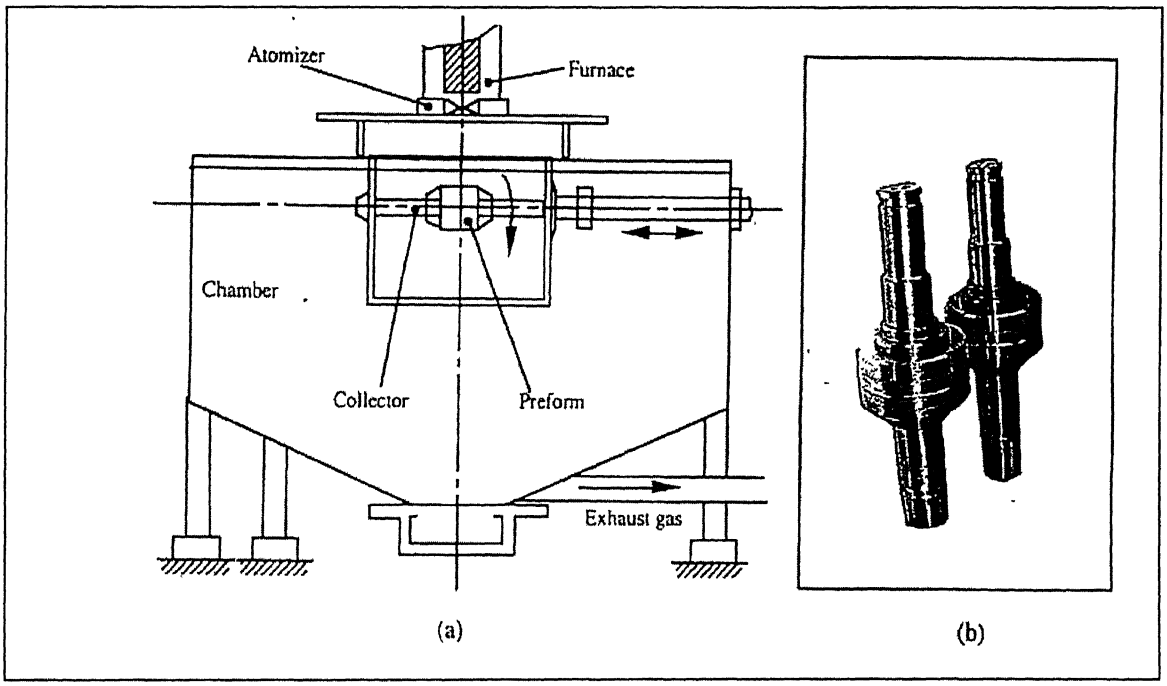

Figure 1.3.7 (a) The equipment used for spray deposition of mill rolls (b) The rolls produced

A notable difference is that, in this case the moving collector (rotating and translating under the droplet spray) utilized to collect spray-atomized droplets in a solid rod instead of a hollow cylinder. The rate of rotation and translation of the substrate is carefully controlled using a computer facility to obtain preforms of the required shape. A

schematic diagram of the unit used for the production of mill rolls is shown in Fig. 1.3.7(a). The rolls produced are shown in Fig.1.3.7 (b).

The advantages of spray deposition processing for roll production are noted as follows [1].

(i) refinement of grain size and carbide size

(ii) elimination of microsegregation

(iii) production of heavily alloyed rolls

(iv) improved hot workability and machinability

(v) uniform microstructure and mechanical properties through out roll diameter

- **Round billets and discs:** Round spray-deposited billets are currently being produced both for experimental purposes and small scale production [2].

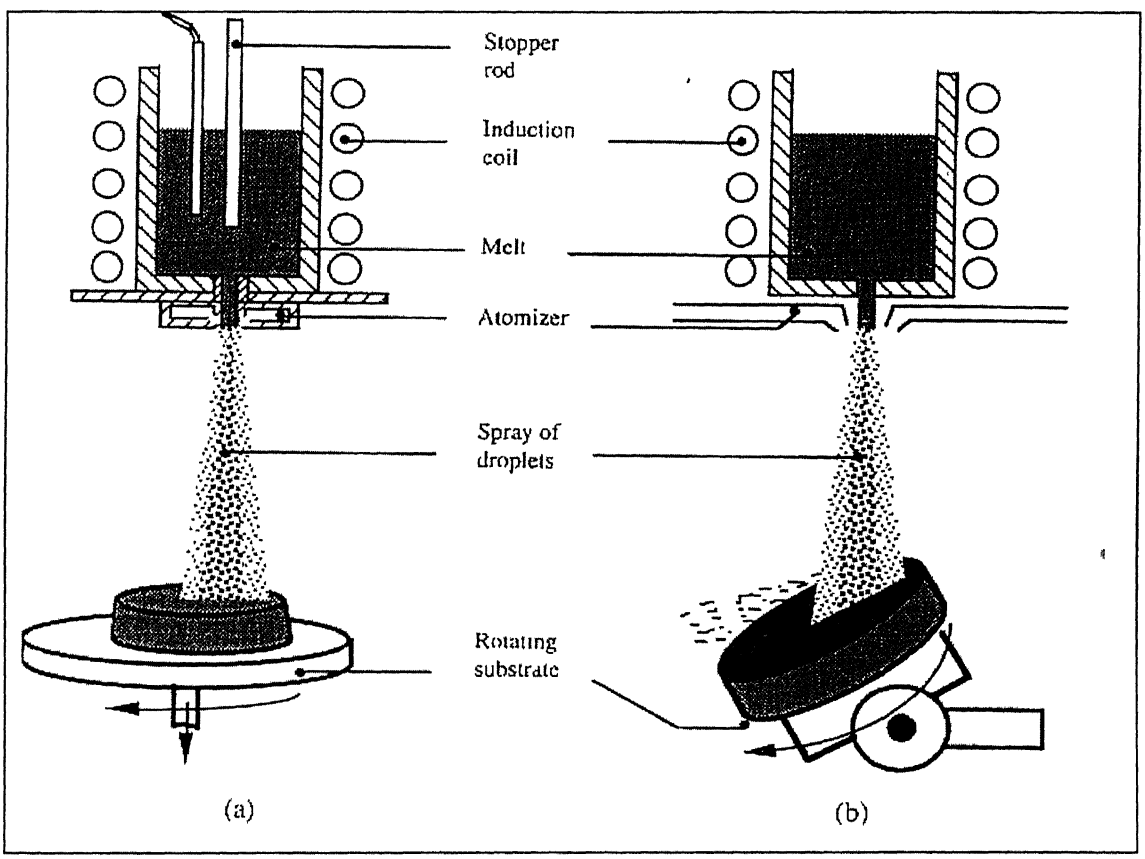

Figure 1.3.8 (a) The spray deposition of round billets using (a) horizontal substrate (b) inclined substrate

Fig. 1.3.8 illustrates schematically the two types of experimental designs that are generally used for the production of round billets through spray deposition processing [9]. Both of the spray deposition units shown in this figure employ similar atomization configurations. The basic difference is in the preform collection mechanism. For the fabrication of round billets, the substrate rotates and withdraws simultaneously under the atomized droplet spray.

The atomized droplets build up gradually on the substrate to form a long billet. In Fig. 1.3.8 (a), the substrate surface is positioned perpendicular to the centerline of the atomization cone. The substrate is off-centered, so that large diameter billets may be built up by rotating the substrate. In Fig. 1.3.8 (b), the deposition substrate surface is maintained at an angle from the centerline of the atomization cone during spray deposition. The objective of positioning the substrate at an angle is to ensure a relatively flat deposition surface and thereby achieve a relatively small variance in billet diameter. When spray-forming near-net-shape spray-deposited discs, the rotating substrate may be positioned perpendicular to the spraying direction. Hence, the dimension of the spray-deposited disc can be varied by adjusting the off-center distance of the rotating disc. Round billets can be hot isostatic pressed or extruded directly to achieve full density and improve mechanical properties. Discs can be densified by a forging or HIP operation.

1.4 OBJECTIVE:

1. To develop a model to describe the droplet dynamics and thermal history as a function of flight distance during its motion to the substrate in the surrounding atomizing gas.
2. To study the influence of different process parameters such as droplet size, initial gas velocity of the atomizing gas, melt superheat on solidification behavior of droplets.
3. To apply the model to study the solidification behavior for different metals and atomizing mediums.
4. To determine the thermal profile in the metal spray deposit.

CHAPTER 2.0 MODEL FORMULATIONS

Spray atomization and deposition is an integral process consisting of 3 steps, namely atomization, droplet flight and deposition. The droplets, which form after atomization travels a predetermined path, defined as the flight distance before impinging a substrate. The different stages have been shown in Fig 2.1.

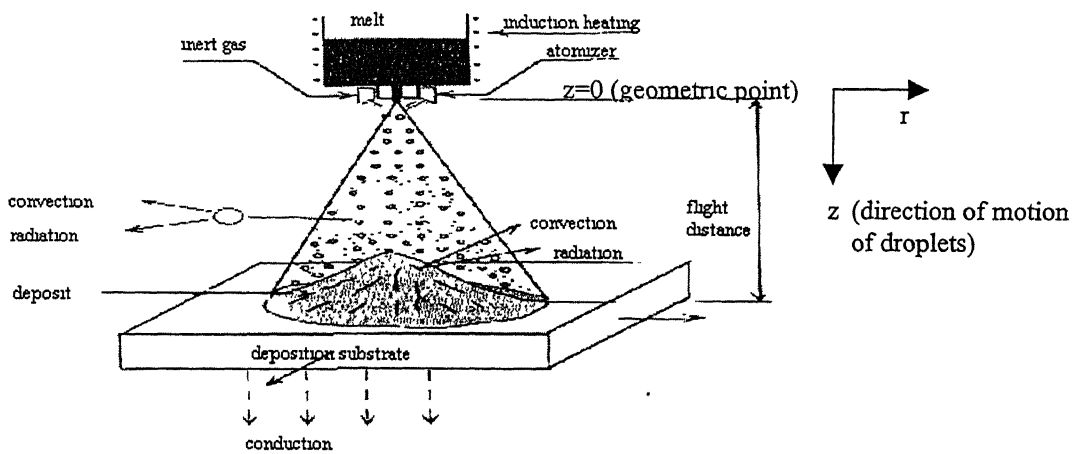

As there is a high temperature gradient exists between the molten droplets and the surrounding gas, the transfer of thermal energy occurs as soon as the droplets begin to move. As a result, the droplets start solidifying. The heat transfer and solidification events that are present during the atomization stage critically influence the microstructure formation during spray atomization and deposition. The total amount of thermal energy that can be released during spray atomization and deposition is fixed. It means that the amount of thermal energy that is dissipated during the droplet travel determines the amount of thermal energy that needs to be released during deposition. Accordingly, the thermal and solidification conditions that are experienced by the spray deposited material are intimately coupled to the heat transfer and solidification conditions of the droplets. When the amount of thermal energy extracted is inadequate, the spray that arrives at the deposition surface generally contains a higher amount of liquid phase. This condition severely limits the geometrical control of the spray-deposited material and leads to the formation of microstructures similar to that of slowly cooled materials that is coarse

grained, severely segregated etc. On the other hand, when an excessive amount of thermal energy is extracted during the droplet flight, the resultant spray-deposited material will be relatively porous and difficult to densify.

In view of this, it is necessary to optimize the extent of solidification of droplets by controlling different process parameters. The extent of solidification of droplets depends on factors such as droplet size, superheat temperature, physical properties of melt, physical properties atomization gas, velocity of droplets and gas. So, suitable models are developed to investigate the interrelation of process parameters and their effect on droplet dynamics, thermal and solidification behavior of droplets. The entire model has been classified into two parts. The first part of the model formulates the effect of process parameters on extent of solidification and temperature of droplets and the second part deals with the enthalpy of spray and thermal profile of the deposit.

2.1 MODEL FORMUALTIONS FOR THERMAL AND SOLIDIFICATION BEHAVIOR OF DROPLETS:

Suitable models are formulated to study the solid fraction and temperature of droplets during its flight downstream the geometric point. All the droplets are considered to be produced at the geometric point of the atomizer. The following assumptions are made:

2.1.1 MODEL ASSUMPTIONS:

- The droplets form instantly during atomization and the same distribution of sizes is maintained through out the motion that is there is no secondary disintegration of the droplet.
- The shapes of the droplets are spherical and there is no subsequent shape change during its motion.
- The particle-particle interaction is ignored.
- There is no chemical reaction occurring between droplets and surrounding gas.
- The motion of droplets is assumed to be along the vertical axis passing through the geometric point.
- Radial acceleration of the droplets is ignored.
- All the droplets have zero velocity at the geometric point.

- Since, the radial acceleration of the droplets is ignored, the velocity of atomizing gas is considered to be decaying downstream in the vertical direction passing through the geometric point.

  This velocity is calculated by [10].

$$V_z = 5.58\times10^{-4}\times\frac{D^{0.48}\times P^{0.96}}{F^{0.75}}\left(\frac{Z_c}{Z}\right)^n \qquad (1)$$

Where D is effective nozzle diameter, P is pressure, F is focal length, Zc is the critical distance up to which the velocity stays constant, n is gas constant, which varies with gas mediums. For Nitrogen n is 0.5313 and for Helium it is 1.636 [10].

2.1.2 VELOCITY PROFILE OF DROPLETS:

The droplet moving in the gas field exchanges its momentum and heat with the surrounding. The rate of heat exchange depends on the droplet velocity. The velocity of a droplet in the gas field is calculated by considering the following forces.

1) Gravitational Forces, F_g
2) Fluid Drag Force, F_d
3) Buoyancy Force of the Fluid, F_b

The direction of forces acting on a droplet has been shown in Fig. 2.1.1 below.

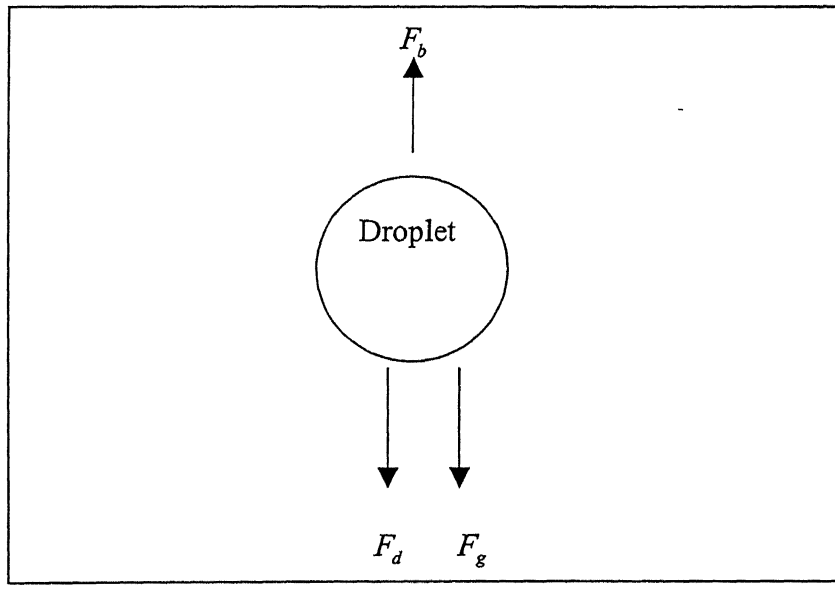

Fig.2.1.1: Forces acting on a droplet

1) Gravitational Force (F_g):

This is expressed as

$$F_g = m_d g \tag{2}$$

$$F_g = \rho_l \frac{\pi}{6} d^3 g \tag{3}$$

Where g acceleration due to gravity, m_d is mass of the droplet.

2) Fluid Drag Force (F_d):

The drag force acting on a spherical body moving in a fluid was discussed by Szekely [11]. The drag force depends on the relative velocity between the gas and the droplet. According to Szekely, the drag force can be calculated from

$$F_d = \frac{A}{2} C_{drag} \rho_g (V_z - V_d) \left| (V_z - V_d) \right| \tag{4}$$

Where A is projected area of the droplet on a plane perpendicular to its motion, C_{drag} is fluid drag coefficient, ρ_g density of gas. This drag force acts in the same direction as the gravitational force, until the gas velocity remains higher than the velocity of droplet and changes its sign when it becomes lower at later stages of flight. The drag coefficient C_{drag} is a function of Reynolds number and is given by [11].

$$C_{drag} = 0.28 + \frac{6}{R_e^{0.5}} + \frac{21}{R_e} \tag{5}$$

This expression is applicable within ranges $0.1 < R_e < 4000$. But in the present study, R_e falls into a wider range i.e. 5 to 8000. Therefore, an improved expression for C_{drag}, As a function of R_e is used [12].

$$C_{drag} = \begin{Bmatrix} \frac{24}{R_e}, 0 < R_e < 1 \\ \frac{24}{R_e^{0.646}}, 1 <= R_e < 400 \\ 0.5, 400 <= R_e < 3\times10^5 \end{Bmatrix} \quad (6)$$

3. Buoyant Force (F_b):

The buoyant force acts in a direction that opposes the motion of a droplet that may be expressed as

$$F_b = \rho_g V g \quad (7)$$

Making a force balance on the droplet the resulting equation is given by

$$m_d a = m_d g + \frac{A}{2} C_{drag} \rho_g (V_z - V_d)|(V_z - V_d)| - \rho_g g V$$

Rearranging the terms;

$$\frac{dV_d}{dt} = \left(1 - \frac{\rho_g}{\rho_l}\right) g + \frac{3}{4} \frac{C_{drag} \rho_g}{d\rho_l} (V_z - V_d)|(V_z - V_d)| \quad (8)$$

Equation –8 is solved for velocity for droplet, along with equations (1) and (6) for gas velocity and drag coefficient.

2.1.4 FORMULATION OF HEAT TRANSFER COEFFICIENT:

The heat transfer between the heated droplet and the surrounding gas is governed by the heat transfer coefficient, which is essential for determining temperature of the droplet. In this case a heat transfer coefficient is required for spherical droplets moving in a flowing gas. In the literature, several empirical correlations are found for a fluid flowing past a sphere. Ranz-Marshall proposed a correlation for heat transfer coefficient for a fluid flowing past a sphere [11]. The correlation is given by

$$Nu = 2 + 0.6\ \mathrm{Re}^{\frac{1}{2}}\ \mathrm{Pr}^{\frac{1}{3}} \quad (9)$$

In equation (9), Nu represents the Nusselt number, which is defined as the ratio of thermal conductance of the droplet/gas interface to that of the atomization gas. It can be shown as

$$Nu = \frac{h_c d}{k_g} \tag{10}$$

Where h_c is heat transfer coefficient, d is droplet diameter and k_g is thermal conductivity of gas. Re represents the Reynolds number. It is defined as the ratio of kinetic forces to viscous forces and can be shown as

$$R_e = \frac{\rho_g |(V_z - V_d)| d}{\mu_g} \tag{11}$$

Pr represents the Prandtl Number that is the ratio of kinematic viscosity to thermal diffusivity. It is represented as

$$P_r = \frac{C_{pg} \mu_g}{k_g} \tag{12}$$

In the present study, equation (13) is used to determine the heat transfer coefficient. Replacing (10)-(12) in equation (9), the final form for heat transfer can be rewritten as

$$h_c = \frac{k_g}{d}\left[2.0 + 0.6\left(\frac{\rho_g |(V_z - V_d)| d}{\mu_g}\right)^{\frac{1}{2}}\left(\frac{C_{pg}\mu_g}{k_g}\right)^{\frac{1}{3}}\right] \tag{13}$$

2.1.3 DETERMINATION OF TEMPERATURE:

The superheated droplet during its motion cool off by losing its heat to surrounding gas by convection and radiation. It is observed that the Biot No. is less than 0.01 for all droplets, which size less than 350 micron in nitrogen medium. So, the temperature gradient across a droplet diameter can be safely neglected. This type of thermal condition is known as Newtonian cooling condition. In Newtonian cooling condition, it is assumed that heat extraction from a droplet is governed by heat convection at the surface [1] and the droplet temperature remains uniform across the diameter. To determine the temperature of a droplet during its flight a thermal energy

balance may be carried out on it. The amount of heat extracted by the gas results in the decrease of enthalpy of the droplet. If the droplet is solidifying, the latent heat also has to be taken into consideration. An energy balance leads to the following equation.

$$V\left(\rho_{sl}C_{psl}\frac{dT}{dt}-\rho_s H_f\frac{df_s}{dt}\right)=-h_c A_d\left(T-T_g\right) \qquad (14)$$

The solidification of pure metal droplets doesn't occur till the droplets are undercooled and arrive at the nucleation temperature. So, up to the nucleation temperature there will be no latent heat of evolution. Hence $\frac{df_s}{dt}$=0. So, the equation (14) can be transformed as

$$V\rho_l C_{pl}\frac{dT}{dt}=-h_c A_d\left(T-T_g\right) \qquad (15)$$

Where ρ_l density of liquid droplet, C_{pl} is specific heat for a pure metal in the liquid state. Equation-(15) can be used to determine the temperature in liquid state. In this equation $T=T_s$ at $t=0$ and $T=T_N$ at $t=t_N$. After nucleation takes place, the growth of the solid phase takes place, which leads to the rapid increase of the temperature, this phenomenon is known as recalescence. The formulation for nucleation temperature and recalescence temperature has been described below.

2.1.3.1 NUCLEATION TEMPERATURE AND RECALESCENCE TEMPERATURE DETERMINATION:

- **Nucleation Temperature Formulation:**

In spray atomization process, the droplet exchanges thermal energy with the atomization environment. The cooling rate involved during the process is very high, so the solidification doesn't start immediately at melting point, rather at a temperature below melting point. This temperature is known as the nucleation temperature, at which one solid nucleus successfully forms from liquid. In rapid solidification processing, the nucleation rate is a function of time until it increases to stay at a constant value, which is known as steady state nucleation rate. The general expression for steady state nucleation rate is [13]

$$I_s=f_0 C_0\exp\left(-\frac{\Delta G_c}{KT}\right) \qquad (16)$$

Where I_s is steady state nucleation rate, f_0 is atom attaching frequency, C_0 is number of atoms per unit volume, ΔG_C is the critical free energy require for nucleation, K is Boltzman's constant. f_0 can be expressed as

$$f_0 = \frac{D_0}{\lambda^2 \alpha}. \tag{17}$$

Where D_0 is self-diffusion coefficient of Aluminum in liquid. λ Is jump distance for f.c.c. crystal i.e $\frac{a_0}{\sqrt{2}}$, a_0 is lattice parameter. ΔG_C is expressed as

$$\Delta G_c = \frac{16\pi \ \sigma_{sl}^{\ 3} T_m^{\ 2} \Omega^2}{3 H_{fm}^{\ 2} \ (T_m - T)^2} \tag{18}$$

σ_{Sl} is the solid liquid interfacial energy, T_m is the melting point, Ω is molar volume and H_{fm} is molar heat of fusion. Solid-liquid interfacial energy σ_l is calculated from [14]

$$\sigma_l = \left(\frac{Z - Z_s}{Z}\right)\left(\frac{H_{fm}}{A_s}\right) + \left(\frac{\rho_s}{\rho_l}\right)^{\frac{2}{3}} (\gamma_{lv})_m \tag{19}$$

Where $\frac{Z - Z_s}{Z} \cong 0.25$ for f.c.c metals and $\cong 0.36$ for b c.c metals A_S is given by molar solid surface area expressed as

$$A_s = 1.12 N^{\frac{1}{3}} \left(\frac{M}{\rho_s}\right)^{\frac{2}{3}} \tag{20}$$

Where N is Avogadro's number, M is molecular weight, $(\gamma_{lv})_m$ and is interfacial tension of liquid metal. Time dependant nucleation rate can be calculated from [15]

$$I_t = I_s \exp\left(-\frac{\tau}{t}\right) \tag{21}$$

Where I_t transient nucleation rate, τ is incubation period. τ can be calculated from [9]

$$\tau = \frac{16 \ KT \ \sigma_{sl} a_0^{\ 4}}{D \left(V_m^{\beta 2}\right)(\Delta G_v)^2} \tag{22}$$

Where V_m^{β} is given by volume per atom, ΔG_V is volume free energy calculated as

$$\Delta G_v = \frac{H_{fv}(T_m - T)}{T_m} \tag{23}$$

Where H_{fv} latent heat of fusion per unit volume. H_{fv} and H_{fm} are related as follows.

$H_{fv} = 3.305 \times 10^5 H_{fm}$ for Aluminium.

$H_{fv} = 1.407 \times 10^5 H_{fm}$ for Copper.

The transient nucleation rate can be rewritten by substituting equations (16)-(20) and (22)-(23) in equation –(21). It is given by

$$It = f_0 C_0 \exp\left(-\frac{16\pi\sigma_{sl}^3 T_m^2 \Omega^2}{3H_{fm}^2 (T_m - T)^2 KT}\right) \exp\left(-\frac{16KT\sigma_{sl} a_0^4 T_m^2}{D_o V_m^{\beta^2} H_{fv}^2 (T_m - T)^2 t}\right) \tag{24}$$

The number of nuclei forming during nucleation can be obtained from an integration of the nucleation rate over the temperature regime between the melting point and nucleation temperatures for a continuous cooling process.

$$N = V \int_{T_m}^{T_N} \frac{I_t}{\left(\frac{dT}{dt}\right)} dT \tag{25}$$

Where N is the number of nuclei, T_N is the nucleation temperature, $\frac{dT}{dt}$ is the cooling rate, V is the volume of liquid droplet. At the nucleation temperature at least one nucleus has formed from the liquid. So, equation (25) can be rewritten as

$$V \int_{T_m}^{T_N} \frac{I_t}{\left(\frac{dT}{dt}\right)} dT = 1 \tag{26}$$

- **Recalescence temperature formulation**

Nucleation is followed by the growth of solid phases. The latent heat of solidification thus released is dissipated into the under cooled liquid that is at a lower temperature. At the same time heat is being removed from the surface of the droplet into the atomization environment. So, the droplet experiences two competing processes. One is heating effect due to the evolution of latent heat where as the other one is cooling effect due to the extraction of heat by the gas. But in an under cooled droplet the solidification rate is very

high. So, the rate of thermal energy release from the liquid-solid interface into the under cooled liquid is much faster than the rate of thermal energy dissipation from the droplet surface into the environment. So, the temperature of the droplet increases, which is termed as recalescence. This recalescence stops when rate of heat extraction becomes equal to the rate of evolution of lateen heat. The fraction of droplet that is solidified after the recalescence and the recalescence temperature plays an important role in subsequent thermal behavior of droplet. So it is essential to determine the recalescence temperature and fraction solidified after recalesence.

The rate of growth of solid phase in slow to moderate under cooled droplet can be calculated by [16]

$$\frac{df}{dt} = \frac{R_i \Delta T}{d} \tag{27}$$

Where $\frac{df}{dt}$ is the rate of growth of solid phase, R_i is interfacial velocity, ΔT is under cooling i.e. $(T_m - T)$ and d is the droplet diameter. In a continuous growth, the rate of crystal growth, R_i can be calculated from [17]

$$R_i = \frac{\beta D H_{fm} (T_m - T)}{a_0 R T_m^2} \tag{28}$$

In the expression β is a dimensionless parameter, which is of the order of 1-100 for diffusion-limited process. $R_i = K_m \Delta T$. This equation implies the interfacial velocity may be approximated as a linear function of undercooling and K_m is linear interface kinetic coefficient. Levi and Mehrabian proposed a lower bound value for K_m when β =1. Therefore, the value of β is taken as 1 in the present study. R is universal gas constant. Substituting Ri in equation-(27), the resulting equation is given by

$$\frac{df}{dt} = \beta \frac{D_0 H_{fm} (T_m - T)^2}{a_0 R d T_m^2} \tag{29}$$

Rate of evolution of latent heat is given by

$$H_1 = H_f \rho_s V \beta \frac{D_0 H_{fm} (T_m - T)^2}{a_0 R d T_m^2} \tag{30}$$

Rate of thermal heat removal from droplet surface

$$H_2 = h_c A_d (T - T_g) \tag{31}$$

The fraction solidified during recalescence period is determined by

$$H_f f = (T - T_N)\left[C_{pl}(1-f) + C_{ps} f\right] \tag{32}$$

For a given value of T rate of evolution of latent heat from equation (30) is compared with rate of heat extraction from equation- (31). At the same T, f is calculated from equation- (32). When $H_1 = H_2$, $T = T_R$ and accordingly from equation- (32), $f_r = f$.

After recalescence the droplet stays in a thermal equilibrium because the rate of extraction of heat by the surrounding gas is equal to the rate of evolution of latent heat by solidification. So, the temperature of the droplet doesn't change with time and stays constant at melting point. So, $\frac{dT}{dt}$=0. Replacing this in equation (14), an expression for solidification rate of a droplet of pure metal can be found out. It can be shown as

$$V\rho_s H_f \frac{df_s}{dt} = h_c A_d (T_m - T_g) \tag{33}$$

After the droplet completely solidifies, the variation of temperature of the droplet with time can be found out from replacing the physical properties of the metal in the solid state and substituting $\frac{df_s}{dt} = 0$ in equation-14. It is given by

$$V\rho_s C_{ps} \frac{dT}{dt} = -h_c A_d (T - T_g) \tag{34}$$

2.1.5 FORMULATIONS FOR THERMAL PROFILE OF THE DEPOSIT AND SUBSTRATE

2.2.1 FORMULATION OF DROPLET SIZE DISTRIBUTION:

Several empirical correlations are available to determine the mean droplet diameter. The correlation used in this model is [16]

$$\frac{d_m}{D_{nl}} = K\left[\frac{\upsilon_l \sigma_l}{\upsilon_g D_{nl} \rho_g V_g^2}\left(1+\frac{m_l}{m_g}\right)\right]^{0.5} \tag{35}$$

Where d_m is the mean droplet diameter, D_{nl} is effective nozzle diameter, K is proportionality constant, υ_l is the kinematic viscosity of liquid, υ_g is kinematic viscosity of gas, V_g is the velocity of gas at geometric point, m_l is the mass flow rate and m_g is given by gas flow rate. σ_l is melt surface tension.

$$m_l = 2A_t\, \rho_l\, C_d (2.0\, g\, H_c)^{\frac{1}{2}} \tag{36}$$

m_g can be calculated from [17]

$$m_g = C_d\, A_t \left[\gamma\, \rho_g\, p_0 \left(\frac{2.0}{\gamma+1}\right)^{\left(\gamma+\frac{1}{\gamma}-1\right)}\right]^{\frac{1}{2}} \tag{37}$$

Where C_d is the discharge coefficient, A_t is area of gas nozzle, p_0 is plenum pressure of atomizing gas, γ is $\frac{C_p}{C_v}$ for atomizing gas, H_c is height of molten metal in the container.

The powder yield in different size range is given by the log-normal distribution function [18]

$$\frac{dw}{dd} = \frac{1}{\sqrt{2\pi}\; d \ln\sigma_g} \exp\left[-\left(\frac{\ln d - \ln d_{mm}}{\sqrt{2}\ln\sigma_g}\right)^2\right] \tag{38}$$

The powder yield in different size range depends on d_{mm} and the geometric standard deviation σ_g.

2.2.2 ENTHALPY OF SPRAY:

The spray contains droplets of various sizes and mass fraction in each size class varies with the log-normal distribution function. In order to calculate the enthalpy of spray, the enthalpy of each size class is needed, which can be found out in this manner.

$$H_{spray} = \sum_i f(d_i) H(d_i) \qquad (39)$$

Where $f(d_i)$ is the mass fraction of each size class and $H(d_i)$ is the enthalpy of each size class.

2.2.3 SOLID FRACTION CONTENT IN SPRAY:

The fraction solid and liquid in the spray can be calculated by calculating the fraction of solid contained in the droplets of each size class multiplied with the mass fraction of that size class.

$$f_s = \sum_i f_s(d_i) f(d_i) \qquad (40)$$

Where $f_s(d_i)$ is the fraction solid present in each size class, f_s is solid fraction of the spray.

2.2.4 FORMULATION FOR TEMPERATURE PROFILE OF DEPOSIT:

During deposition, the spray is allowed to fall on a substrate, which stays at a much lower temperature. Therefore, the heat gets transferred by conduction through the bottom and also some amount of heat gets convected out from the top of the deposit by the atomizing gas. So, during deposition there is a redistribution of energy occurs in the deposit and hence the temperature profile of the deposit changes with time.

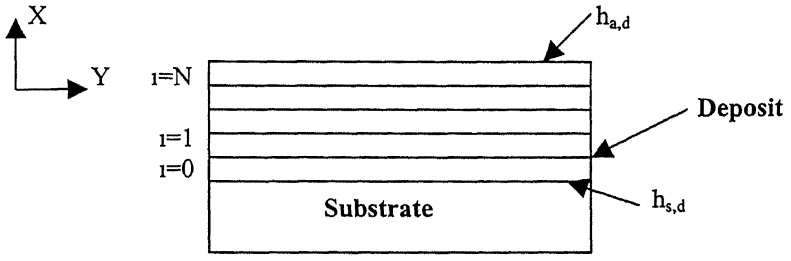

Fig.2.2.4.1: Grid pattern for deposit

Certain assumptions are made in order to determine the thermal profile.

1. Rectangular coordinates are used to determine the temperature profile.

2. The heat conduction is assumed to be significant in the direction of growth of deposit, which is in X-direction as shown in the above figure. So, temperature gradient occurs in the X-direction only.

3. At each time step, a new layer is added. During each time step, the latent heat present in the liquid portion of the spray is assumed to be conducted out through the deposit, so the temperature of the top layer stays at the melting point during each time step.

The governing one-dimensional conduction heat transfer equation is found to be

$$\frac{\partial T}{\partial t} = \left(\frac{k_s}{\rho_s C_{ps}} \right) \frac{\partial^2 T}{\partial x^2} \qquad (41)$$

Where, k_s is the thermal conductivity in the solid state.

With Initial Condition:

$$T[\imath] = T_0$$

Boundary condition at substrate/deposit interface

$$-k_s \frac{\partial T}{\partial x} = h_{s,d}(T - T_s) \qquad (42)$$

Where $h_{s,d}$ is the heat transfer coefficient between deposit and substrate interface and T_s is the temperature of the top of the substrate.

Boundary condition at deposit-gas interface at top

$$-k_s \frac{\partial T}{\partial x} = h_{a\,d}(T - T_g) \tag{43}$$

Where $h_{a,d}$ is the heat transfer coefficient between top of the deposit and the atomizing gas.

2.2.5 FORMULATION OF TEMPERATURE PROFILE OF THE SUBSTRATE:

The temperature of the substrate during deposition changes due to the heat flux that comes from the top of the deposit. The transient temperature profile of the substrate significantly affects the heat transfer rate from the deposit. So, it is needed to determine the temperature profile of the substrate at each time interval along with the temperature profile of the deposit. The assumptions made for calculation is given below.

1. Significant amount of heat transfer takes place in the vertical direction, so the temperature gradient occurs in the X-direction as shown in the figure. Temperature variations in the other directions are neglected.

The governing conduction equation is formulated to be

$$\frac{\partial T}{\partial t} = \left(\frac{k_{sub}}{\rho_{sub}\, C_{psub}} \right) \frac{\partial^2 T}{\partial x^2} \tag{44}$$

with Initial condition $T[t] = T_{0,s}$

Boundary Condition at deposit and substrate interface

$$k_{sub} \frac{\partial T}{\partial x} = h_{d,s}(T - T_d) \tag{45}$$

Boundary condition substrate and gas interface

$$-k_{sub} \frac{\partial T}{\partial x} = h_{a,s}(T - T_g) \tag{46}$$

CHAPTER 3 METHOD OF CALCULATION

3.1 SINGLE DROPLET SOLIDIFICATION:

A computer program is developed for calculation of temperature and fraction solid as a function of flight distance. The flow chart for the program is shown in Fig. 3.1.

The program takes physical properties of gas and metal, physical constants as input data. It reads maximum distance, minimum droplet size and distance step. In the program the maximum distance is taken as 1m and the distance step is 0.0001m.

At geometric point, that is at X=0; the gas velocity is initialized to $V_{g,0}$, the droplet velocity is initialized to zero, the temperature of the droplet is the superheat temperature and the calculations are carried out for a single droplet of fixed size.

At a next distance step, i. e. X=X+ΔX, the velocity of gas is calculated from equation-(1). The droplet velocity is calculated from equation- (8). The Euler's numerical scheme[19] is used for the initial distance step, i.e. for i=1. The equation-(8) can be shown as

$$V_d[i] = V_d[i-1] + dt \times \left(1 - \frac{\rho_g}{\rho_l}\right) g + \frac{3}{4} \frac{C_{drag} \rho_g}{d \rho_l} \left(V_z[i-1] - V_d[i-1] \times \left|\left(V_z[i-1] \times V_d[i-1]\right)\right|\right)$$

For distance steps greater than i=1, the velocity of droplet is calculated by solving the same equation using Adams-Bash forth second order technique [19] for better accuracy. It can be shown as

$$V_d[i] = V_d[i-1] + \frac{dt}{2.0} \times \left(3.0 \times \left(1 - \frac{\rho_g}{\rho_l}\right) g + \frac{3}{4} \frac{C_{drag} \rho_g}{d \rho_l} \left(V_z[i-1] - V_d[i-1]\right) \times \left|\left(V_z[i-1] - V_d[i-1]\right)\right|\right)$$

$$- \frac{dt}{2.0} \times \left(\left(1 - \frac{\rho_g}{\rho_l}\right) g + \frac{3}{4} \frac{C_{drag} \rho_g}{d \rho_l} \left(V_z[i-2] - V_d[i-2]\right) \times \left|\left(V_z[i-2] - V_d[i-2]\right)\right|\right)$$

During calculation of droplet velocity from the above expression, gas velocity drag co-efficient is calculated and substituted in the expression.

FLOW CHART:

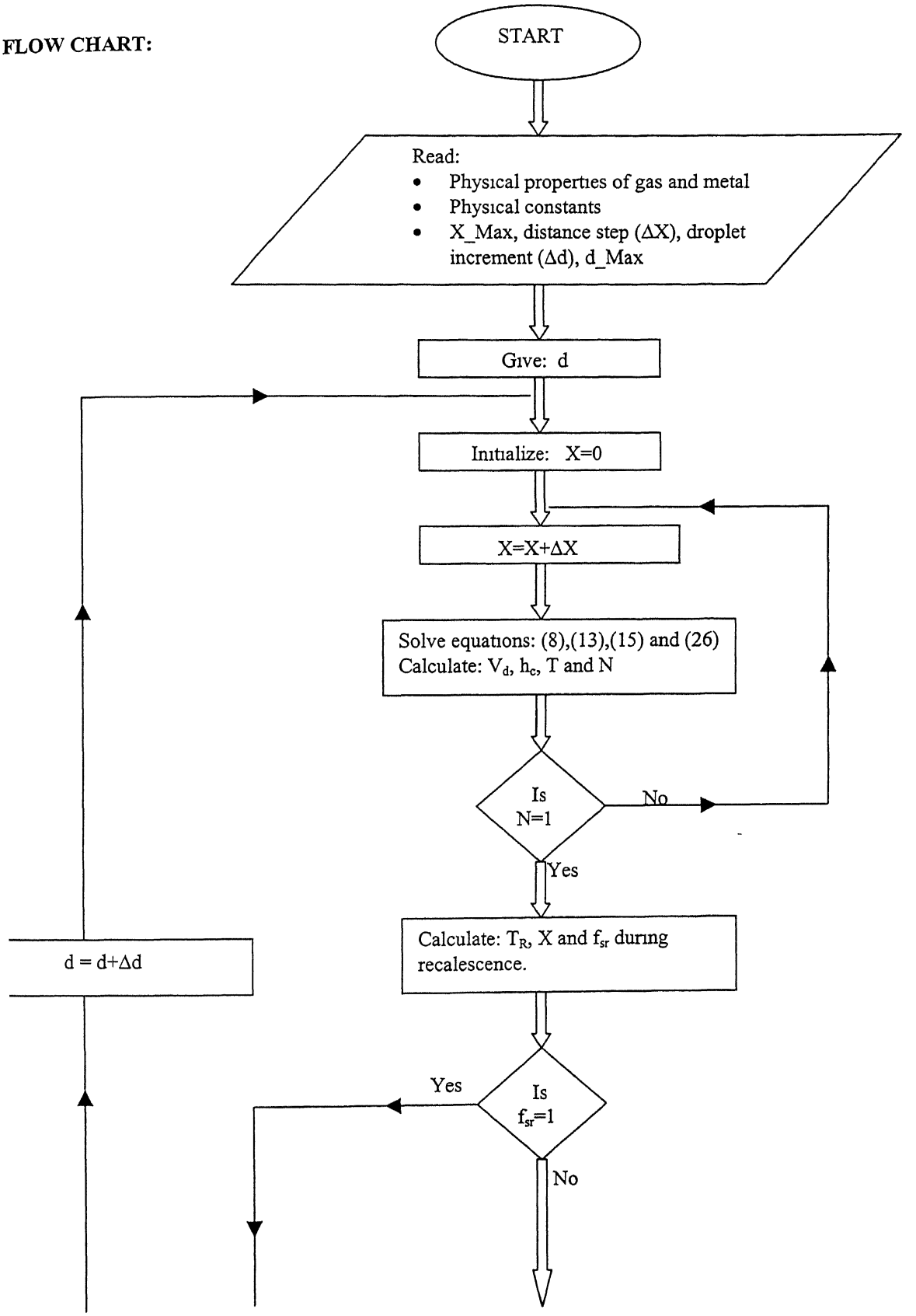
START
Read:
• Physical properties of gas and metal
• Physical constants
• X_Max, distance step (ΔX), droplet increment (Δd), d_Max
Give: d
Initialize: X=0
X=X+ΔX
Solve equations: (8),(13),(15) and (26)
Calculate: V_d, h_c, T and N
Is N=1
No
Yes
Calculate: T_R, X and f_{sr} during recalescence.
Is f_{sr}=1
Yes
No
d = d+Δd

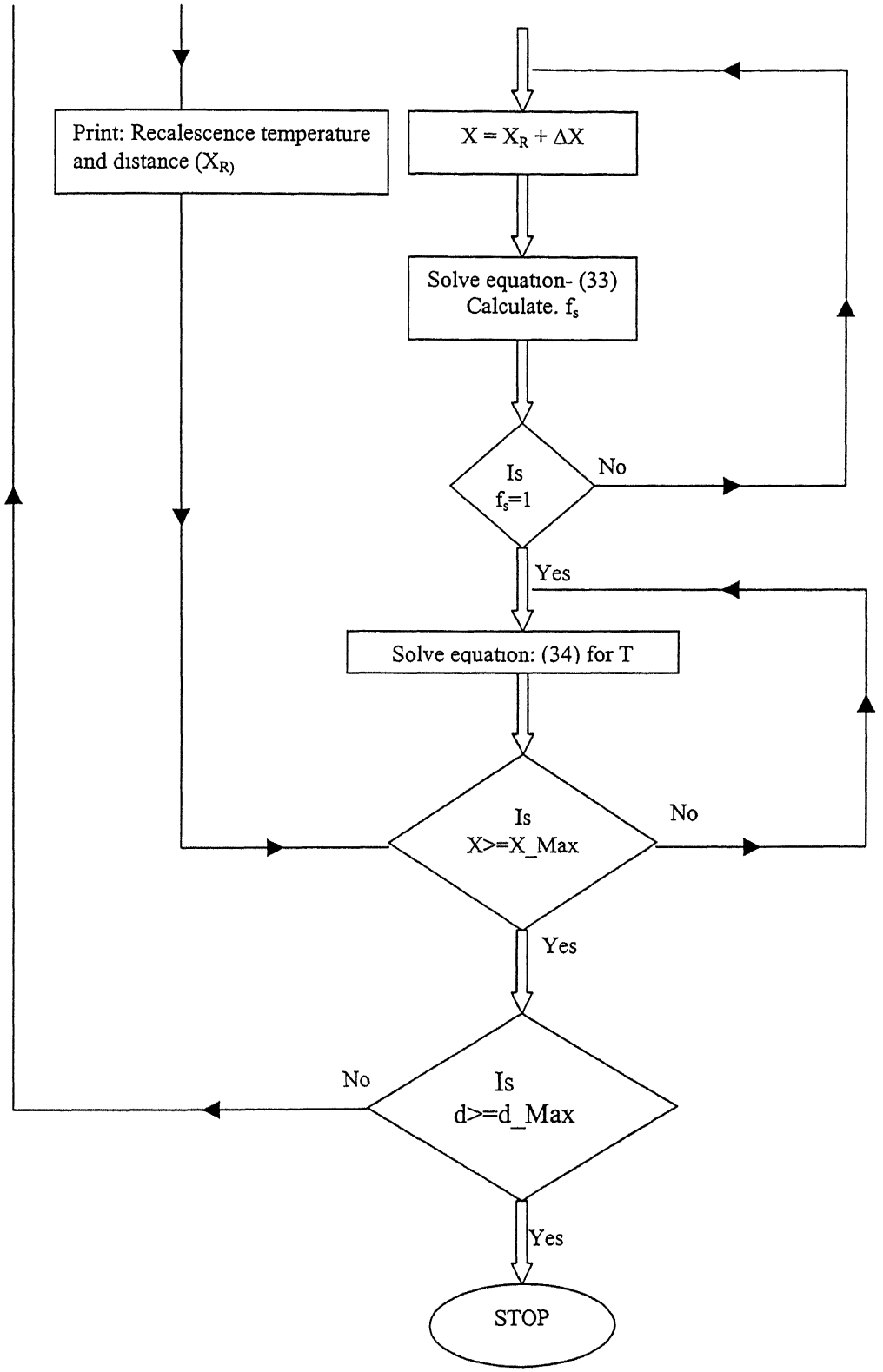

Fig. 3.1: Flow chart for the computer program generated.

After calculating velocity, heat transfer co-efficient is calculated and substituted in equation, in which the droplet velocity and gas velocity is substituted in all distance steps.

After that, the temperature of the droplet is calculated from the equation (15). Similarly to solve it, Euler's numerical scheme is used, for the first distance step (i=1); it is calculated from;

$$T[i] = T[i-1] + dt \times \left(-\frac{6.0 \times h_c[i-1]}{d \times \rho_l \times C_{pl}} \left(T[i-1] - T_g \right) \right)$$

For subsequent distance steps (i>1), it is calculated using a more accurate method, that is

$$T[i] = T[i-1] + \frac{dt}{2.0} \left(\left(3.0 \times \left(\frac{-6.0 \times h_c[i-1] \times \left(T[i-1] - T_g \right)}{d \times \rho_l \times C_{pl}} \right) - \left(-\frac{6.0 \times h_c[i-2] \times \left(T[i-2] - T_g \right)}{d \times \rho_l \times C_{pl}} \right) \right) \right)$$

When the temperature of the droplet goes below melting point, nucleus number is calculated. In order to calculate nucleus number, numerical integration of the equation is carried out. The transient nucleation rate I_t is calculated from equation- (24). For a very small time step Δt, there is a linear relationship between nucleation time and nucleation rate. During the time step Δt, temperature changes from T_1 to T_2. So if the nucleation rate is I_{t1} at T_1 and t_1, after a short time period Δt, the nucleation rate increases to $I_1(t+\Delta t)$ and the increase in nucleation density equals to ΔN_1. As the time goes up from t_1 to $(t_1+\Delta t)$ the temperature changes continuously from T_1 to T_2. So the nucleation rate must be in between I_1 and I_2 and the increase in nucleation density is between ΔN_1 and ΔN_2. In order to simplify the calculation, mathematics average is used to represent the variations of nucleation rate I at $(t+\Delta t)$ is derived to be

$$I(t + \Delta t) = I(t_1) + \left(\frac{I_1 + I_2}{2.0} \right) \Delta t$$

and the increase in nucleus density from t to $t+\Delta t$ is

$$\Delta N|_{t+\Delta t} = I(t_1)\Delta t + \left(\frac{I_1 + I_2}{4.0}\right)\Delta t^2$$

Total number of nucleus forming is the summation of increase in nucleus density in each time step Δt times the droplet volume:

$$\sum_{t_l=t_0}^{t} \Delta NV = \pi \frac{d^3}{6} \sum \Delta N_{tl}$$

The temperature, at which the nucleus appeared, is referred as nucleation temperature.

After nucleation takes place, the fraction solidified at the end of recalescence, temperature and distance covered during recalescence is calculated. In order to calculate recalescence temperature and fraction solidified at the end of recalescence, equation (27) to (32) is used.

From equation- (30) rate of evolution of latent heat is calculated. From equation - (31) rate of extraction of heat by atomizing gas is calculated and is compared with rate of evolution of latent heat. As the rate of evolution of latent heat is much higher than that of extraction by gas, the temperature rises rapidly. Assuming a linear increase, temperature is increased by a small step and the rate of evolution of latent heat and the extraction of heat is compared at all steps. The recalescence temperature is that temperature when rate of evolution of latent heat becomes equal to the rate of heat extraction by gas. Fraction solidified at the end of recalescence is calculated from equation (32) by substituting the recalescence temperature. The distance covered during recalescence is calculated by calculating the time and multiplied with velocity of droplet during recalescence. This distance is added with the distance covered by the droplets after nucleation.

If the fraction solidified at the end of recalescence (f_s) is one, it means the droplet has completely solidified and hence the temperature of droplet in the solid state is calculated from equation- (34) for its subsequent flight.

If the droplet has not completely solidified at the end of recalescence, distance is increased by a step and for this step solid fraction is calculated from equation- (33), a numerical scheme is used, as it is a first order ODE. It is solved by

$$f_s[i] = f_s[i-1] + \frac{dt}{2.0}\left[\frac{3.0\times\left(\left(6.0\times h_c[i-1]\times\left(T_m - T_g\right)\right)\right)}{d\times\rho_s\times H_f} - \left(\frac{6.0\times h_c[i-1]\times\left(T_m - T_g\right)}{d\times\rho_s\times H_f}\right)\right]$$

The solid fraction is calculated till it completely solidifies. Then the temperature of the droplet in the solid state is calculated from equation- (34) till the maximum distance is reached.

After calculating these quantities for a given droplet, the droplet size is increased by a step and the distance is initialized to zero. Again the same procedure is repeated to calculate temperature and solid fraction along flight distance. For this bigger droplet the same procedure is repeated till the maximum droplet size is reached.

3.2. THERMAL PROFILE OF THE DEPOSIT AND SUBSTRATE:

3.2.1 THEMAL PROFILE OF THE DEPOSIT:

In order to find out the thermal profile of the growing deposit, the one-dimensional heat transfer conduction equation-41 need to be solved with initial and boundary conditions.

The solution procedure is described as follows. Equation-41 can be discretized in an implicit scheme. It is assumed that there is as initial deposit, which has a got a uniform temperature which is then divide into a certain number of grids. At each time step, one layer of deposit is added to the previous deposit, which in turn increases the number of grids to N+1 from N.

The discretization can be shown as

$$\frac{T_i^{n+1} - T_i^n}{\Delta t} = \left(\frac{k_S}{\rho_S C_{ps}}\right)\frac{T_{i+1}^{n+1} - 2.0\,T_i^{n+1} + T_{i-1}^{n+1}}{\Delta x^2}$$

$$\Rightarrow T_i^{n+1} = T_i^n + \left(\frac{\alpha\Delta t}{\Delta x^2}\right)\left(T_{i+1}^{n+1} - 2T_i^{n+1} + T_{i-1}^{n+1}\right)$$

Where $\alpha = \dfrac{k_S}{\rho_S C_{ps}}$

$$\Rightarrow -\upsilon\, T_{i+1}^{n+1} + (1+2\upsilon)\, T_i^{n+1} - \upsilon\, T_{i-1}^{n+1} = T_i^n$$

Where $\upsilon = \dfrac{\alpha \Delta t}{\Delta x^2}$

Equation –42 can be descritized as

$$-k_S \frac{\left(T_0^{n+1} - T_1^{n+1}\right)}{\Delta x} = h_{s,d}\left(T_0^{n+1} - T_S\right)$$

$$\Rightarrow \left(-\frac{k_S}{\Delta x} - h_{s,d}\right) T_0^{n+1} + \frac{k_S}{\Delta x} T_1^{n+1} = -h_{s,d}\, T_S$$

Similarly, equation-43 can be descritezed as

$$-k_S \frac{\left(T_N^{n+1} - T_{N+1}^{n+1}\right)}{\Delta x} = h_{a,d}\left(T_N^{n+1} - T_g\right)$$

$$\Rightarrow \left(-\frac{k_S}{\Delta x} - h_{a,d}\right) T_N^{n+1} + \frac{k_S}{\Delta x} T_{N-11}^{n+1} = -h_{a,d}\, T_S$$

To find out the temperature profile, GS-SOR technique is used. Equation-41 is used to determine the temperature at interior points, where as the discretized form of equations are used to determine the temperature at boundary points. At each time step, a new layer is added up, the number of grids increases from N to N+1. Then the new profile is found out for all points. The process is continued till the desired time.

3.2.2 THERMAL PROFILE OF THE SUBSTRATE:

In order to find out the temperature profile of the substrate, it is divided into N number of grid points.

The governing conduction equation-44 is discretized with an implicit scheme as follows

$$\frac{T_i^{n+1} - T_i^n}{\Delta t} = \left(\frac{k_{sub}}{\rho_{sub} C_{psub}}\right) \frac{T_{i+1}^{n+1} - 2.0\, T_i^{n+1} + T_{i-1}^{n+1}}{\Delta x^2}$$

$$\Rightarrow T_i^{n+1} = T_i^n + \left(\frac{\alpha_{sub}\Delta t}{\Delta x^2}\right)\left(T_{i+1}^{n+1} - 2T_i^{n+1} + T_{i-1}^{n+1}\right)$$

Where $\alpha_{sub} = \dfrac{k_{sub}}{\rho_{sub} C_{psub}}$

$$\Rightarrow -\upsilon_{sub}\, T_{i+1}^{n+1} + (1 + 2\upsilon_{sub})\, T_i^{n+1} - \upsilon_{sub}\, T_{i-1}^{n+1} = T_i^n$$

Boundary condition-45 can be discretized as

$$-k_{sub}\frac{\left(T_N^{n+1} - T_{N-1}^{n+1}\right)}{\Delta x} = h_{d,s}\left(T_N^{n+1} - T_d\right)$$

$$\Rightarrow \left(-\frac{k_{sub}}{\Delta x} - h_{a,d}\right)T_N^{n+1} - \frac{k_s}{\Delta x}T_{N-1}^{n+1} = -h_{d,s}\, T_d$$

Similarly boundary condition-46 can be discretized as

$$-k_{sub}\frac{\left(T_0^{n+1} - T_1^{n+1}\right)}{\Delta x} = h_{a,s}\left(T_0^{n+1} - Tg\right)$$

$$\Rightarrow \left(-\frac{k_{sub}}{\Delta x} - h_{a,s}\right)T_0^{n+1} - \frac{k_s}{\Delta x}T_1^{n+1} = -h_{a,s}\, Tg$$

Here also, the discretized equation-44 along with discretized boundary conditions- 45 and -46 are used to determine the temperature profile of the substrate. A GS-SOR technique is used for calculating the temperature. At each time step the new substrate temperature is found out.

4.1.1 VELOCITY PROFILE OF DROPLETS:

Fig. 4.1 1-4 show the variation of velocity of Al and Cu droplets in Nitrogen and Helium gas medium at an initial gas velocity of 200m/s and 400m/s It can be seen from all figures that the droplet velocity initially increases and then gradually decreases for all sizes. A 10μm droplet in all figures acquires a higher velocity in its initial flight than a 300μm droplet. This behavior can be expressed from equation-8, where velocity of a droplet varies inversely to its diameter So, a 10μm droplet accelerates faster than a 300μm droplet. As a result the maximum velocity of a 10μm droplet is much higher than a 300μm droplet As soon as the droplet velocity crosses the gas velocity, the drag force defined in equation-4 and used in equation-8, becomes negative which opposes the motion of the droplets. As a consequence, the velocity of a droplet decreases. However, the position at which the drag force becomes negative depends on droplet size, initial gas velocity and physical properties of atomizing gas medium. A 10μm Al droplet at 200m/s velocity and in nitrogen medium touches the gas velocity at 0.02m where as a 300μm Al droplet under the same condition equals the gas velocity at 0 42m. At an initial gas velocity of 400m/s in Fig 4.1.2 the same 10μm droplet touches the gas velocity at 0.03m from geometric point.

It can be observed that the maximum velocity and the distance, at which the droplets achieve maximum velocity, vary with the type of metal, the atomizing gas medium and the initial gas velocity. Table 2 -4 summarizes the effect of these parameters on the maximum velocity of droplets.

Table-2: **Nitrogen Atomizing Gas Medium**

At Initial Gas Velocity of 200m/s					
Droplet Size(μm)	$V_{max,Al}$ (m/s)	Position (m)	$V_{max,Cu}$ (m/s)	Position (m)	Ratio($V_{max,Cu}$ /$V_{max,Al}$)
10	131	0 026	93	0.049	0 71
50	67	0.093	45	0.201	0 67
100	50	0.163	33	0.393	0.66
300	31	0.402	20	0.850	0.67
At Initial Gas velocity of 400m/s					
10	255	0.027	173	0.058	0.67
50	126	0.105	84	0 226	0.66
100	95	0.181	61	0.407	0.64
300	59	0 437	37	0.92	0.63

Table-3: **Helium Atomizing Medium**

At Initial Gas Velocity of 200m/s					
Droplet Size (μm)	$V_{max,Al}$ (m/s)	Position (m)	$V_{max,Cu}$ (m/s)	Position (m)	Ratio($V_{max,Cu}$ /$V_{max,Al}$)
10	94	0.019	59	0 025	0 64
50	32	0.035	19	0 049	0.62
100	21	0.046	12	0.065	0 58
300	11	0.071	27	0.099	0.63
At Initial Gas velocity of 400m/s					
10	164	0.020	100	0.028	0.61
50	58	0.038	34	0.054	0.59
100	38	0.05	22	0.071	0.58
300	19	0.075	12	0.107	0.63

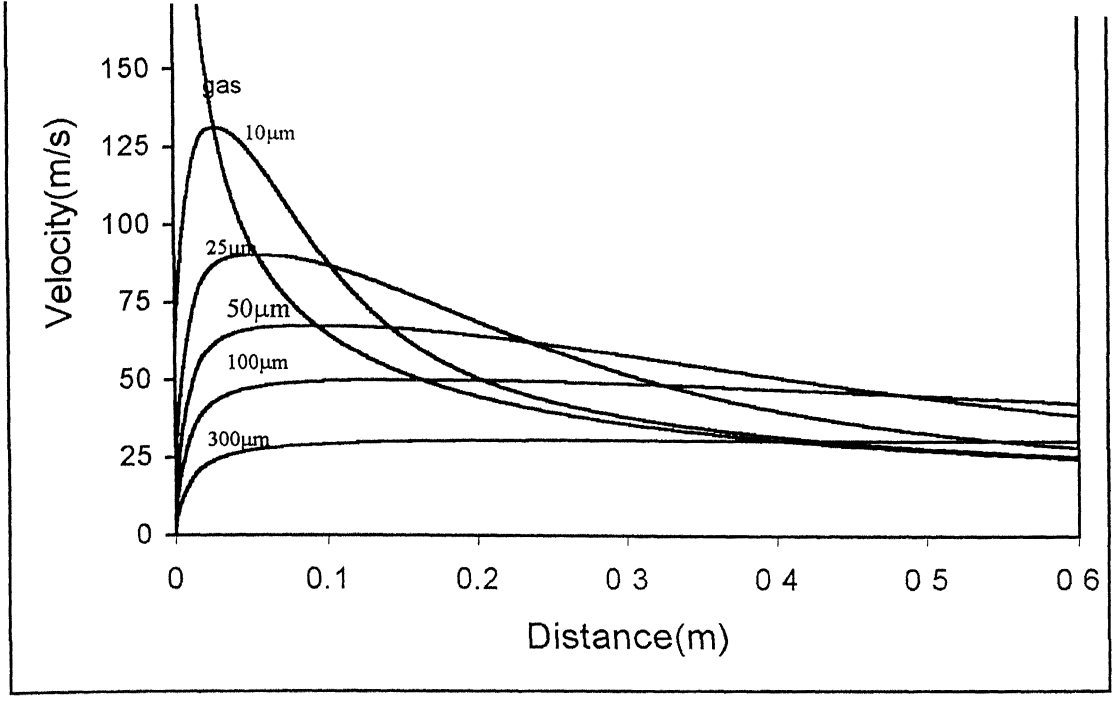

Fig 4 1 1· Velocity profile of Al droplets at an initial gas velocity of 200m/s

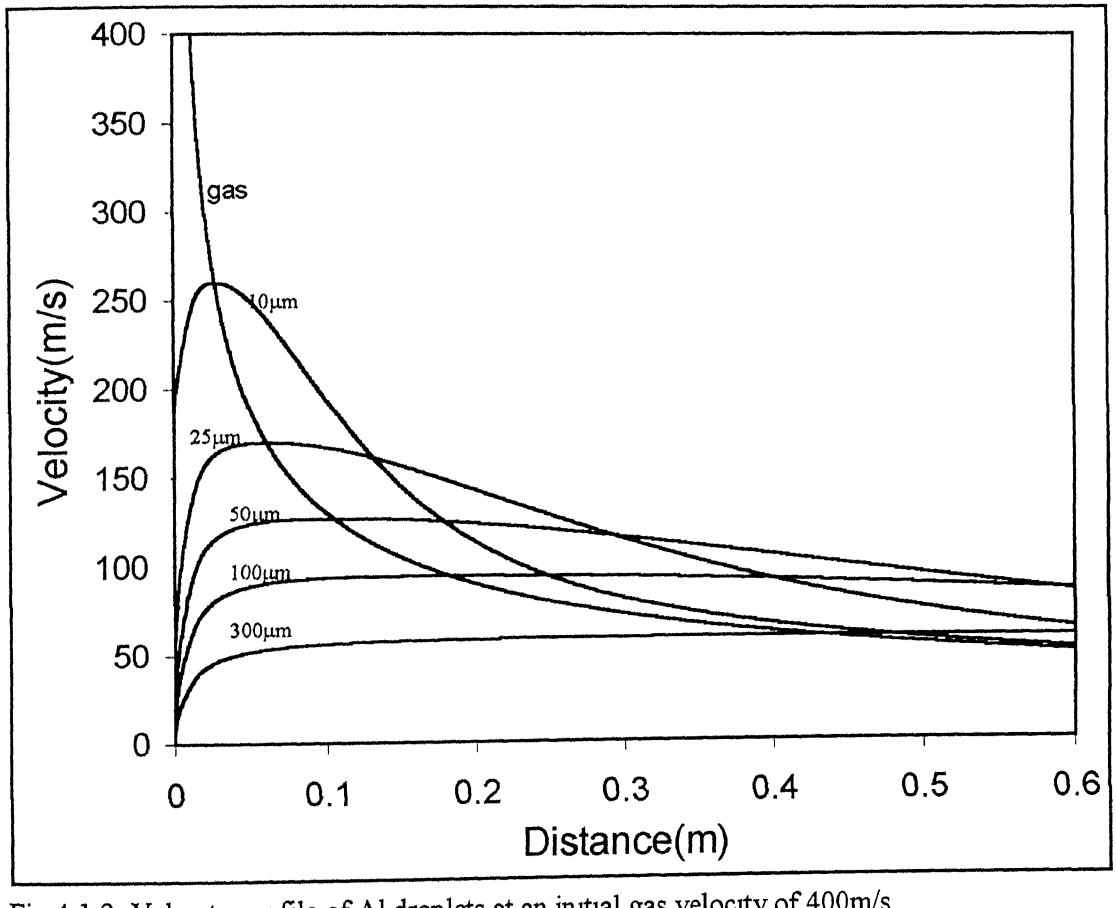

Fig.4.1 2: Velocity profile of Al droplets at an initial gas velocity of 400m/s

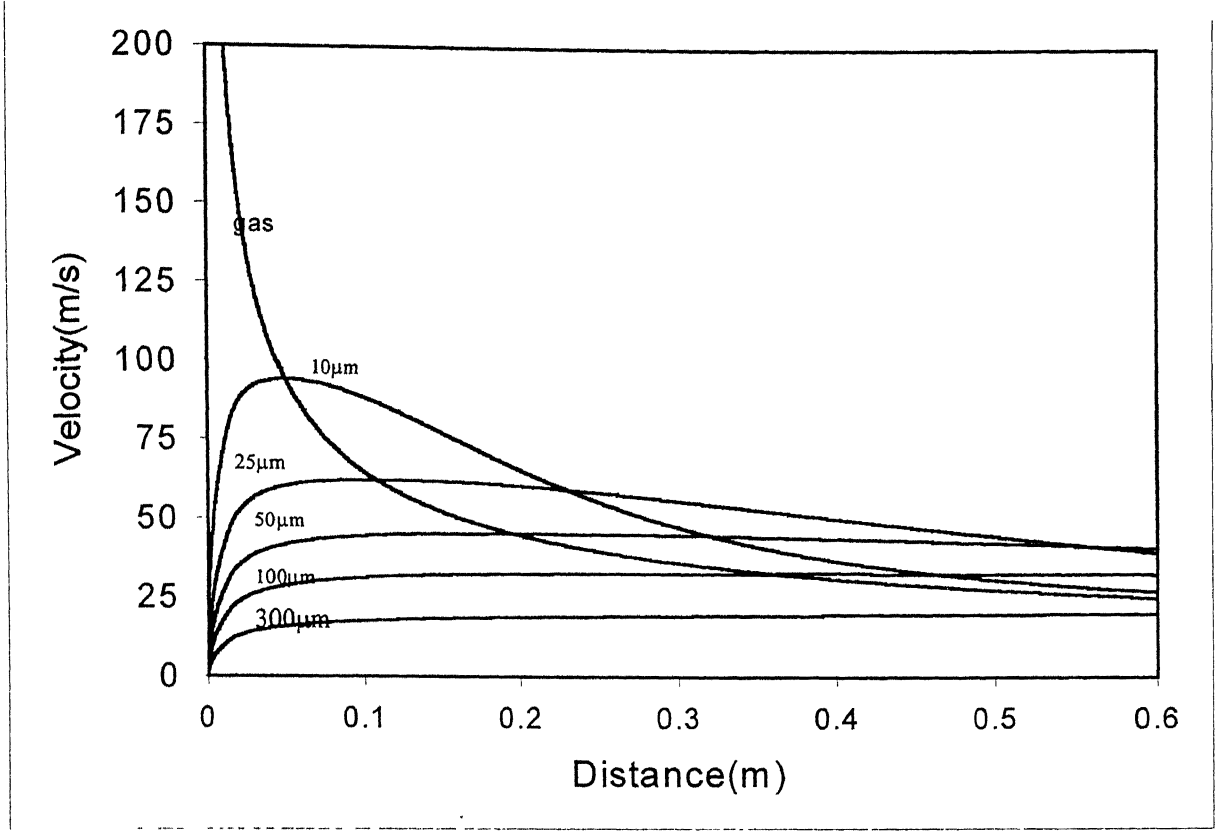

Fig. 4.1.3: Velocity profile of Cu droplets in Nitrogen medium at an initial gas velocity of 200m/s

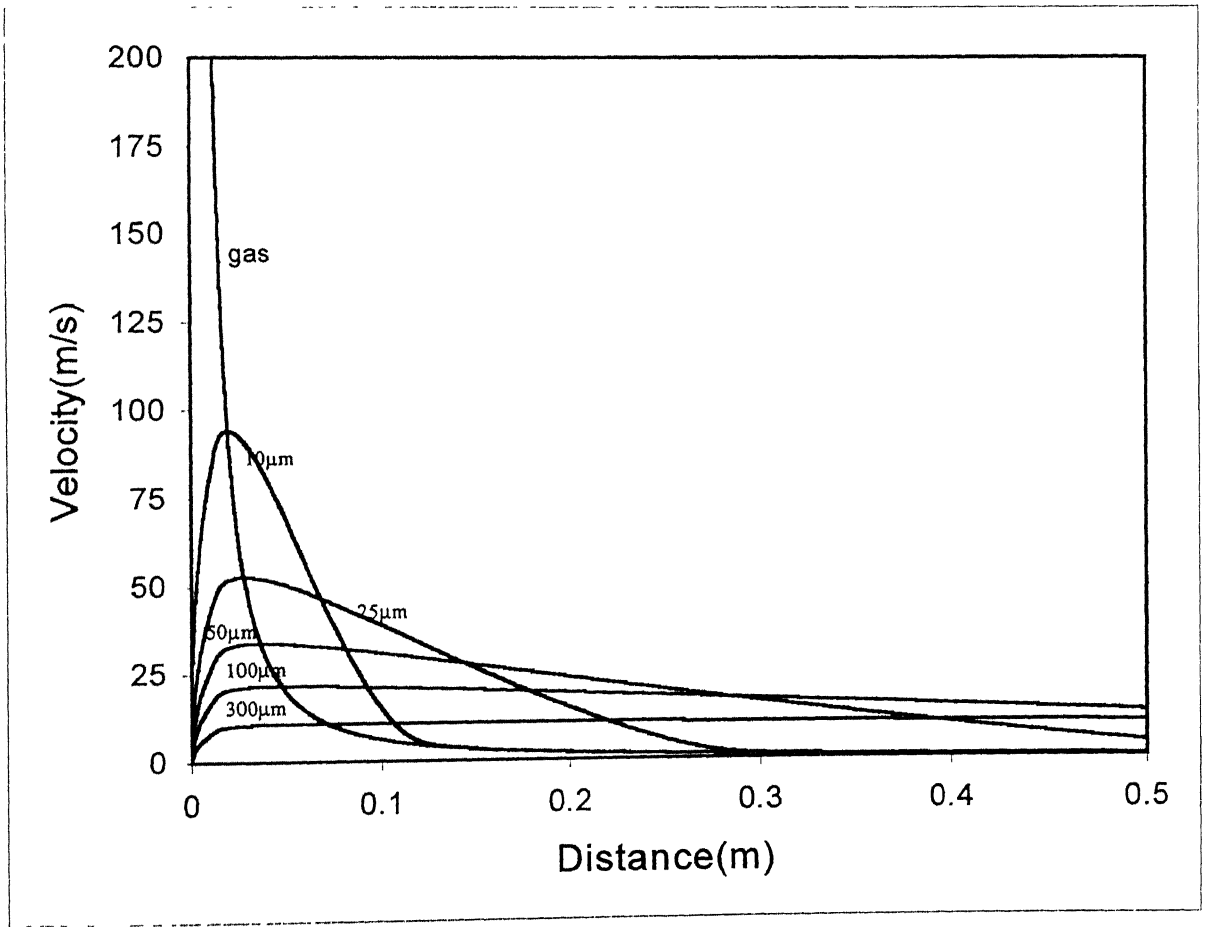

Fig. 4.1.4: Velocity profile of Al droplets in Helium medium at 200m/s initial gas velocity.

Table-4: Ratio of maximum velocities of Al and Cu at 200m/s and 400m/s in nitrogen

Droplet Size(μm)	Vmax,Al(400)/Vmax,Al(200)	Vmax,Cu(400)/Vmax,Cu(200)
10	1.94	1.86
50	1.88	1.86
100	1.9	1.85
300	1.9	1 85

It can be seen from the above table that the maximum velocity of Cu droplets of all sizes is lower than Al droplets irrespective of the initial gas velocities and gas medium. The ratio of VCu/VAl is varying from 0.58 to 0 71. This decrease in magnitude of the velocity of copper can be explained from equation-8, where velocity varies inversely with density. Cu has a density of 8 94gm/cc where as Al has a density of 2.7 gm/cc An increase in density with a factor of 3 3 decreases the velocity of droplets in the range of 0 58-0 71 However, the gas medium has an influence on the maximum velocity of droplets. It can be seen from the above tables that droplets of all sizes achieve a lower magnitude of maximum velocity in helium medium than in nitrogen medium. From equation-4 it is noticed that the drag force depends on the density of the gas. In case of helium, the density is 8.2 times lower than nitrogen. Hence, the drag force is also much lower and the droplets achieve lower velocity in comparison to nitrogen medium An increase in initial gas velocity results in higher drag force and hence the droplets move with a higher velocity. From the Table-4 it can be observed that the two fold increase in gas velocity results in almost 1.9 time increase in maximum velocity

From Table-2 and 3, it can be seen that for all droplets the position at which they acquire maximum velocity vary with their size, type of metal and gas medium. It is observed that with increase in droplet size, the position of occurrence of maximum velocity shifts away from geometric point. A 10μm Al droplet achieves a maximum velocity at 0.026m from geometric point, where as a 300μm Al droplet achieves the same at 0.4m from geometric point. It can also be seen that for all droplet sizes, Cu droplets attend the maximum velocity at a longer distance than Al droplets. It is because of its higher density, for which its acceleration is slower. A 100μm Cu droplet attends the maximum velocity at 0.39m from geometric point where as an Al droplet achieves the same much earlier at 0.16m. Similarly,

in helium medium, the position at which they acquire maximum velocity is much lower than in nitrogen. However, the effect of droplet size and type of metal on the position remains same as happens in case of nitrogen medium.

4.1.2 HEAT TRANSFER COEFFICIENT:

Fig 4.1 5-8 show the variation of heat transfer coefficient with flight distance for Al and Cu droplets in Nitrogen and Helium gas medium at an initial gas velocity of 200m/s and 400m/s It can be observed that the heat transfer coefficient decreases at a slower rate initially up to a distance of Zc for all droplets. From equation –1 it can be observed that the velocity of gas doesn't decay up to critical distance Zc From equation-(13), it can be observed that heat transfer coefficient depends on relative velocity between gas and size of droplet Here, the rate of decrease of heat transfer coeffcient is proportional to the rate of decrease of relative velocity. So, from Fig 9, it can be seen that relative velocity varies at a lower rate in the region. Hence, the heat transfer coefficient decreases at a lower rate. After that the heat transfer coeffcient decreases rapidly with distance to a minimum value for all droplets. It is because as per equation-1, the gas velocity decays rapidly with distance. So, the relative velocity decreases rapidly, which can be seen from Fig. 9. Hence, from equation-13, the heat transfer coeffcient decreaes rapidly to attain a minimum value when the relative velocity between gas and velocity is zero. After that the relative velocity increases as because the droplet velocity surpasses the gas velocity and hence the heat transfer coeffcient again increases for all droplets. After increasing up to a certain distance the heat transfer coeffcient reaches a maximum for all droplets and then slowly decreases

The distance at which the droplets attain a minimum value of heat transfer coeffcient depends on droplet size, initial gas velocity and the gas medium A 10μm Al droplet in N_2 medium and at 200m/s initial gas velocity has a minimum heat transfer coeffcient at 0.026m, where as a 300μm droplet attains a minimum at 0.28m from geometric point. In helium medium, a 10μm Al droplet has the minimum heat transfer coeffcient at 0.02m where as a 300μ m droplet has a minimum heat transfer coeffcient at 0.07m. The effect of initial gas velocity on heat transfer coeffcient variation can be seen

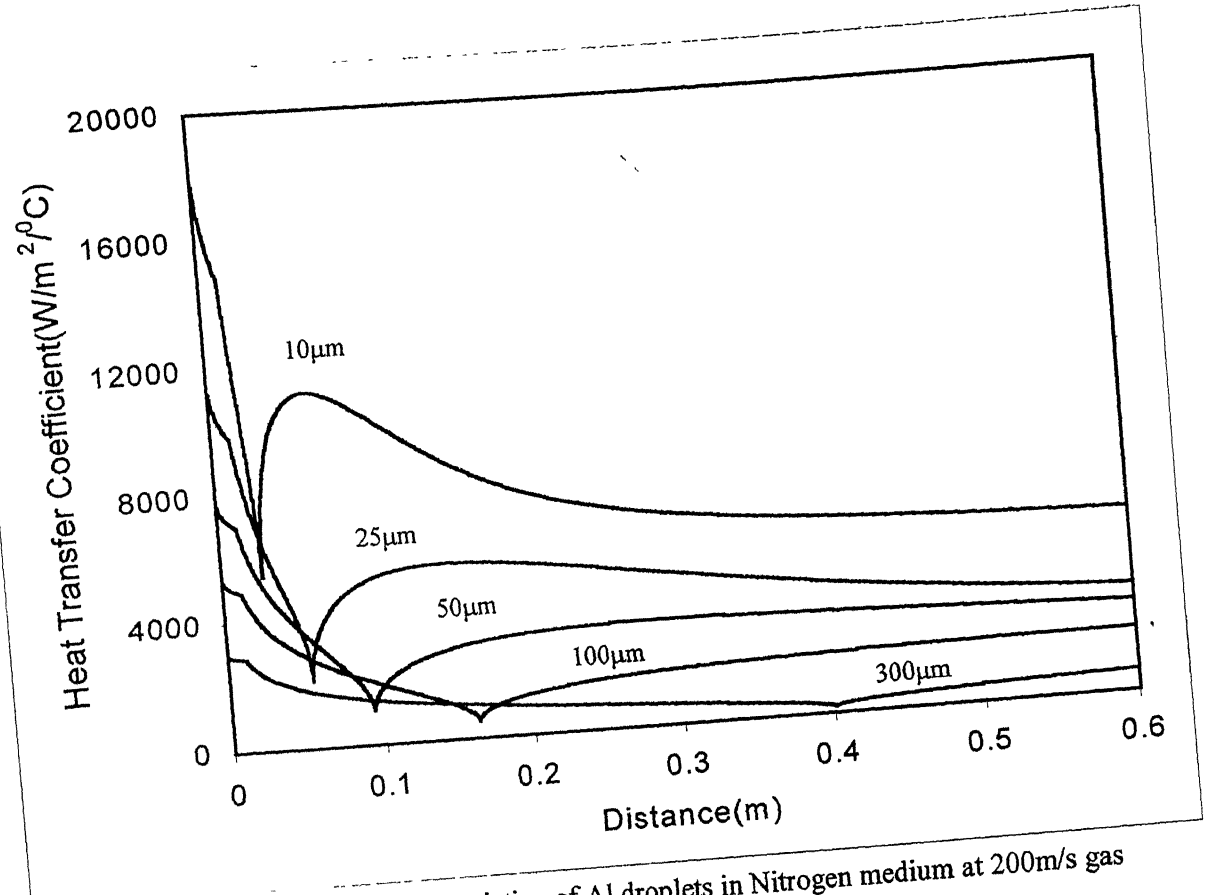

Fig. 4.1.5: Heat Transfer Coefficient variation of Al droplets in Nitrogen medium at 200m/s gas velocity

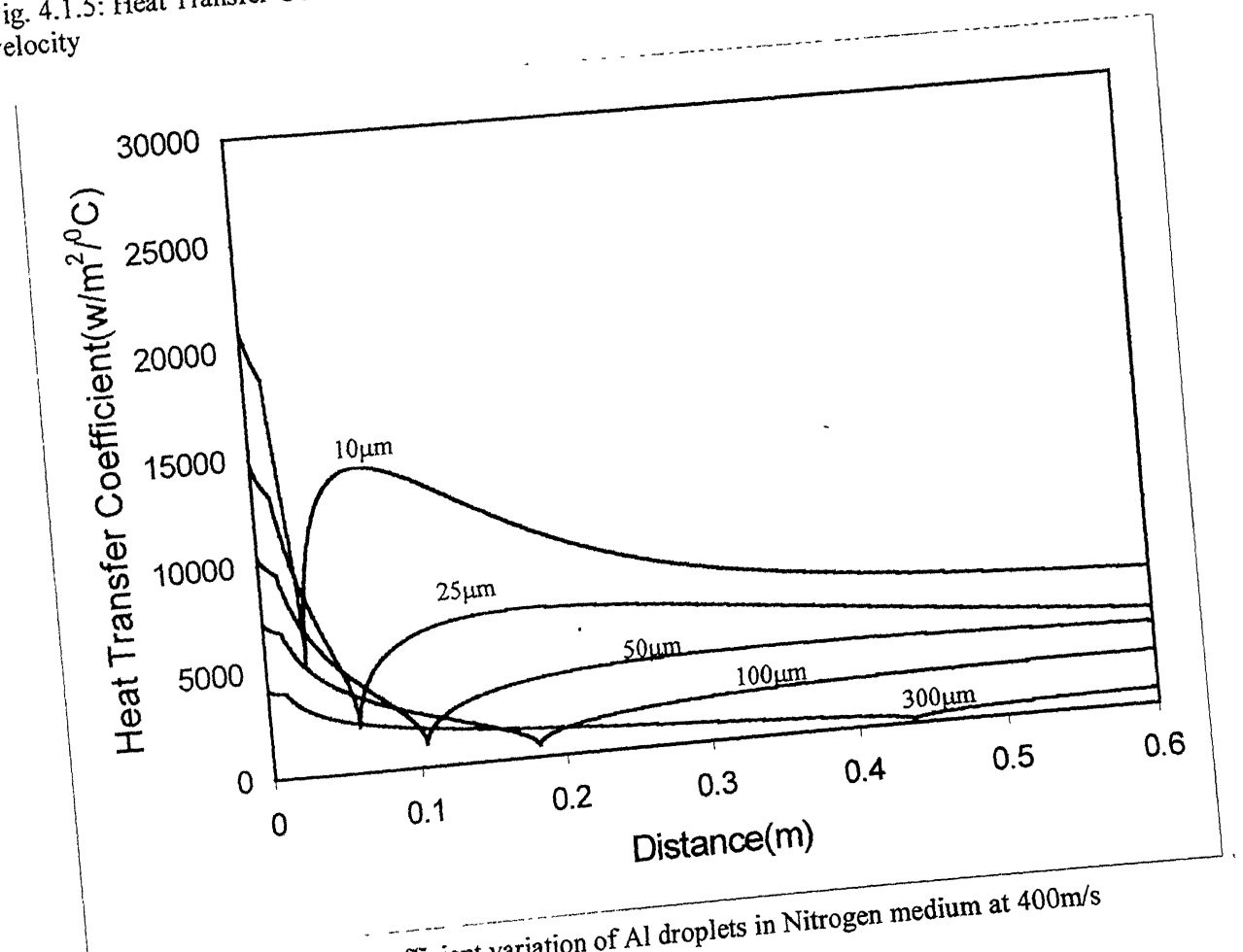

Fig.4.1. 6: Heat Transfer Coefficient variation of Al droplets in Nitrogen medium at 400m/s initial gas velocity

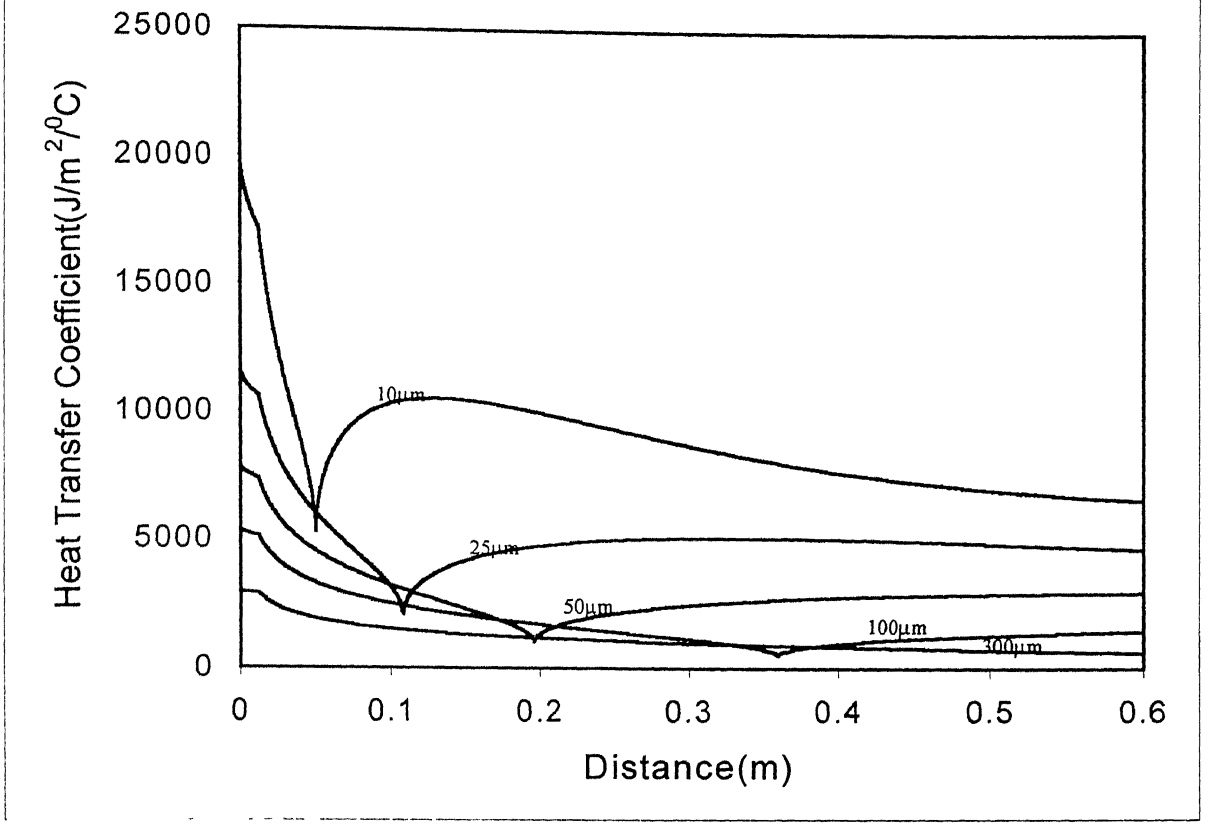

Fig. 4.1.7: Heat Transfer Coefficient variation of Cu droplets in Nitrogen medium at an initial gas velocity of 200m/s velocity.

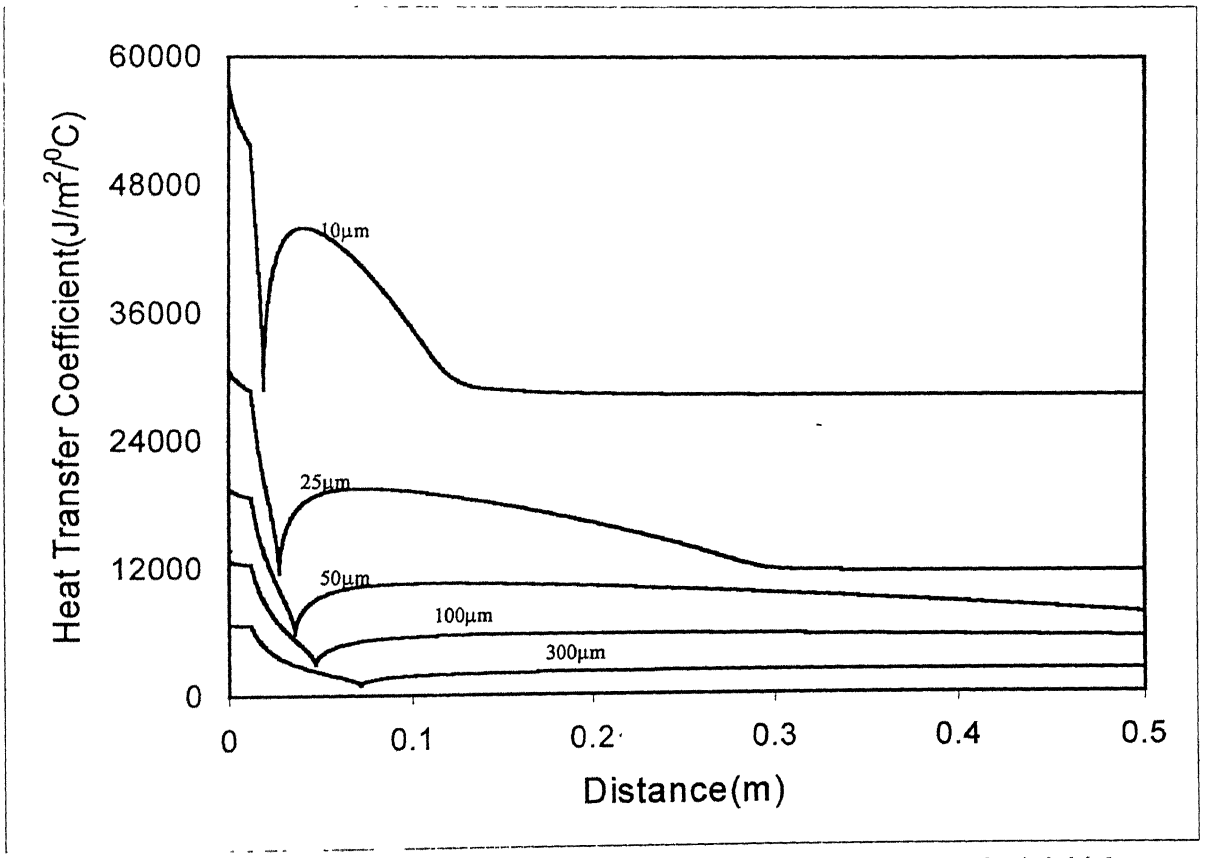

Fig. 4.1.8: Heat Transfer Coefficient variation of Al droplets in Helium medium at 200m/s initial gas velocity.

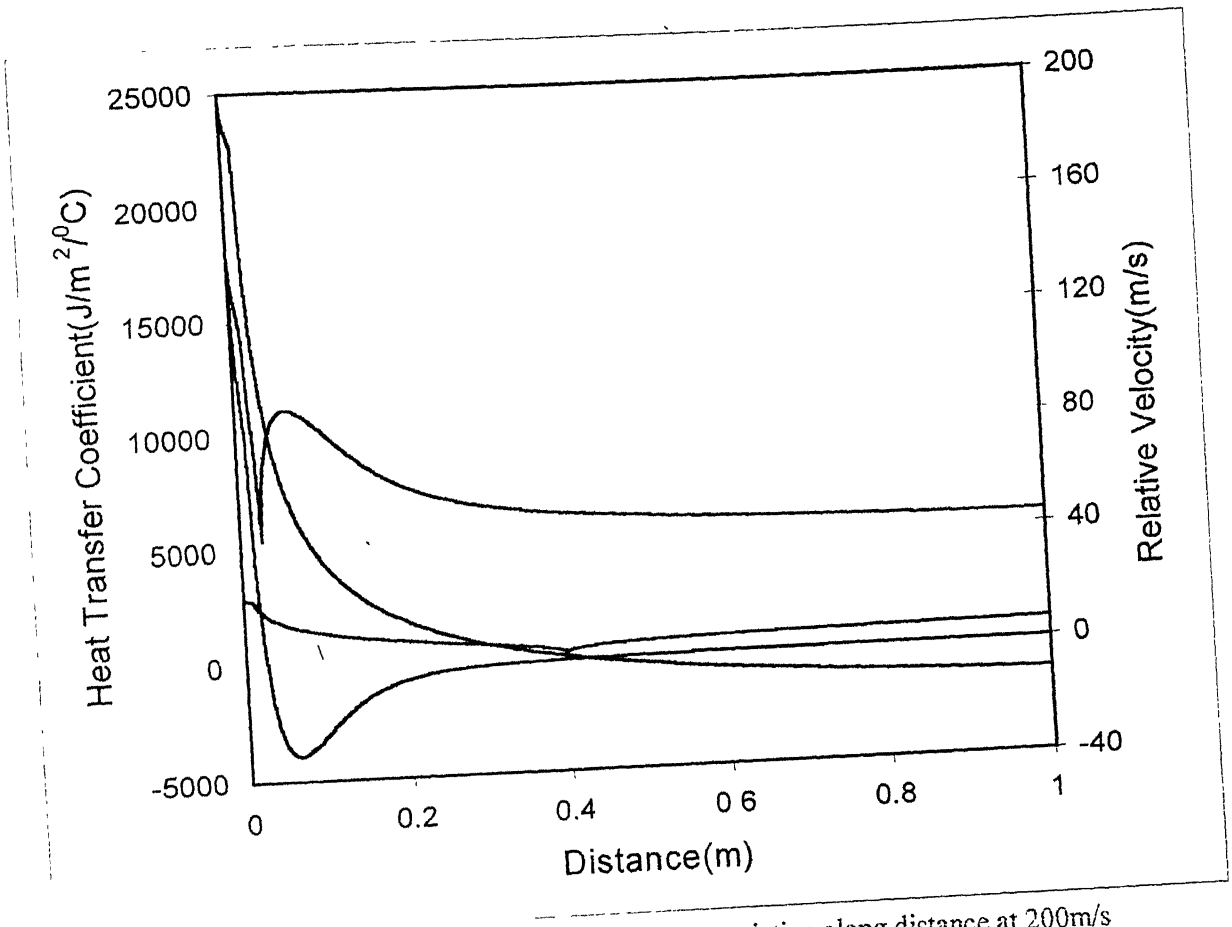

Fig. 4.1.9: Relative velocity and Heat Transfer coefficient variation along distance at 200m/s initial gas velocity in Nitrogen atmosphere.

from Fig-5 and 6 For Example, at 200m/s initial gas velocity, a 300μm droplet has a minimum heat transfer coeffcient at 0.28m where as at 400m/s initial gas velocity, the same droplet has a minimum heat transfer coeffcient at 0 42m from geometric point.

4.1.3 TEMPERATURE PROFILE OF THE DROPLETS:

Fig 10-13 show the temperature of Al and Cu droplets as a function of vertical flight distance in nitrogen and helium medium at an initial gas velocity of 200m/s and 400m/s. At geometric point all the droplets are at 30^0C superheat. In all the figures 25μm, 50μm, 100μm, 300μm droplets are shown as a function of flight distance. It can be seen that all droplets undercool and attain a minimum temperature at different flight distance prior to start of solidification. This minimum temperature is known as nucleation temperature. The droplets begin to solidify which results in evolution of latent heat. After that the temperature of all the droplets increase rapidly due to the phenomena of recalescence. Recalescence happens when the rate of evolution of latent heat is much higher in comparison to the rate of heat extraction by the surrounding gas. It can be seen that the maximum increase in temperature depends on the droplet size. Aluminum droplets of sizes less than 7μm couldn't reach the melting point, where as all droplets greater than that size could reach up to the melting point. Thereafter, the droplet temperature doesn't change with distance, which is due to the heat balance consideration (rate of latent heat evolution is equal to rate of heat extraction by gas) till it completely solidifies. After that it can be seen that the temperature of the droplet decreases in the solid state as a function of flight distance. The variation of temperature of droplets with distance gets influenced by medium and initial gas velocity. It can be observed that nucleation temperature of the droplets get influenced by these parameters

पुरुषोत्तम कालीनाथ केलकर पुस्तकालय
भारतीय प्रौद्योगिकी संस्थान कानपुर
अवाप्ति क्र० A 141825

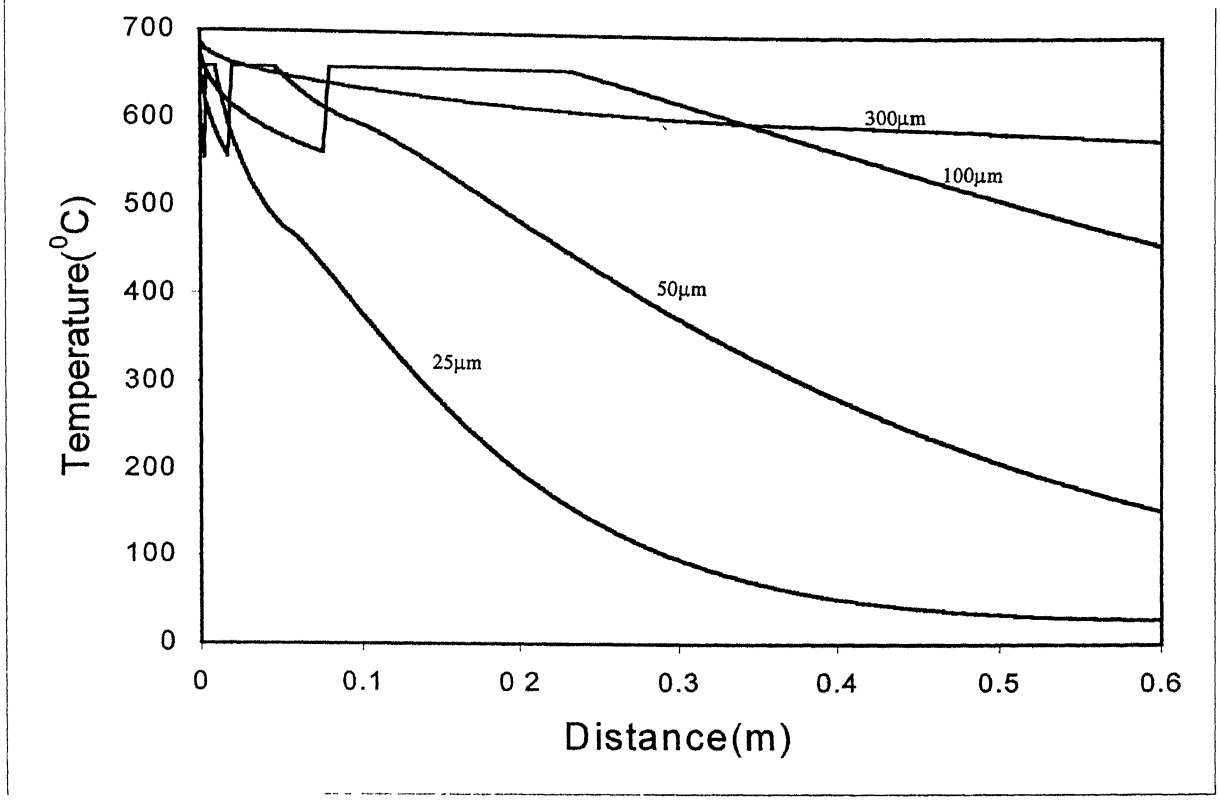

Fig. 4.1.10: Temperature variation of Al droplets in Nitrogen medium at an initial gas velocity of 200m/s.

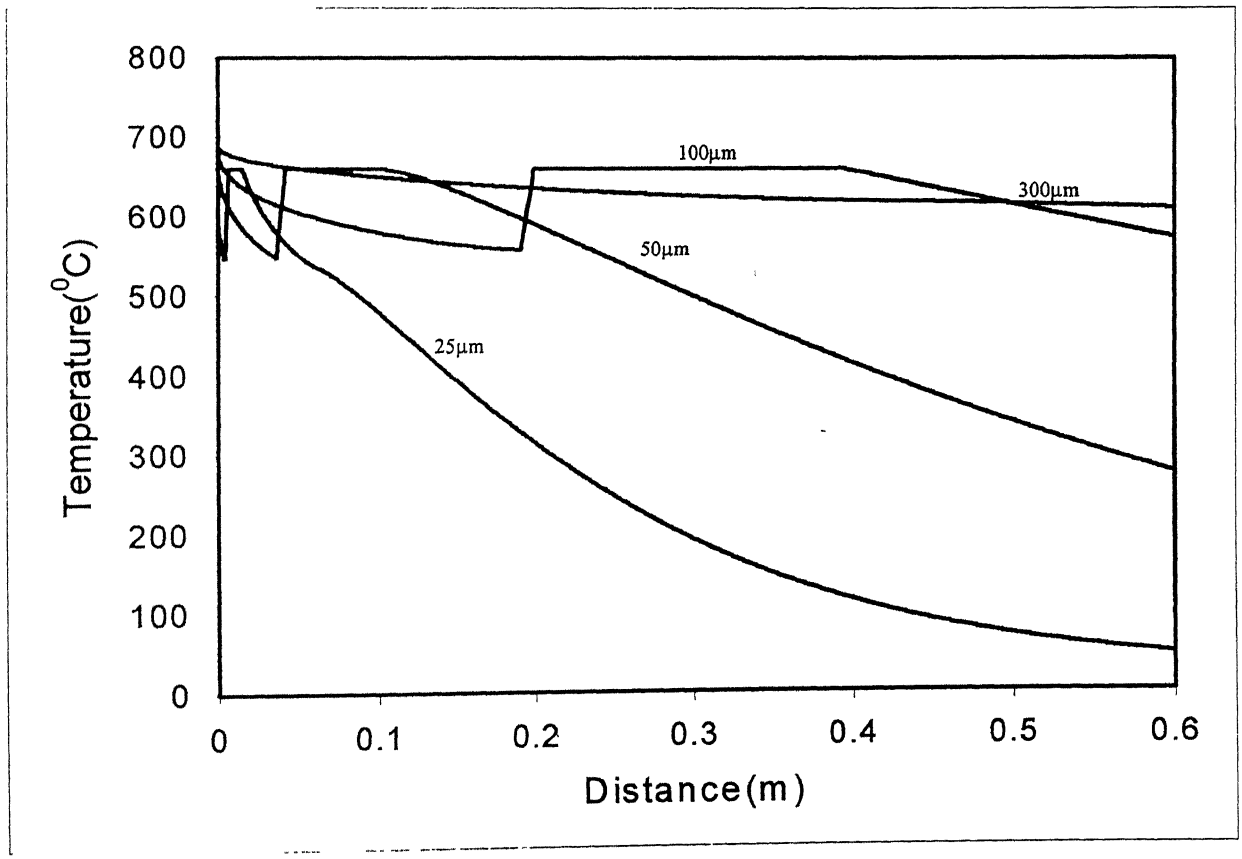

Fig. 4.1.11: Temperature variation of Al droplets in Nitrogen gas at an initial gas velocity of 400m/s.

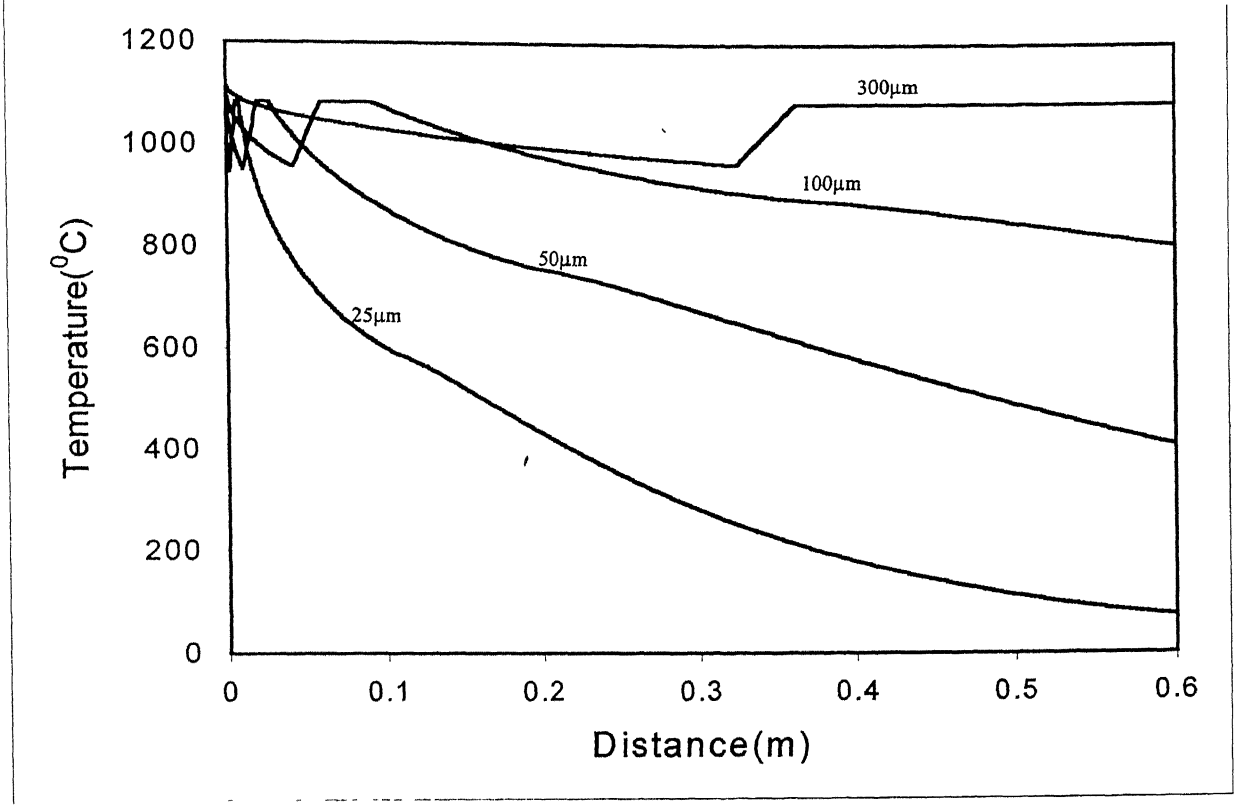

Fig. 4.1.12: Temperature variation of Cu droplets in Nitrogen atmosphere at an initial gas velocity of 200m/s.

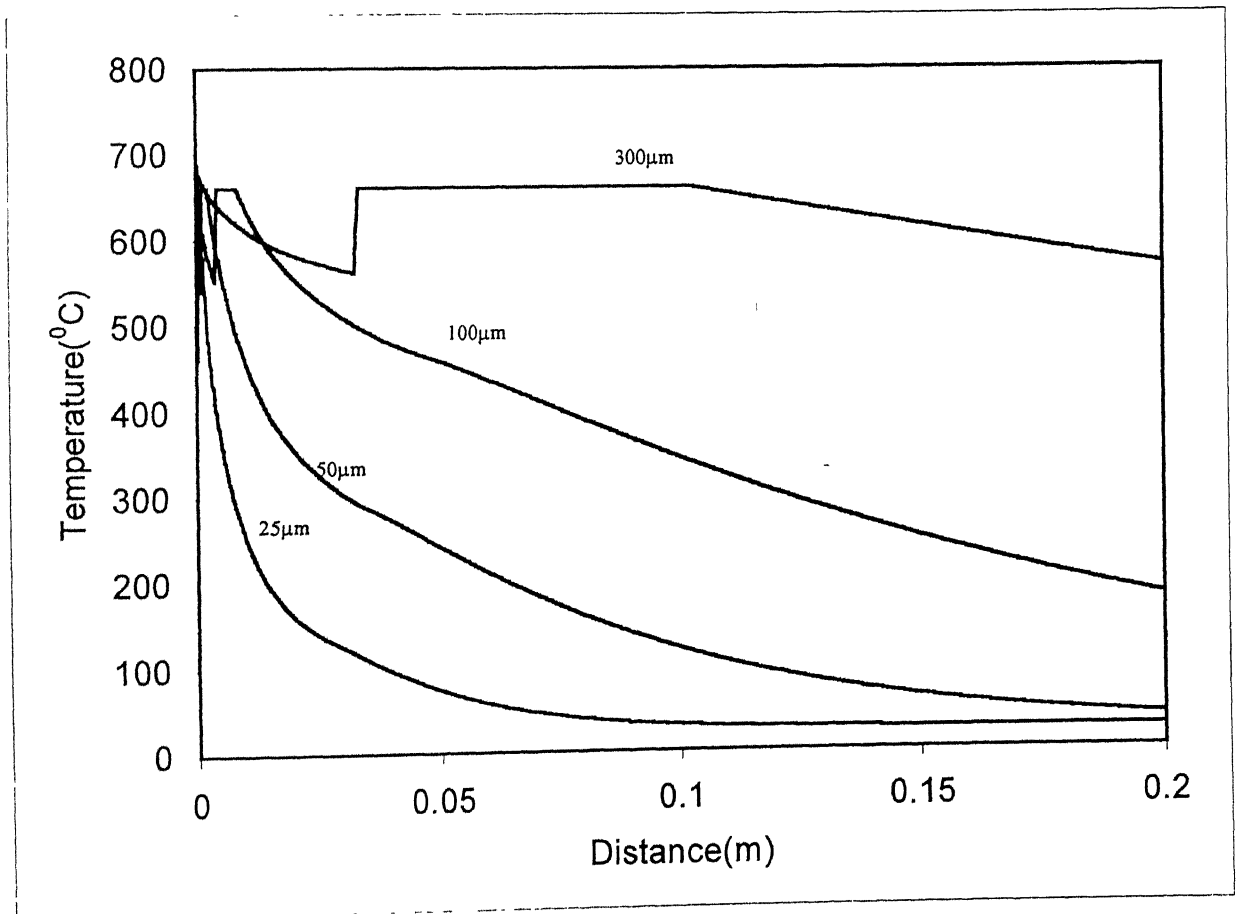

Fig. 4.1.13: Temperature variation of Al droplets in helium medium at 200m/s gas velocity.

4.1.3.1 Effect of initial gas velocity and medium on nucleation temperature:

Fig 14 shows the variation of nucleation temperature with droplet size in helium and nitrogen atomizing medium at an initial gas velocity of 200m/s and 400m/s. It can be seen that nucleation temperature varies with droplet size The nucleation temperature is lower for smaller droplets than bigger ones The nucleation temperature of droplets depends on $(T_m-T_N)/T_m)$ and cooling rate. Higher value of $(T_m-T_N)/T_m)$ and that of cooling rate will give lower nucleation temperature according to equation–(24) and (26). Typically, the nucleation temperature of a 10μm Al droplet in nitrogen is 385^0C where as a 200μm droplet in the same medium has a nucleation temperature of 556^0C. Similarly, for the reasons mentioned above in helium medium, all the droplets have a lower nucleation temperature or higher undercooling in comparison to nitrogen medium.

Fig 15 is plotted between reduced supercooling $(T_m-T_N)/T_m$ where T_m in Kelvin against size for Al and Cu metals. It can be seen that Cu droplets have lower value of reduced super cooling than Al. This can be observed from equations A-2 and A-4 in the Appendix-A, where the coefficient of $T_m/(T_m-T)$ for Cu is lower than that of Al. Hence nucleation rate It is much higher for Cu than Al. To have the nucleation frequency for nucleation, a 10μm cu droplet need a reduced super cooling of 0.502 where as the same size Al droplet need a reduced supercooling of 0.702. The results are compared with the achievable undercooling in helium medium available in the literature. It can be seen that Al droplets of below 16μm have a reduced undercooling, higher than the given data in literature. In literature, the data are given for steady state nucleation where as in the present calculation the results are shown for transient nucleation. It is observed that the droplets undercooled higher during transient nucleation than in steady state nucleation It can be observed from equations A-3 and A-5 in the Appendix-A, where I_t is a fraction of Is and it increases with time to become equal to steady state nucleation. So, to achieve the nucleation frequency for nucleation, in transient nucleation the time require is higher than steady state nucleation rate and hence the undercooling is higher.

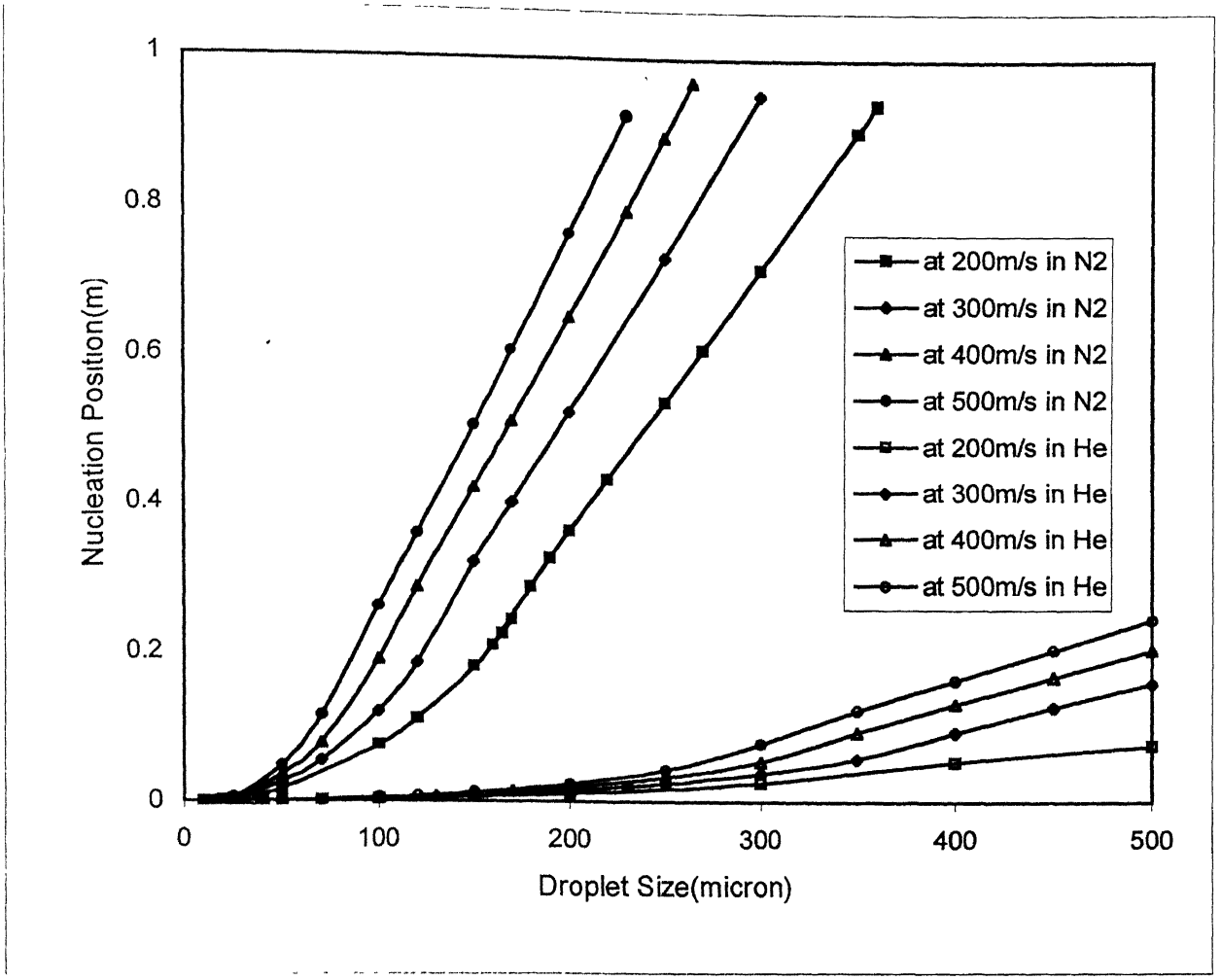

Fig. 16: Variation of Nucleation position of Al droplets with gas velocity and medium.

4.1.3.2 Effect of initial gas velocity and gas medium on nucleation position:

Fig 16 shows the effect of initial gas velocity and gas medium on nucleation position of droplets Al droplets at a superheat of 30^0C are taken for calculation. It can be seen that on increasing the gas velocity, nucleation position of droplets shift to a longer distance Quantitatively, at 200m/s initial gas velocity, a 200μm droplet nucleates at 0.36m from geometric point where as at 500m/s of initial gas velocity the nucleation event of the same droplet takes place at 0.7m from geometric point. It is because higher velocity of gas results in higher amount of drag force; hence the droplets attain a higher velocity. This results in shifting the position. The same trend is also observed in case of helium medium, the nucleation event is found to be taking place at much shorter distance from the geometric point

4.1.4 SOLIDIFICATION OF DROPLETS:

Figs. 17-20 show the variation of solid fraction of Al and Cu droplets in nitrogen and helium atomizing medium at an initial gas velocity of 200m/s and 400m/s. The figures are drawn for the droplets of 25μm, 50μm, 100μm and 300μm size. It can be seen that the total amount of solidification occurs in two stages: initial and final. The initial stage is characterized in the figure by a sudden increase in the solid fraction, where as the final stage is characterized by a continuous increase in solid fraction with distance. The sudden increase in solid fraction is due to the phenomenon of recalescence where as in the final stage, the increase in solid fraction with distance is due to the equilibrium solidification as discussed in 4 1.3. In the recalescence stage, the solid fraction increases linearly with distance. It is because in equation- (29), solid fraction varies linearly with distance. It can be seen from all figures that the flight distance require for onset of solidification increases with droplet size. The reason can be noticed from equation-33, where the rate of growth of solid fraction depends on heat transfer coefficient. It is discussed before that bigger droplets are associated with lower heat transfer coefficient and hence lower cooling rate. So, the removals of heat, in case of bigger droplets take more time than smaller droplets. Hence, the bigger droplets move more distance before solidification starts. Typically, a 25μm Al droplet starts to nucleate at 0.01m from geometric point, where as a 300μm

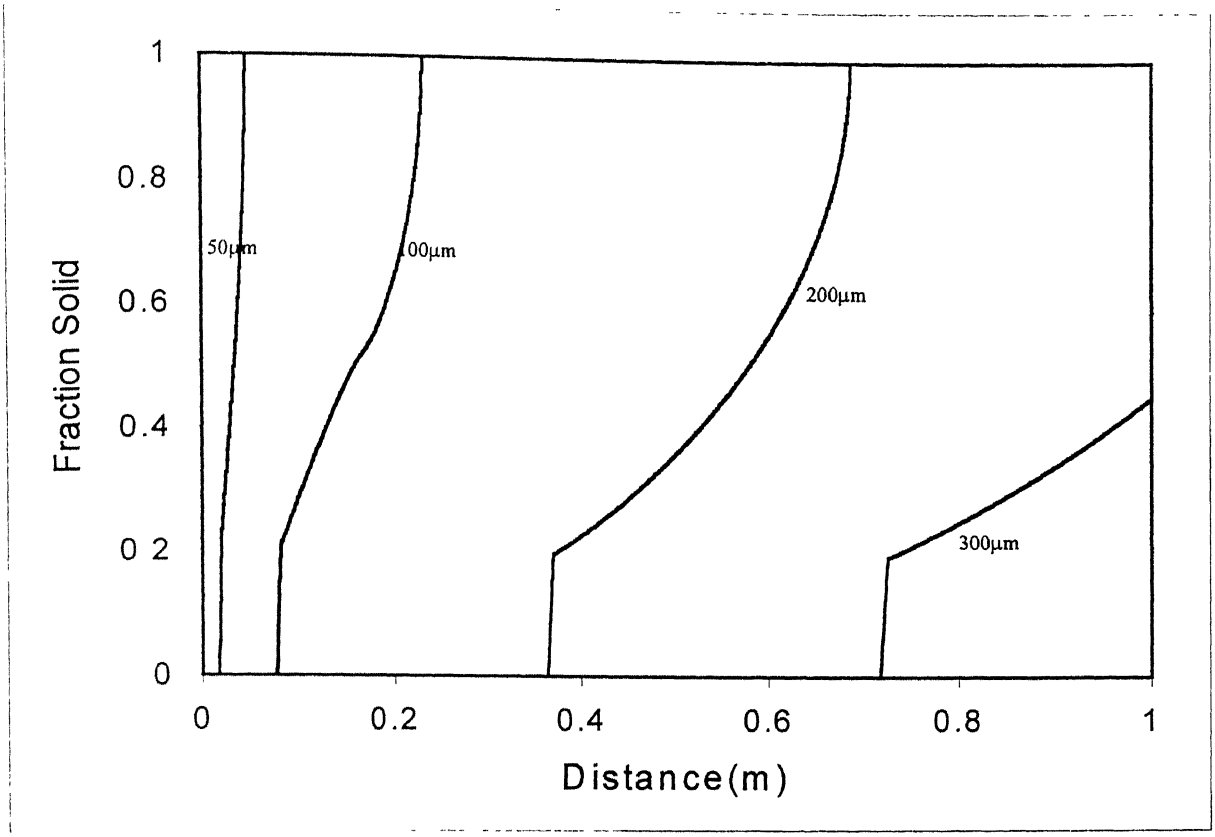

Fig. 4.1.17: Fraction Solid variation of Al droplets in Nitrogen atmosphere at 200m/s initial gas velocity.

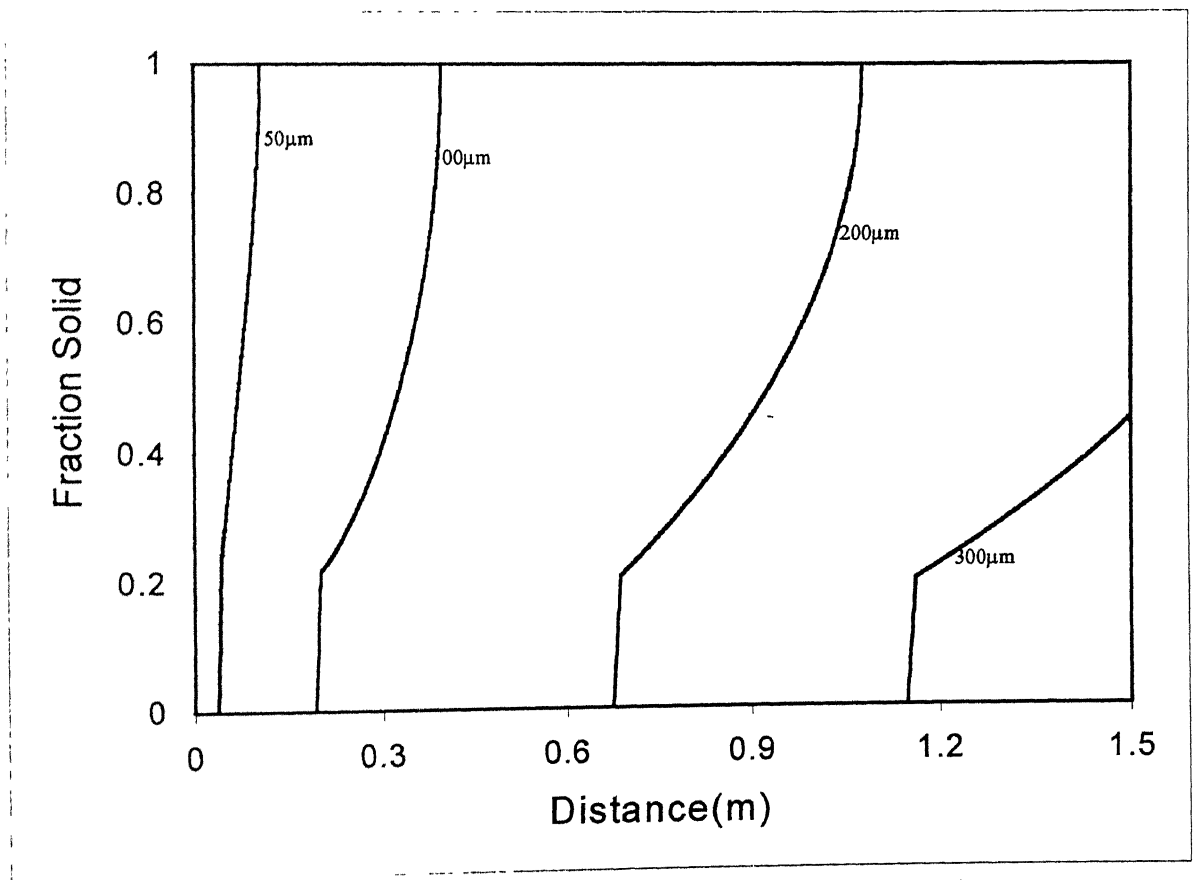

Fig. 4.1.18: Fraction Solid variation of Al droplets in Nitrogen medium at 400m/s initial gas velocity

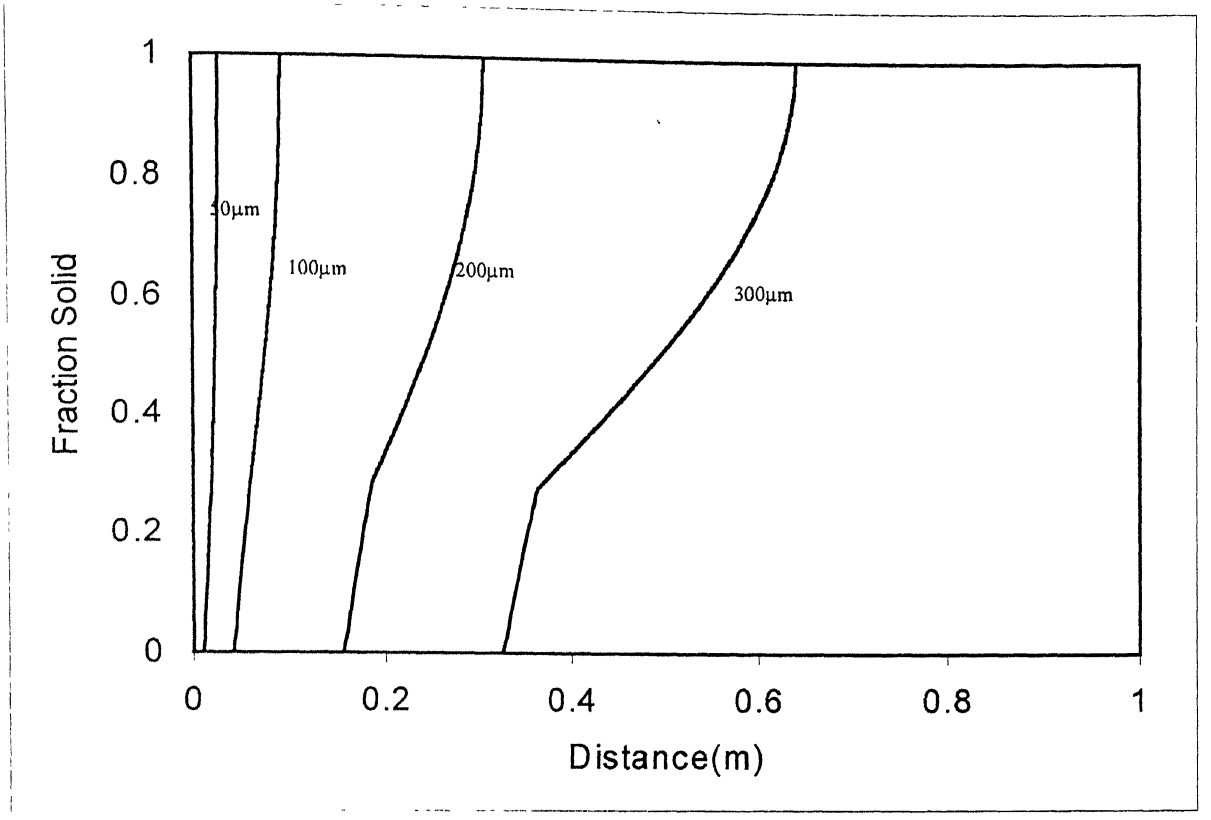

Fig. 4.1.19: Fraction Solid variation of Cu droplets in Nitrogen medium at an initial gas velocity of 200m/s velocity.

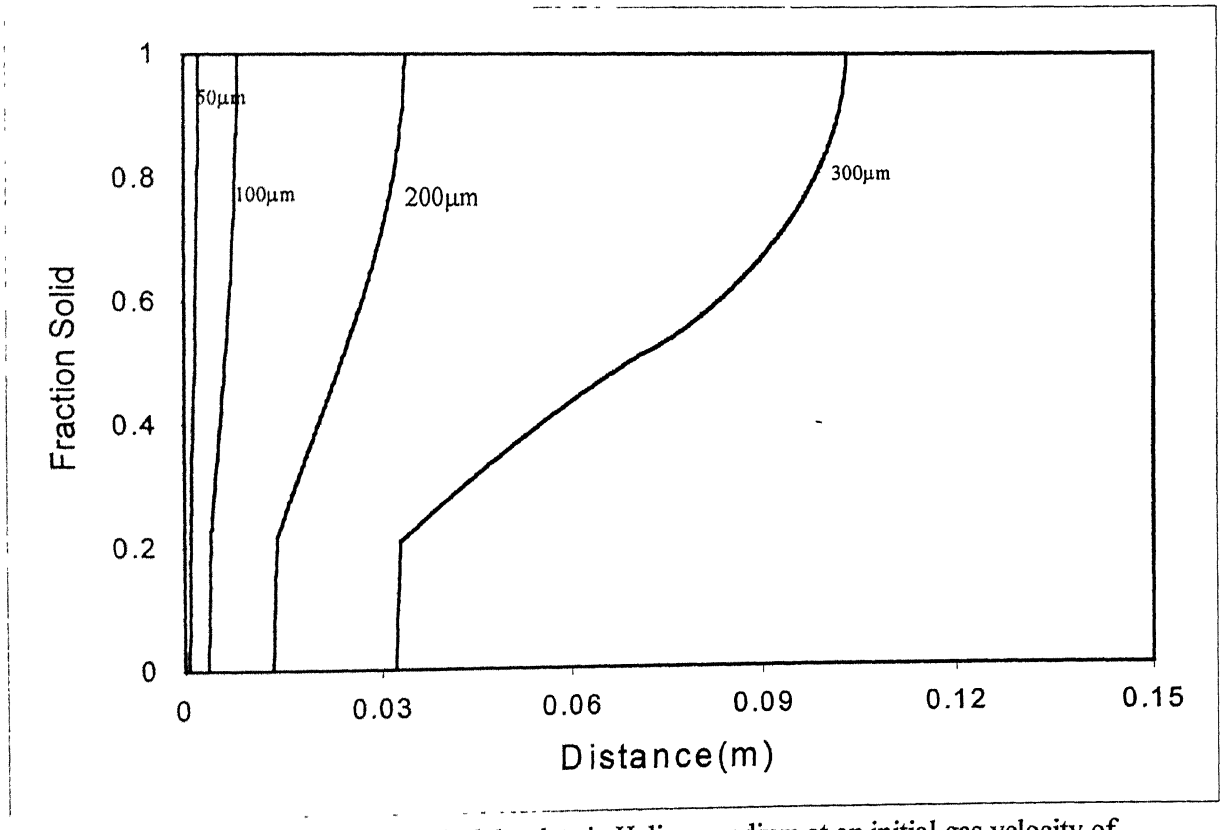

Fig. 4.1.20: Fraction Solid variation of Al droplets in Helium medium at an initial gas velocity of 200m/s velocity.

droplet starts to nucleate at 0.73m at an initial gas velocity of 200m/s On comparing Fig 17 and Fig 18, which are plotted at 200m/s and 400m/s initial gas velocity, it can be seen that the nucleation position and total solidification distance increases with velocity For example, a 100μm Al droplet completely solidify at 0.2m where as in 400m/s of initial gas velocity it completely solidifies at 0 4m from geometric point. The effect of gas medium on the profile of solid fraction variation can be seen from Fig.19. Here also, it can be seen that all the curves have two distinct stages but the start of solidification takes place at a much lower distance than in nitrogen medium. A 300μm Al droplet starts to solidify at 0.03m from geometric point During solidification, the complete distance of solidification and time vary with initial gas velocity, gas medium and superheat.

4.1.4.1 Effect of gas medium on fraction solidified at the end of recalescence:

Fig 21 shows the fraction solid at the end of recalescence of Cu and Al droplets in nitrogen and helium medium at an initial gas velocity of 200m/s. During recalescence a significant fraction gets solidified which has an effect on total solidification distance and time of droplets. Droplets below certain size get completely solidified during recalescence. All Al droplets below 7μm in nitrogen get completely solidified where as in helium medium droplets below 15μm get solidify completely. All Cu droplets of 6μm and below in nitrogen medium solidifies during recalescence where as in helium medium droplets below 14μm get completely solidified. It can be seen that the fraction solid at the end of recalescence decreases rapidly with droplet size and becomes almost constant afterwards for both Cu and Al and in both mediums. It can be seen that Cu droplets have a higher solid fraction at the end of recalescence. For example, a 50μm Al droplet has a solid fraction at the end of recalescence is 0.22 where as a Cu droplet has 0.32. It is observed that in helium medium the fraction solidified at the end of recalescence is higher. For example. a 20μm droplet in nitrogen medium has a solid fraction of 0.22, where as the same droplet in helium medium has a solid fraction of 0.55. It means that helium imparts a higher solid fraction at the end of recalescence. The same effect is also observed for Cu droplets. The reason being the higher rate of cooling, which result lower nucleation temperature. From equation – 29, it can be seen that the growth of solid phase depends on amount of undercooling.

4.1.4.2 Effect of gas medium and initial gas velocity on solidification distance of Al and Cu:

Fig. 22 compares the solidification distance of Al and Cu in nitrogen and helium medium. The results are shown for two initial gas velocities that is 200m/s and 400m/s. It can be seen that the solidification distance continuously increases with droplet size. Bigger droplets solidify at a longer distance than smaller droplets. The effect of gas velocity can be prominently seen in the figure. The solidification distance for both droplets of Al and Cu and in two mediums increases with initial gas velocity. For example, a 200μm Cu droplet solidify at 0.34m at 200m/s where as at 400m/s it solidifies at 0.77m from geometric point. The helium medium has a significant effect on solidification distance of droplets. It can be seen that all droplets of both Al and Cu solidify at a much shorter distance in helium than in nitrogen. It is because of its higher thermal conductivity, which ensures a higher rate of heat extraction Hence, droplets tend to solidify at a shorter distance. For example; a 100μm droplet in helium medium solidifies at 0.007m at 200m/s initial gas velocity, whereas in nitrogen medium it solidifies at 0.23m from geometric point.

It can be noticed that at all gas velocities and mediums, Cu droplets take longer distance than Al droplets for complete solidification. For example, at 200m/s initial gas velocity, a 100μm Cu droplet solidify at 0.17m where as an Al droplet solidifies at 0.23m.

Fig. 23 shows the ratio of distance covered by Al droplets in nitrogen and helium medium after 50% solidification and complete solidification. The initial gas velocity is maintained at 200m/s. It can be seen that the trend of variation is same for the two curves. The ratio initially increases up to 130μm size and then gradually decreases. However, the ratio is higher at complete solidification for droplets of all sizes.

4.1.4.3 Effect of gas medium and velocity on solidification time:

Fig. 24 shows the effect of initial gas velocity on total solidification time of Al droplets. The effects of two different atomizing medias are also shown in the figure. It can be seen that on increasing the atomization gas velocity, the time of solidification of all droplets decreases. Typically, a 200μm droplet with an initial velocity of 200m/s in nitrogen

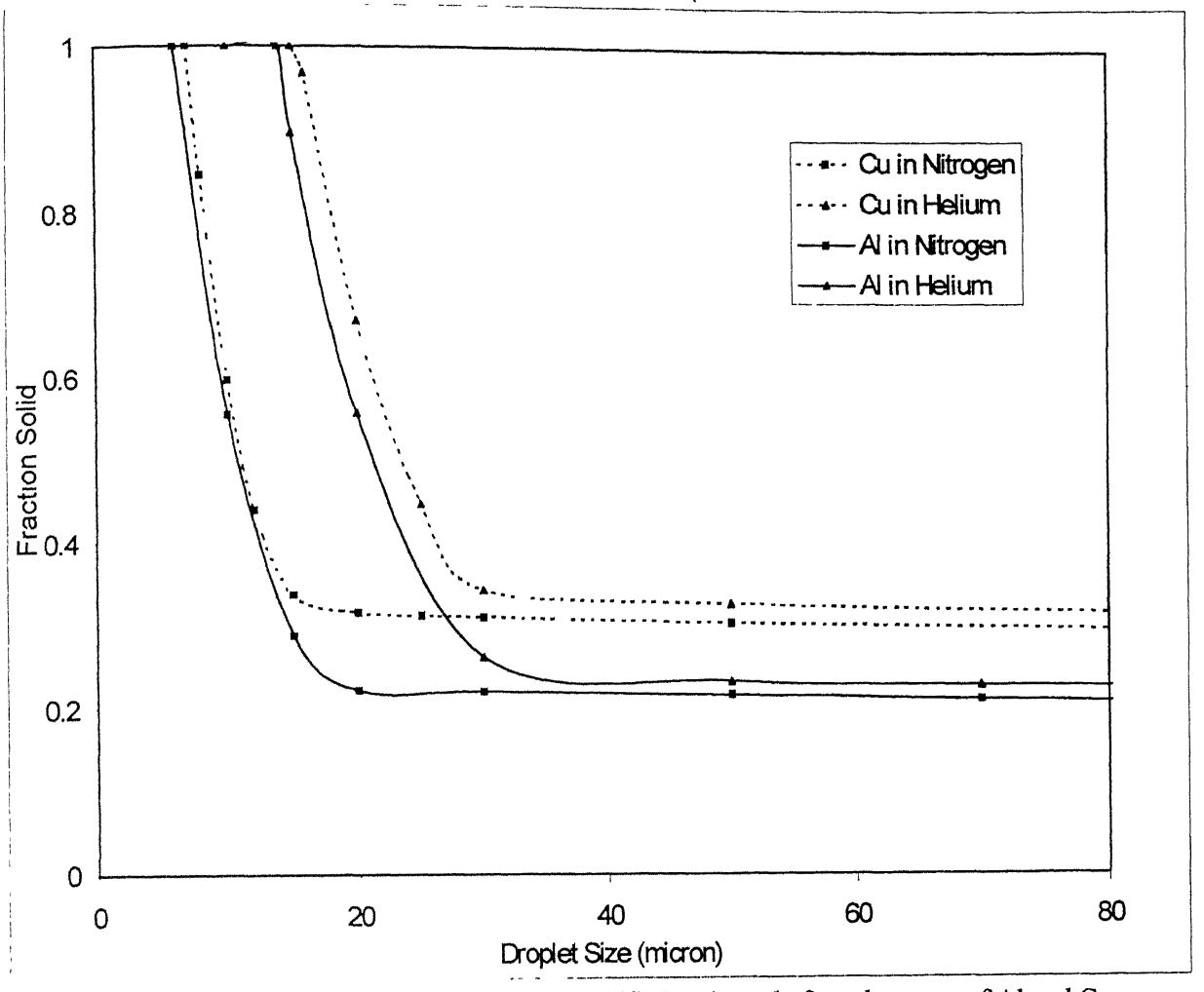

Fig.4.1.21: Effect of gas medium on fraction solidified at the end of recalesecnce of Al and Cu droplets.

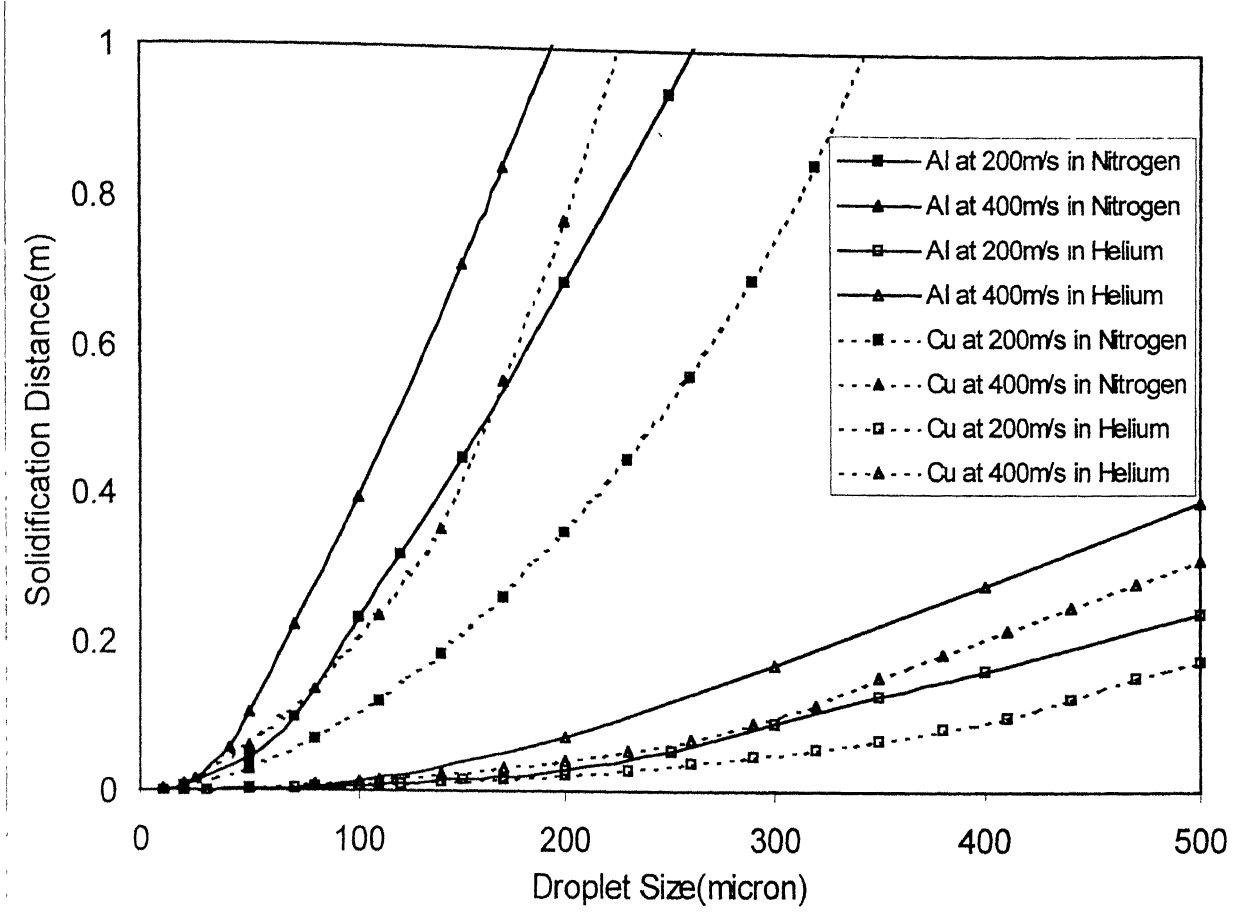

Fig.4.1.22. Effect of initial gas velocity and medium on complete solidification distance of Al and Cu droplets.

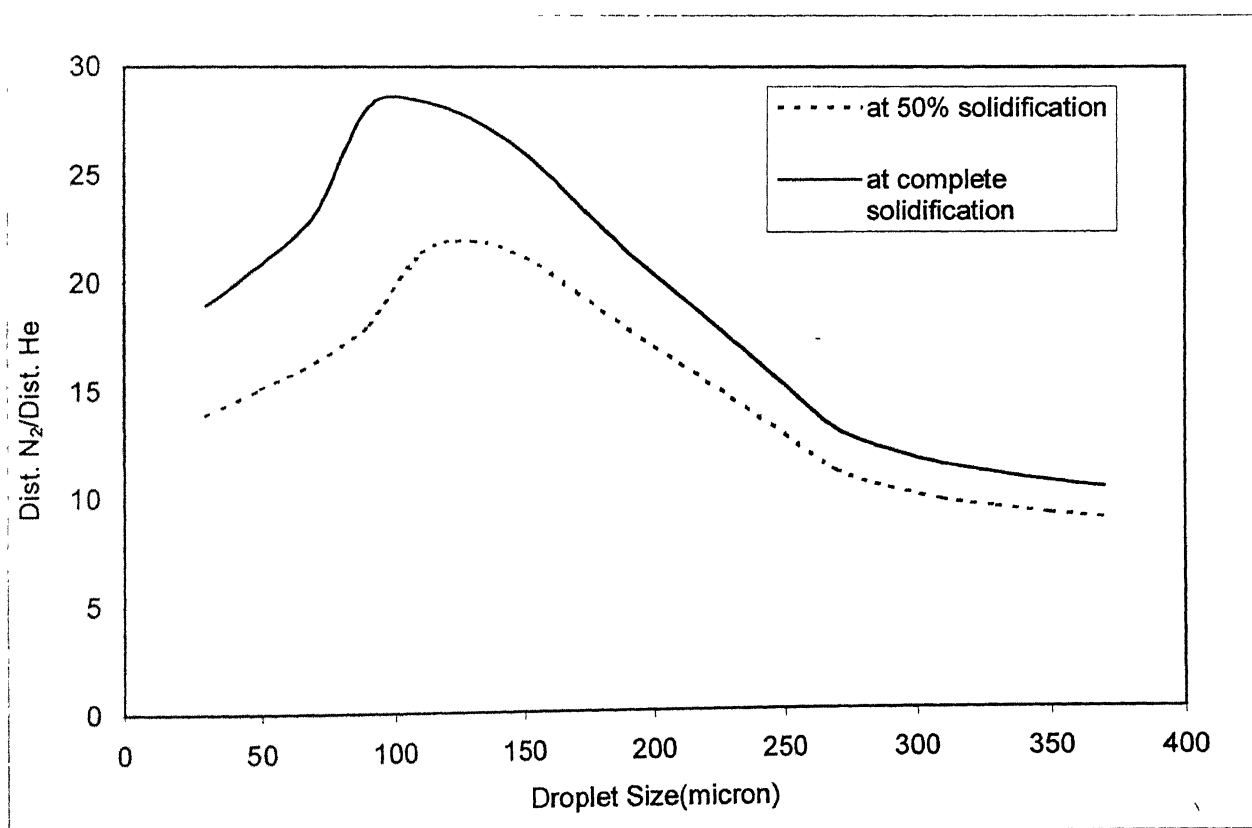

Fig.4.1.23: Ratio of distance covered in He and Nitrogen medium at 50% and complete solidification.

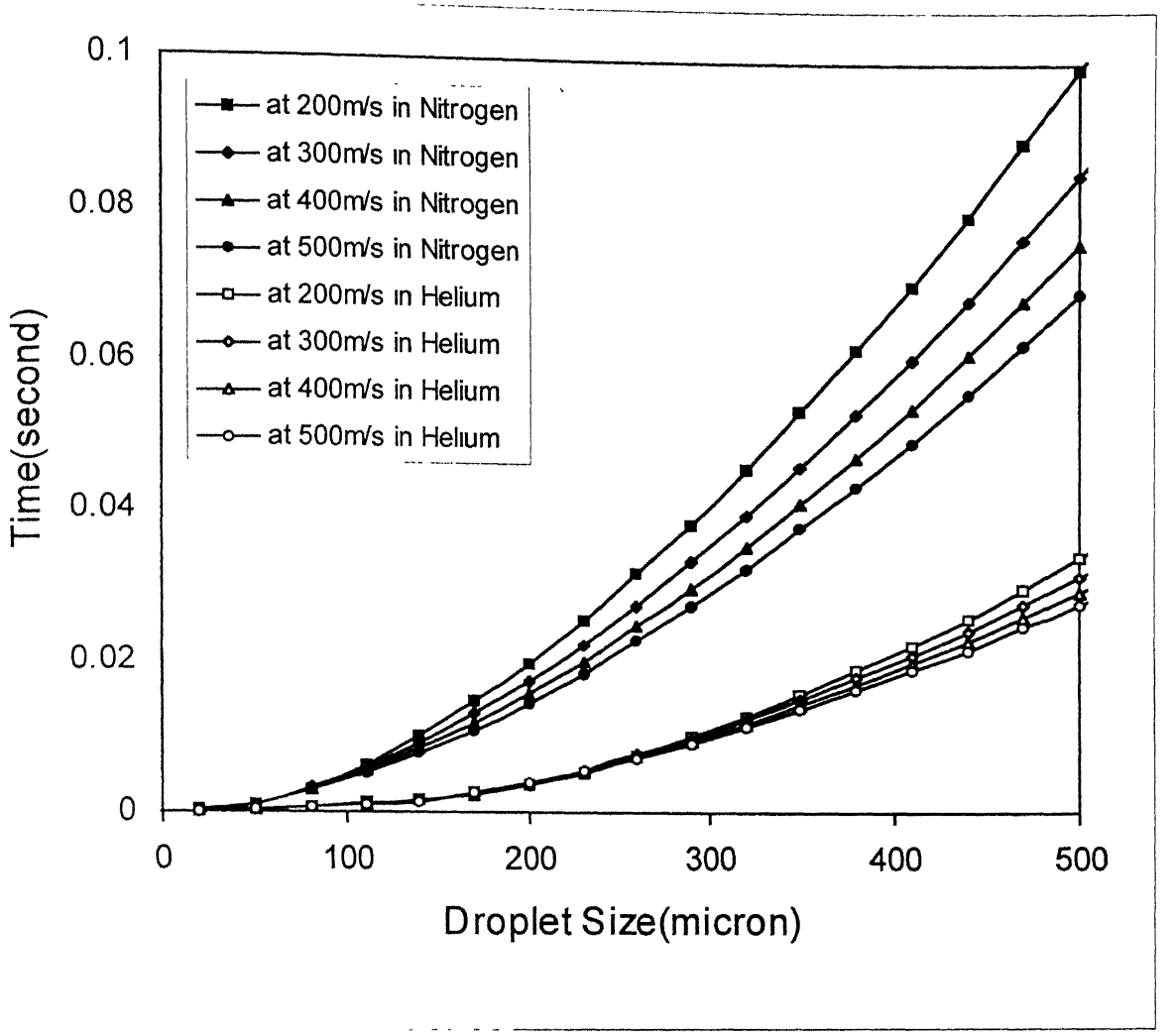

Fig.4.1.24: Effect of Nitrogen and Helium gas medium on complete solidification time of Al droplets.

medium gets completely solidify at a time of 19 7ms where as the same droplet at 500m/s in the same medium gets completely solidify at 14.5ms. It is because increasing the velocity results in increasing the heat transfer coefficient and hence very high rate of cooling. From equation-14, it can be seen that rate of growth of solid fraction depends on heat transfer coefficient, so increase in velocity result in higher rate of growth of solid fraction. Hence, solidification completes early. Comparing the time of solidification with helium medium, a 200μm Al droplet at 200m/s initial gas velocity completely solidify in 3.6ms where as the same droplet in nitrogen medium solidifies in 19.7ms.

4.1.4.4 Effect of superheat on complete solidification distance:

Fig 25 shows the effect of superheat on complete solidification distance of droplets. It is observed that all droplets with increasing amount of superheat solidify at longer distances. The same behavior is noticed in two mediums. A 200μm droplet with 50^0C superheat solidifies at 0.76m in nitrogen medium where as at 200^0C superheat it completely solidifies at 1 2m from the pint of atomization. In helium medium the same droplet with a superheat of 500C solidify at 0 12m whereas at 200^0C it solidifies at 0.24m. The reason for this can be understood as increasing superheat result in increasing the heat content. So, removal of extra amount of heat takes longer time and hence the droplets travel a longer distance.

4.1.4.5 Effect of superheat on complete solidification time:

Fig. 26 shows the effect of superheat on complete solidification time of droplets. The effect is shown in two atomizing gas mediums. It is noticed that increasing the superheat result in increasing the solidification time. A 200μm Al droplet with a superheat of 50^0C solidifies in 21.8ms where as the same droplet with a superheat of 200^0C solidifies at 34.9ms in nitrogen medium. In helium medium the same size droplet solidifies at 4.7ms with 50^0C superheat where as with 200^0C superheat the droplet solidifies in 8.71ms.

4.1.4.6 State (Temperature and solid fraction) of the droplets at a fixed position from geometric point:

Fig. 27-29 show the temperature and solid fraction of droplets at 0.3m, 0 4m, and 0.5m from geometric point. In all the plots, solid fraction and temperature are plotted against droplet size. Each curve gives an impression about the size ranges, which stays in solid, semisolid ad completely liquid at increasing distances from geometric point.

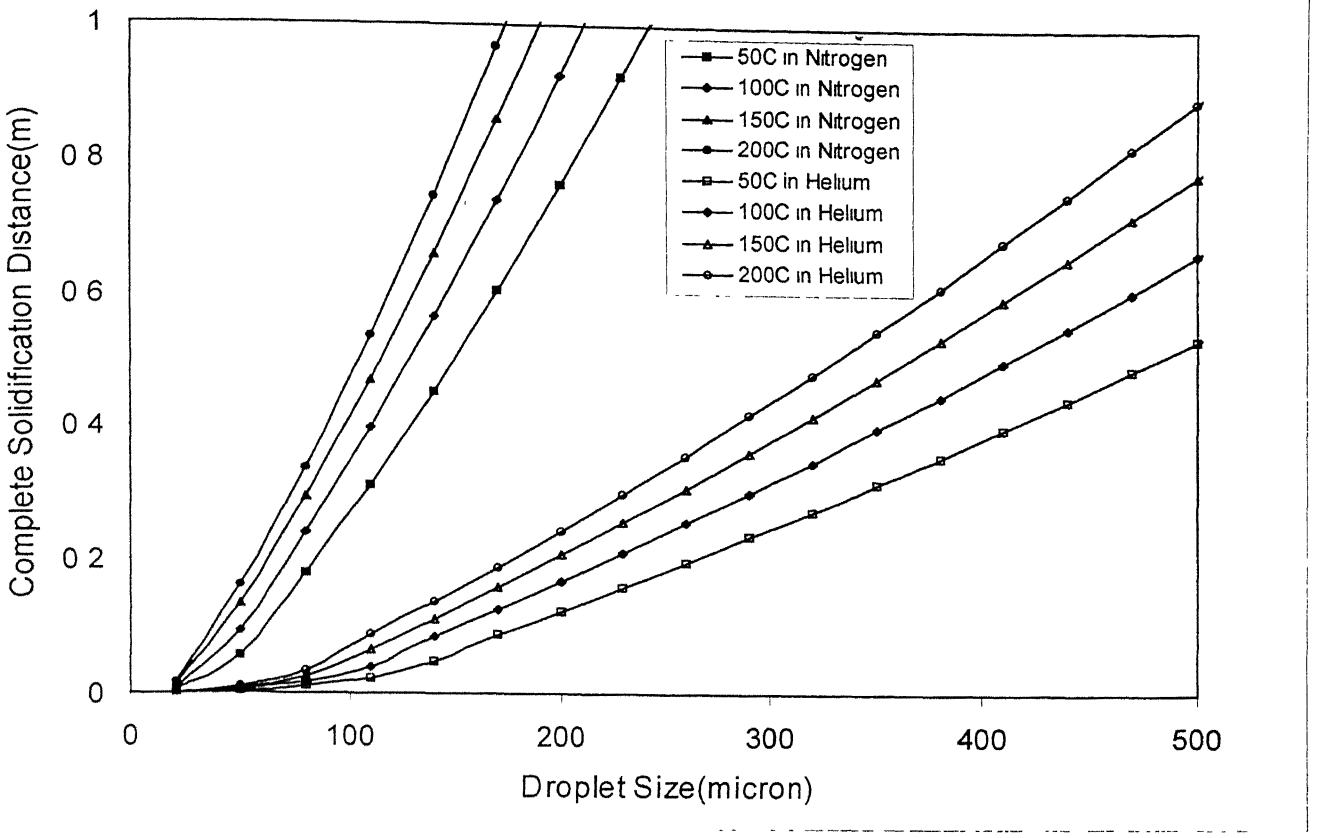

Fig.4.1 25: Effect of superheat on solidification distance of Al droplets at an initial gas velocity of 200m/s.

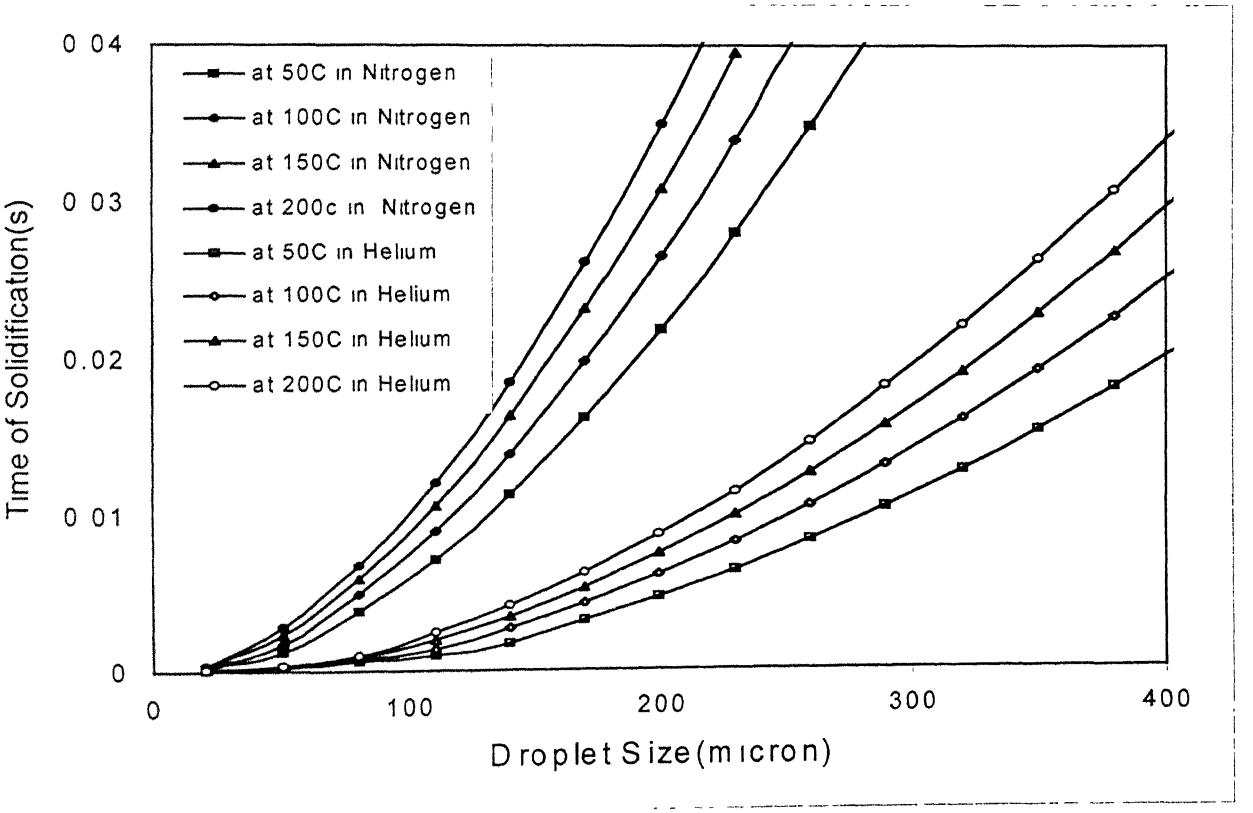

Fig.4.1.26: Effect of superheat on complete solidification time of Al droplets at 200m/s initial gas velocity

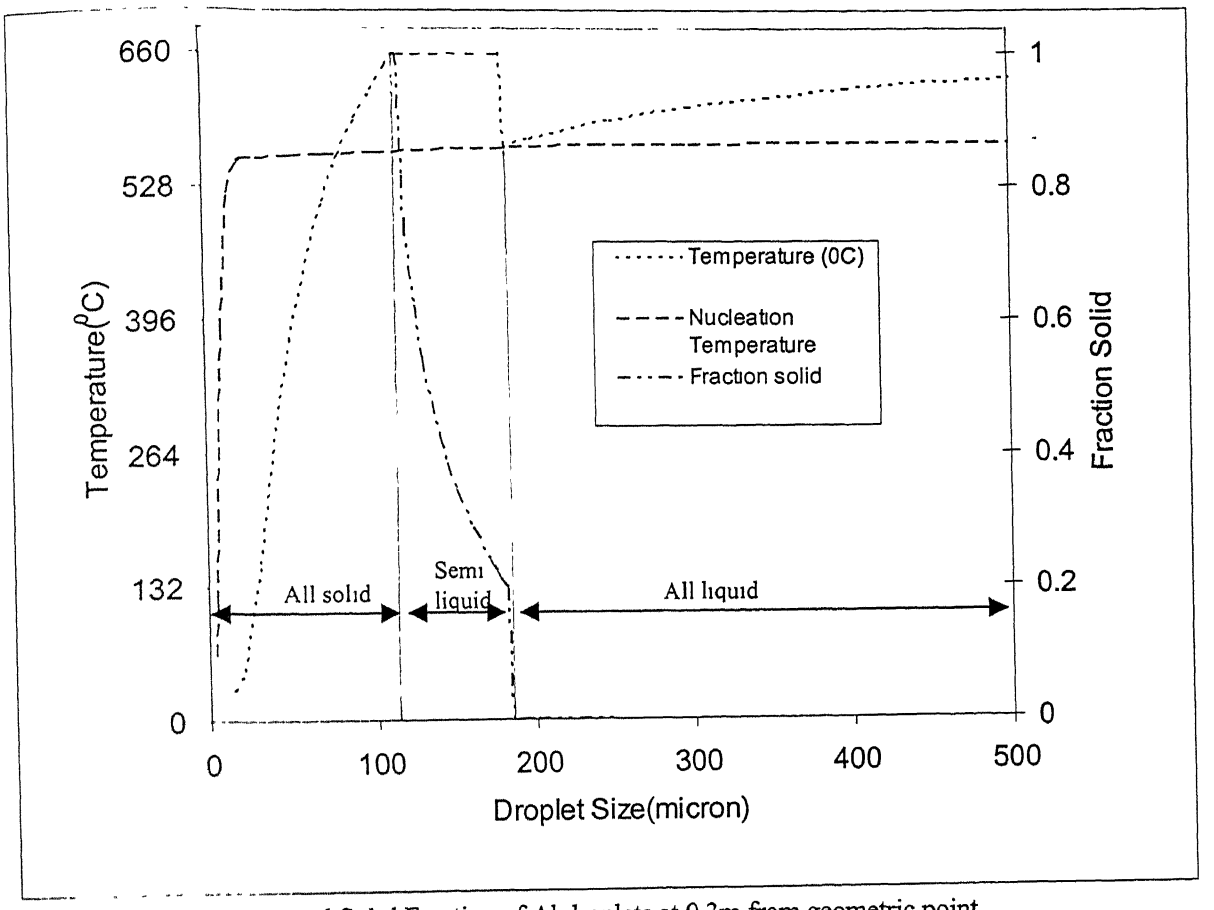

Fig.4.1.27 Temperature and Solid Fraction of Al droplets at 0.3m from geometric point

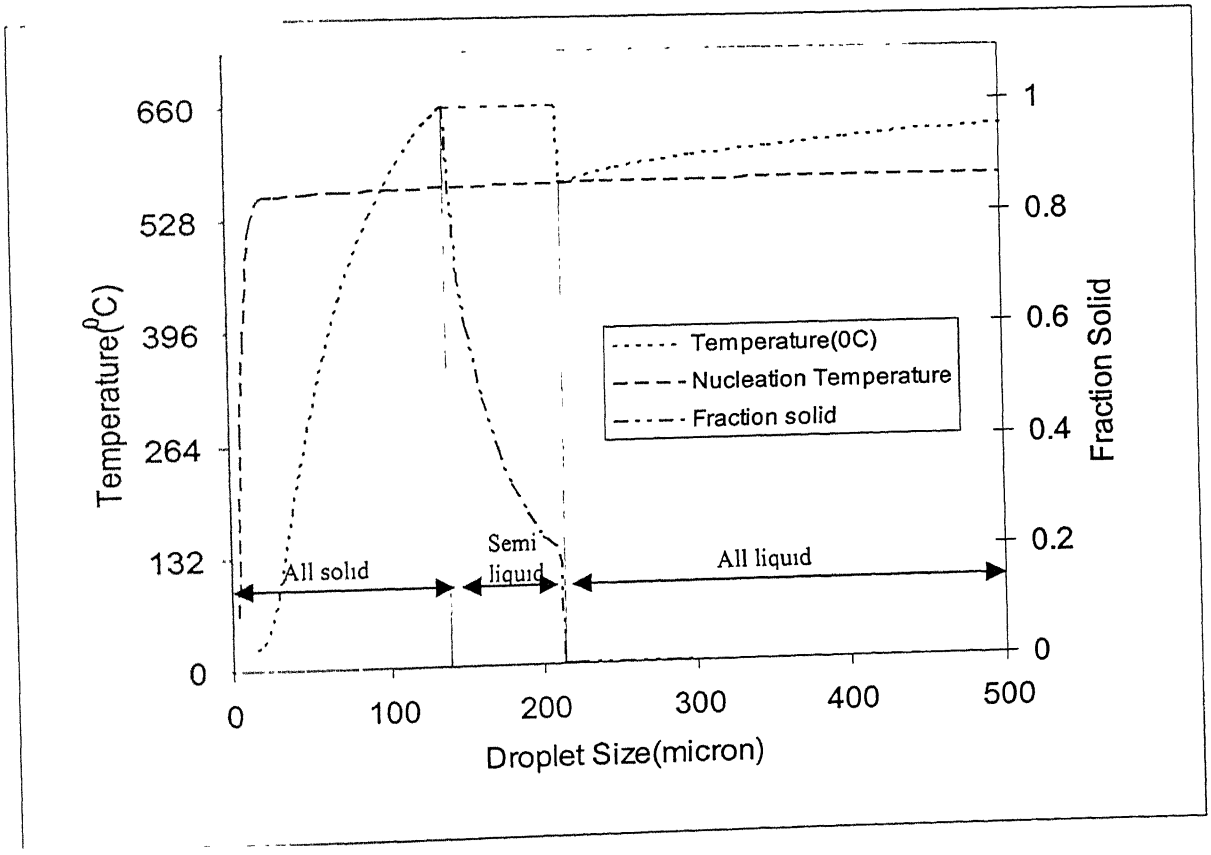

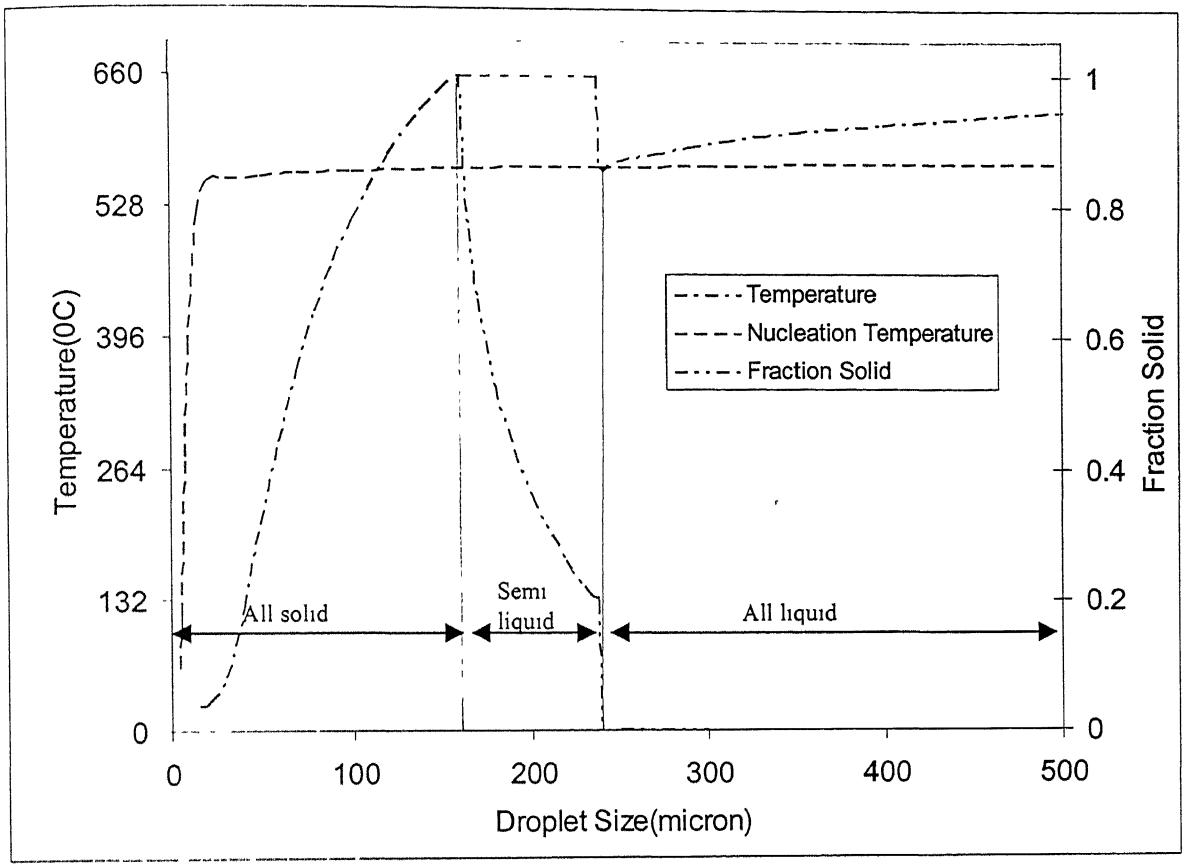

Fig.4.1.29 Temperature and Solid Fraction of Al droplets at 0.5m from geometric point

Table-5 The state of the droplets at different position from the geometric point

Position (m)	Completely solid	Partially solid/liquid	Completely liquid
0.3	d<110	110<d<188	d>188
0.4	d<115	115<d<208	d>208
0.5	d<160	145<d<238	d>238

It is noticed that as the position of consideration increases from geometric point, the droplet size in all classes increases.

4.2 Thermal profile of the deposit:

Fig 4.2.1 shows the thermal profile of the deposit at different time intervals. In this representation the substrate temperature, though varies with time and thickness of the deposit, is taken to be constant and is equal to 200^0C. It can be seen that the temperature of the deposit increases with the increase in thickness of the deposit for all times. For a given thickness increase in time decreases the deposit temperature. The heat transfer coefficient at the substrate-billet interface has taken as $1000 W/m^2/^0C$ from literature. The results are shown at 10s, 20s, 30s, 40s, and 50s after the start of deposition. Further work is needed to show the influence of substrate temperature variation on the thermal behavior of the droplet.

4.3 VALIDATION:

The theoretical distance of complete solidification for Pb calculated from model is compared with available experimental result [12]. The graph is shown in Fig. 4.3. It can be seen that the theoretical value is lower than the experimental one below the 200μm and above that the predicted value goes higher than the experimental one. However, the theoretical model predicts the solidification distance with a variation of 17.7% from the experimental result.

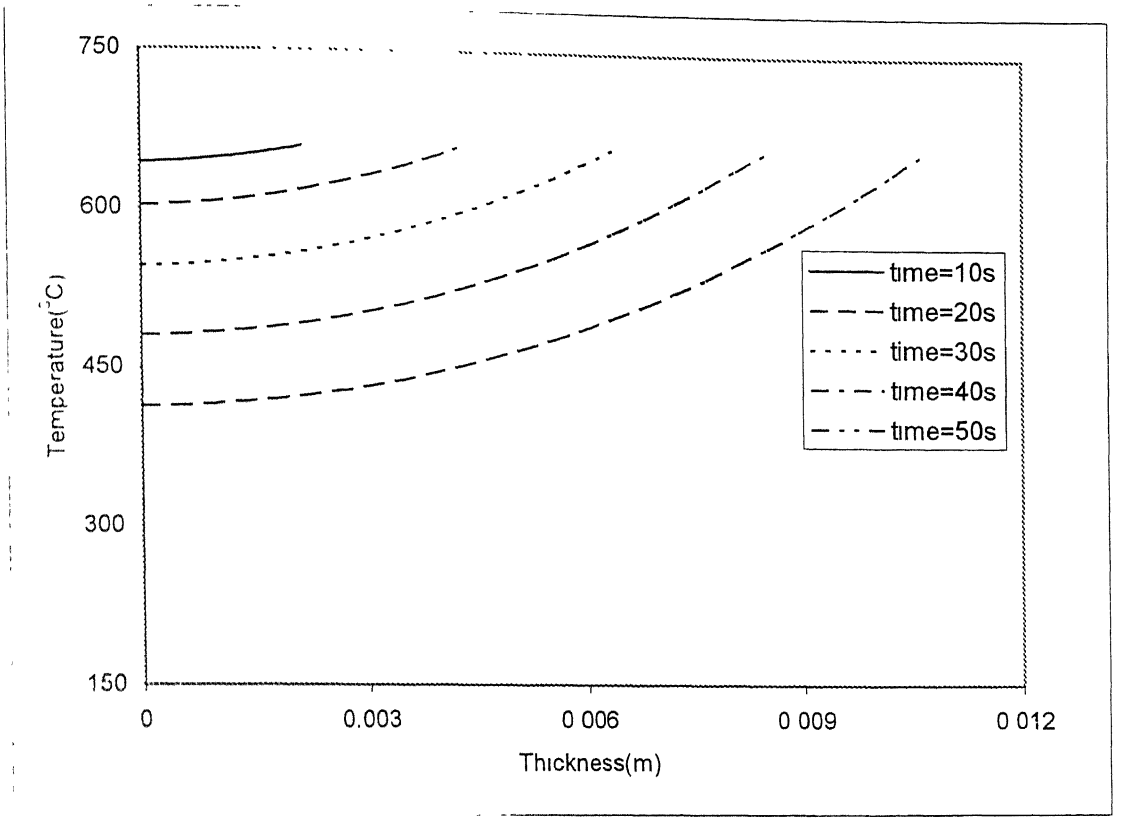

Fig 4 2 1 Temperature along the thickness of the deposit at different time intervals

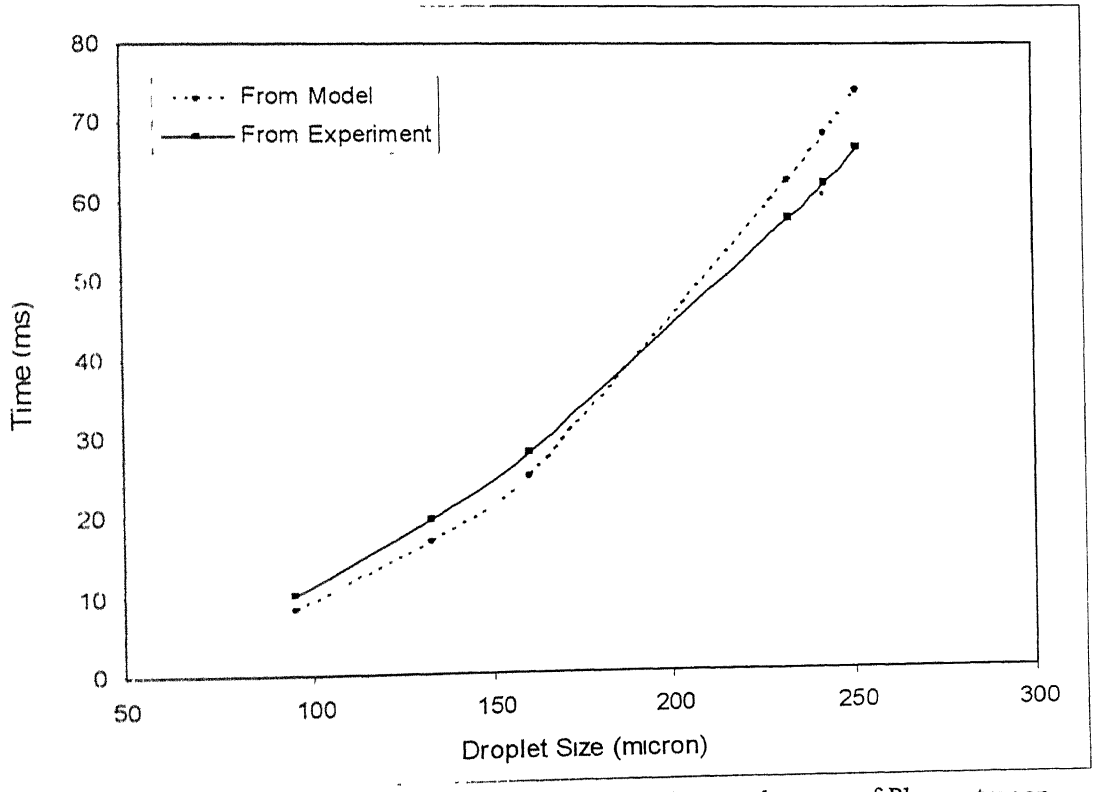

Fig 4.3. Comparison of theoretical and experimental solidification distance of Pb in nitrogen atmosphere

CHAPTER 5 CONCLUSIONS

Following conclusions are made.

1. It is found that smaller droplets move with a faster velocity in the beginning of their motion and after a certain distance the velocity of smaller droplets goes below the bigger droplets. Hence, the velocity profile of a droplet depends on its size.

2. The heat transfer coefficient of a droplet is intimately related with the relative velocity between the droplet and atomizing gas. It is noticed that smaller droplets have a higher heat transfer coefficient than bigger droplets at all positions.

3. The nucleation temperature of a droplet is found to depend on the size of the droplet. Smaller droplets are observed to be having lower nucleation temperature than bigger droplets. It is also observed that in helium medium the droplets nucleated at a lower nucleation temperature than nitrogen medium.

4. The fraction solidified at the end of recalescence is observed to depend on the amount of undercooling. The amount solidified at the end of recalescence decreases with increase in droplet size. It is also noticed that the fraction solidified at the end of recalescence is higher in helium medium than in nitrogen medium.

5. The gas medium plays an important role in total solidification distance and time of droplets. It is observed that all droplets in helium medium solidify at much shorter distance than in nitrogen medium.

6. The initial gas velocity, superheat temperature of the molten metal is responsible for variation of complete solidification distance and time. It is observed that with increase in gas velocity the solidification distance increases but the total solidification time decreases. An increase in superheat temperature resulted in increase of solidification time and distance.

7. The Cu droplets are observed to be solidifying at shorter distance than Al droplets.

8. The temperature profile of the deposit is observed to be a function of substrate temperature. The amount of heat removal by the substrate influences the temperature profile of the deposit.

FUTURE WORK:

In the present study, an effort has been made to investigate the effects of process parameters on solidification behavior of pure metals. This study can be extended for different alloys. Models can be developed to determine the solidification behavior of alloys and effect of process parameters on it. In the present study the thermal profile of the deposit is found out by solving one dimensional heat conduction equation in rectangular coordinates. However, the study can be extended for true geometry of the preform that is cylindrical coordinates can be considered to determine the temperature profile. Model can be formulated for higher dimensional conduction equation.

REFERENCES

1. J. Lavernia, Yue Wu, Spray Atomization and Deposition, pp. 8,28.40,44,299, John Wiley and Sons,1996

2. J. Lavernia, J.D. Ayers and T.S. Srivatsan (1992) Int. Mater. Rev., 37,1,2,253

3. A.R.E Singer (1970) Met. And Mater., 4,246

4. R.G. Brookes, A.G. Leatham, J.S. Coombs and C. Moore (1977), Metall. and Met. Form., 9,157

5. A.R.E. Singer (1985) J. Inst. Met., 100,185

6. A.R.E. Singer (1985) Int. J. Powder Metall. Powder Tech., 21(3), 219

7. H.C. Fiedler, T.F. Sawyer, R.W. Kopp, and A.G. Leatham (1987) J. Met., 39 (8), 28

8. Y.Ikawa, T. Itami, K. Kumagai et. Al (1990) ISIJ International, 30, 756.

9. A.G. Leatham and a. Lawley (1993) Int. J. Powder Metall., 29,321

10. Koria, Singh and Dube, PhD Thesis, 1999

11. J. Szekely, Fluid Flow Phenoemena in Metals Processing, pp.261, Academic Press, New York (1979)

12. B.Li., X. Liang, J.C. earthman and E.J. lavernia, Acta. Mater., Vol. 44, No. 6, pp. 2409-2420, 1996

13. J.P Hirth, Metallurgical Transactions A, Vol 9A, pp 401-404, March 1978

14. Lawrence E. Murr, Interfacial Phenomena in Metals and Alloys

15. J.W. Christian, Theory of Transformations in Metals and Alloys, 2nd ed., Pergamon Press, Oxford united Kingdom, 1975, pp. 442-48

16. C.G. Levi, R. Mehrabian, Metallrgical Transactions, 13a, 1982, pp. 221

17. J.W. Cahn, W.B. Hillings, G.W. Sears, Acta. Metall., 12, pp. 421

18. H. Lubanska (1970) J.Met., 22 (2), 45

19. S.K. Gupta, Numerical Methods for Engineers,pp.129

APPENDIX-A:

Calculation of coefficient of $\frac{T_m^2}{(T_m - T)^2}$ in equation- (24):

The expression for transient nucleation rate is given in equation -24. It is given by

$$It = f_0 C_0 \exp\left(-\frac{16\pi\sigma_{sl}^3 T_m^2 \Omega^2}{3H_{fm}^2 (T_m - T)^2 KT}\right)\exp\left(-\frac{16KT\sigma_{sl} a_0^4 T_m^2}{D_o V_m^{\beta^2} H_{fv}^2 (T_m - T)^2 t}\right) \quad \text{--------- ---A1}$$

For Al:

$$f_0 = \frac{D_0}{\lambda^2 \alpha} \text{ i.e. } \frac{4.0\times10^{-10}}{\left(\frac{4.04\times10^{-10}}{\sqrt{2}}\right)^2 \times 4}$$

$$= 2.475\times10^9 /\text{s}$$

$$C_0 = \frac{6.023\times10^{23}}{27}\times 2.7\times10^6$$

$$= 6.023\times10^{28} \text{ atoms/m}^3$$

$$It = 1.49\times10^{38}\exp\left(-\frac{16\times\pi\times0.852^3\times10^{-10}\times T_m^2}{3\times10739^2\times1.38\times10^{-23}(T_m - T)^2 T}\right)$$

$$\exp\left(-\frac{16\times1.38\times10^{-23}\times0.852\times\left(4.0\times10^{-10}\right)^{-4} T_m^2}{4.0\times10^{-10}\times\left(1.66\times10^{-29}\right)^2\left(3.55\times10^9\right)^2 (T_m - T)^2 t}\right)$$

$$= 1.490\times10^{38}\exp\left(-651119.36\times\frac{T_m^2}{(T_m - T)^2 T}\right)\exp\left(-3.506\times10^{-12}\frac{T_m^2}{(T_m - T)^2 t}\right) \quad \text{---------A-2}$$

$$\frac{I_t}{I_s} = \exp\left(-3.506\times10^{-12}\frac{T_m^2}{(T_m - T)^2 t}\right) \quad \text{----------A-3}$$

For Cu:

$$f_0 = \frac{D_0}{\lambda^2\alpha} == 3.137\times10^9 \text{ /s}$$

$$C_0 = \frac{6.023\times10^{23}}{63.5}\times 8.96\times10^6$$

$$= 8.479\times10^{28} \text{ atoms/m}^3$$

$$It = 2.66\times10^{38}\exp\left(-\frac{16\times\pi\times0.512^3\times7.102^2\times10^{-12}\times T_m^2}{3\times13041.63^2\times1.38\times10^{-23}(T_m-T)^2T}\right)$$

$$\exp\left(-\frac{16\times1.38\times10^{-23}\times0.512\times\left(3.6\times10^{-10}\right)^{-4}T_m^2}{4.0\times10^{-10}\times\left(1.179\times10^{-29}\right)^2\left(1.836\times10^{9}\right)^2(T_m-T)^2t}\right)$$

$$= 2.66\times10^{38}\exp\left(-48325.56\times\frac{T_m^2}{(T_m-T)^2T}\right)\exp\left(-1.814\times10^{-11}\frac{T_m^2}{(T_m-T)^2t}\right) \text{---------- A-4}$$

$$\frac{I_t}{I_s} = \exp\left(-1.814\times10^{-11}\frac{T_m^2}{(T_m-T)^2t}\right) \text{---------- A-5}$$

APPENDIX B:

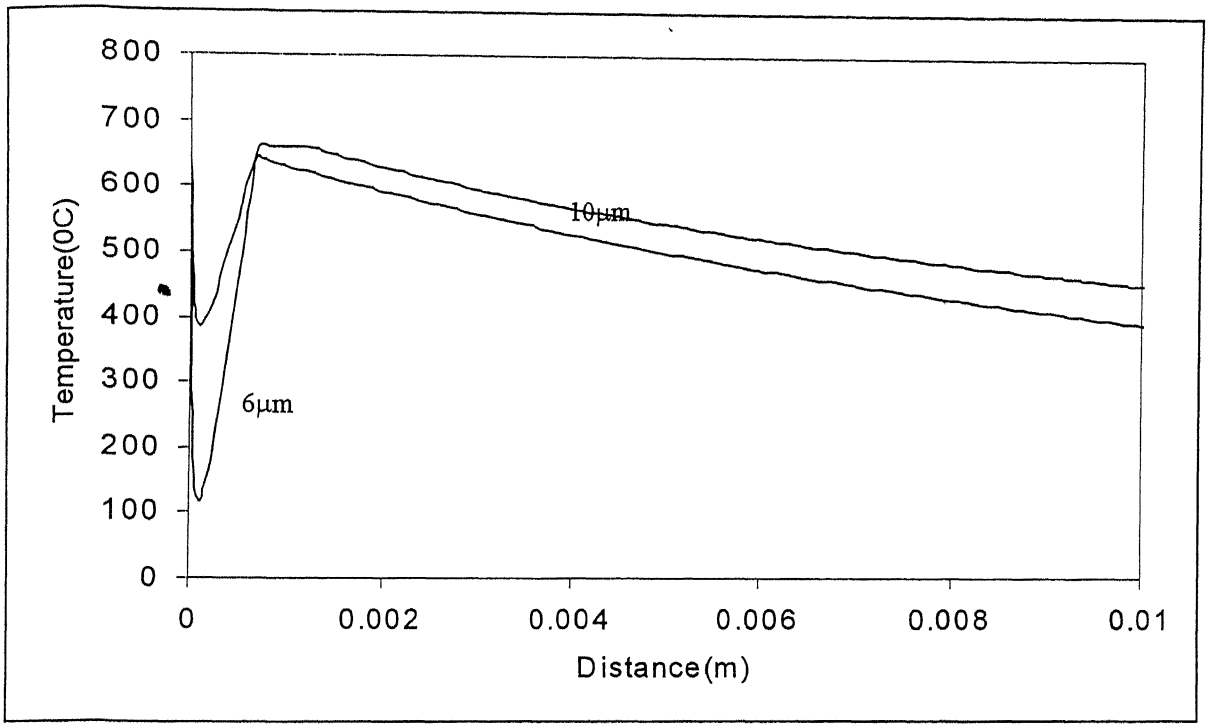

Fig.B-1: Figure shows the hypercooled Al droplet of 6μm which completely solidifies before reaching melting point The medium is nitrogen and the initial gas velocity is 200m/s

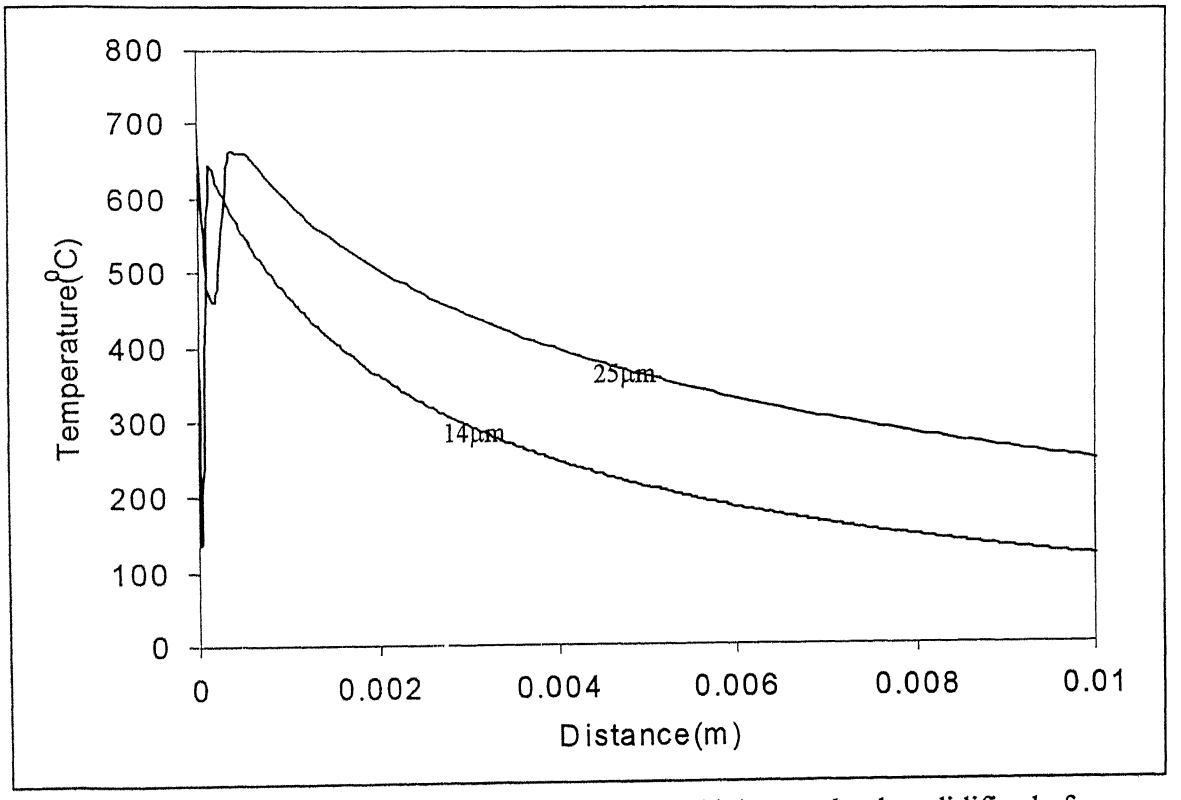

Fig. B-2: Shows the hypercooled Al droplet of 14μm which completely solidifies before reaching melting point in helium medium The other droplet 25μm has solidification at melting point.